Seismic Performance of Circular Columns Rehabilitated with Sprayed-GFRP Composites

by

Syed Abdullah Mohit

A Thesis submitted to the Faculty of Graduate Studies of

The University of Manitoba

in partial fulfillment of the requirements of the degree of

MASTER OF SCIENCE

Department of Civil Engineering

University of Manitoba

Winnipeg, MB, Canada

ABSTRACT

Rehabilitation of reinforced concrete (RC) structures has become a vital issue. Large number of structures constructed before 1970 are reported as seismically-deficient due to inadequate detailing or environmental degradation. Conventional rehabilitation methods such as steel plates and RC jacketing increases the structural mass, changes aesthetic of the structure, needs heavy equipment, time consuming and still vulnerable to steel corrosion. On the other hand, fibre reinforced polymer (FRP) wraps need extra surface preparation and its application on irregular structures is complicated. Recently, the new sprayed-FRP composites technique is introduced to overcome these limitations. This study investigates the seismic behaviour of RC circular columns rehabilitated using sprayed-glass fibre reinforced polymer (sprayed-GFRP) composites. Six large-scale RC circular columns were constructed in laboratory and tested under a combination of reversal-cyclic load and a constant axial load. The applied axial load was equal to 20% of axial load carrying capacity of the column. All specimens were deficient in lap splice length at footing-column joint and had a diameter of 305-mm with 1,525-mm shear span (length). A 3.0-mm and 6.0-mm thick sprayed-GFRP coating was used for rehabilitation of the specimens. Two specimens were strengthened without prior loading, two specimens were rehabilitated after being partially damaged (up to 2.5% drift ratio) and two specimens were rehabilitated after being fully-damaged. Results showed that sprayed-GFRP of 3-mm thickness is inadequate for rehabilitation of the fully damaged column. However, it can be used for strengthening and rehabilitation of partially-damaged columns. Sprayed-GFRP of 6-mm thickness not only increased the drift capacity of the column but also successfully restored the full capacity of seismically damaged RC columns.

To my beloved parents and sister

Thanks for your continuous prayer, support and care

ACKNOWLEDGEMENT

My first and sincere appreciation goes to my advisor Dr. Ehab El-Salakawy, PEng, FCSCE, Professor of Structural Engineering in the Department of Civil Engineering at the University of Manitoba. His continuous guidance and support has immensely helped me throughout this work. His support during the most difficult phases of my work was remarkable. I am so proud to work with him. I would also like to thank him for all I have learned from him, and for encouraging and helping me to shape my ideas and interests.

I would like to express my deep gratitude to my colleagues, Dr. Karam Mahmoud, Dr. Anant Parghi, Mr. Shervin Ghomi, and Mr. Mohammed Galal El-Gendy whose suggestions for my work were phenomenal.

Special thanks to Dr. Raghavan Jayaraman, PEng, Associate Professor in the Department of Mechanical Engineering at the University of Manitoba for allowing me to use his research facility.

The financial support of the University of Manitoba Graduate Fellowship (UMGF), NSERC-Engage grant and MITACS-Accelerate are gratefully acknowledged.

The outcome of this project would not have been possible without the help and assistance of the W. R. McQuade structures laboratory technical staff, Dr. Chad Klowak, PEng, Brenden Pachal and Grant Whiteside.

Thanks to my special mentor Mr. S. M. Hasanur Rahman for being there for me, during both good and bad times.

Lastly, and most importantly, I would like to thank my father, my mother, and my sister. Words cannot describe the sacrifices my parents have made for me, to assure a bright future; without them I would not have been here.

TABLE OF CONTENTS

LIST OF TABLES

LIST OF FIGURES

LIST OF NOTATIONS

a	Depth of equivalent stress block, mm
A_b	Area of a single rebar, mm^2
A_c	Area of core of spirally-reinforced compression member measured to outside diameter of spiral, mm^2
A_{cc}	Area under confined concrete, mm^2
A_{ch}	Cross-sectional area of a structural member measured to outside edges of transverse reinforcement, mm^2
A_{comp}	Concrete area under compression, mm^2
A_g	Gross area of section, mm^2
A_p	Area of prestressing tendon, mm^2
A_{sh}	Total effective cross-sectional area of transverse reinforcing steels in the direction under consideration, mm^2
A_{sp}	Cross-sectional area of spiral reinforcement, mm^2
A_{st}	Total area of longitudinal reinforcement, mm^2
A_t	Area of one leg of closed transverse torsion reinforcement, mm^2
$A_{v,min}$	Area of shear reinforcement perpendicular to the axis of a member within the distance *s*, mm^2
$A_{\beta_1 c'}$	Area under unconfined concrete, mm^2
b_w	Beam web width or diameter of circular section, mm
b_c	Core dimensions to centerlines of peripheral hoop in X-direction of rectangular cross sections, mm^2

C_c Compression force due to concrete, N

c_b Distance from extreme compression fibre to neutral axis at balanced condition, mm

c' Distance from the neutral axis to the position where the compression strain is ε_c' in the concrete, mm

C_{cc} Compression force due to confined concrete, N

C_s Force on bars in compression, N

d Effective depth of section, mm

D Section diameter for circular column, mm

d_b Longitudinal bar diameter, mm

d_c Core dimensions to centerlines of peripheral hoop in Y-direction of rectangular cross sections, mm^2

d_s Diameter of spiral between bar centres, mm

d_v Effective shear depth taken as the greater of 0.9*d* or 72*h*, mm

E_c Modulus of elasticity of concrete, GPa

E_{frp} Modulus of elasticity of FRP, GPa

E_f Modulus of elasticity of fibre, GPa

E_m Modulus of elasticity of resin or matrix, GPa

E_s Modulus of elasticity of steel bar, GPa

f_c' Specified compressive strength of concrete, MPa

f_{cc}' Confined concrete strength, MPa

f_f, Tensile strength of fibre, MPa

f_{frp}, Tensile strength of FRP, MPa

f_{lfrp}	Lateral confining pressure from FRP, MPa
f_m	Tensile strength of resin or matrix, MPa
f_{pr}	Stress in prestressing tendons at factored resistance, MPa
F_s	Force in steel bar, N
f_s	Stress in steel longitudinal reinforcement, MPa
F_{sj}	Force on intermediate steel bars, N
f_{ufrp}	Ultimate tensile strength of FRP, MPa
f_y	Specified yield strength of non-prestressed reinforcement or anchor steel, MPa
f_{yh}	Yield strength of transverse reinforcing steel, MPa
f_{yt}	Specified yield strength of transverse reinforcement, MPa
h	Total section height, mm
k_e	Reduction factor for confined concrete strength
k_{ef}	Confinement efficiency coefficient
l_{sp}	Length of transverse reinforcement in one loop, mm
M_f	Factored moment about the centroid of critical section of the column, N.mm
N_f	Factored axial load normal to the cross section occurring simultaneously with V_f including compression, N
p	Spiral pitch, mm
P_f	Factored axial load, N
P_r	Axial load resistance of column, N
$P_{r,max}$	Maximum factored axial load resistance for a reinforced concrete column, N
P_{ro}	Factored axial load resistance of column at zero eccentricity, N

P_{sus}	Sustained axial load, N
R	Section radius of circular cross section, mm
R_f	Fibre concentration in matrix, %
s	Center-to-center spacing of adjacent transverse confining steels, mm
s'	Clear spacing between adjacent transverse confining steel, mm
S_{Ze}	Equivalent value of crack spacing parameter that allow the influence of aggregate size, mm
t	Confinement thickness, mm
t_{frpex}	Required extra confinement thickness in lap splice region, mm
T_s	Tension force on longitudinal bars, N
T_{FRP}	Tension force on FRP, N
V_c	Shear resistance attributed to the concrete factored by ϕ_c, N
V_f	Volumetric ratio of fibres
V_m	Volumetric ratio of resin
V_r	Factored shear resistance of section, N
V_{rmax}	Maximum allowable shear resistance, N
V_s	Shear resistance provided by shear reinforcement factored by ϕ_s, N
w_c	Weight of composite sample, gm
w_f	Weight of fibre in composite sample, gm
w_i'	Distance between adjacent longitudinal steel in rectangular cross-sections, mm
y	Distance of the C.G. of concrete area under compression from the center of cross section of the column, mm

α_1	Ratio of average stress in rectangular compression block to the specified concrete strength
β	Factor taking into account the shear resistance of cracked concrete
β_1	Ratio of depth of rectangular stress block to depth of neutral axis
δ	Design lateral drift ratio
ε_{cu}	Ultimate strain of concrete
ε_c'	Strain in concrete at f_c'
ε_{cc}'	Strain in concrete at f_{cc}'
ε_s	Strain in steel bars
ε_x	Longitudinal strain at mid depth of member due to factored load
ε_y	Yield strain of steel bars
θ	Angle created at the centre of column cross section by area under compression, rad
θ_v	Angle of inclination of diagonal compressive stress to the longitudinal axis of member
ρ_c	Composite density, g/cm^3
ρ_{cc}	Area ratio of total longitudinal steel to concrete core
ρ_f	Fibre density, g/cm^3
ρ_s	Ratio of volume of spiral reinforcement to total volume of core confined by the spiral (measured out-to-out of spirals)
ρ_x	Matrix density, g/cm^3
ϕ	Material resistance factor
ϕ_a	Resistance factor for structural steel
ϕ_c	Resistance factor for concrete

ϕ_s Resistance factor for non-pre-stressed reinforcing bars

CHAPTER 1 – INTRODUCTION

1.1 General

Earthquake has been a major concern in structural design due to its devastating consequences. Therefore, researchers around the world have been working agitatedly to improve the design guidelines for better seismic performance of the structures. Over the last few decades, there has been a significant improvement in seismic design of reinforced concrete (RC) structures. Newly constructed structures, particularly, the high rise RC buildings have shown satisfactory seismic behaviour during recent earthquake events. However, recent advancement in seismic design has also raised concerns about the seismic performance of existing structures. Several RC structures constructed throughout the 20^{th} century were reported to be intensively damaged after recent earthquake events. Additionally, these structures deteriorated due to aging and adverse environmental conditions. Lately, more than half of the bridges in USA were reported not suitable for conventional use and in need of immediate repair work (Lee et al. 2008).

Rehabilitation of existing and damaged RC structures is more economic than reconstruction in many cases. Several rehabilitation techniques have been developed over the last few decades such as RC or steel plate jacketing; significantly increasing the cross-section of structural members. These rehabilitation techniques often lead to a large increase in the self-weight of the structure which consequently causes preposterous expenditure. Also, steel plates and reinforcements used in these types of rehabilitation work are vulnerable to corrosion. Hence, fibre reinforced polymers (FRP) materials were introduced in the rehabilitation of RC structures due to their lightweight, higher strength, substantial durability and corrosion resistance. However, using FRP materials in retrofitting was perceived as economically-deficient due to high material production cost as well as complex application process. Moreover, it showed some shortcomings while rehabilitating

structures with irregular shapes and difficult access (Banthia and Boyd 2000; Lee et al. 2016). Therefore, researchers have recently developed a new method to repair or rehabilitate RC structures; namely sprayed-FRP composites rehabilitation technique. In this technique, FRP fibres of specific length are sprayed over the concrete surface along with resin and catalyst to form a layer of composite material, with randomly oriented fibers, up to a certain thickness. To date, very few studies have been carried out to determine the feasibility of this technique. Nevertheless, some of the studies have reported its easy application and cost effectiveness over other existing retrofitting methods (Lee 2012).

1.2 Problem Definition

A large number of existing buildings and highway bridges in North America were built when the standards for seismic design were at an early stage of development. Therefore, the columns in most of these structures were constructed with inadequate lap splice length and/or transverse reinforcement compared to those required by the recent seismic design codes. This deficiency often leads to reduction in flexural strength by concrete cover spalling followed by lap splice debonding under seismic load (Haroun & Elsanadedy 2005). Recently, the earthquake hazard levels have been increased for many regions throughout the globe, which also creates some concern on the seismic performance of existing structures. Moreover, the truck loads have increased significantly over the years and often the transportation authority had to put restriction on the traffic volume over the existing bridges. In addition, RC columns are more vulnerable to long-term structural strength deterioration and durability problems due to its location in buildings and bridges. Thus, repair and strengthening of columns in existing structures have become very essential in order to meet the current structural requirement and traffic demand. The rapid deterioration of RC infrastructure and the limited funding available for maintenance have

promoted the use of FRP laminates as a sustainable repair and strengthening materials (ACI 440.2R-17). However, FRP sheet rehabilitation systems come with several challenges, for example: require prior surface treatment, difficulty in application at joints and on irregular shaped structures, relatively expensive and sensitivity to rough concrete surface (Karbhari 2007).

A proposed retrofitting technique, the sprayed-FRP system, can be used in strengthening of RC structures to avoid the adverse issues associated with FRP laminates. Previous research demonstrated that the sprayed-FRP rehabilitation system can considerably increase the load carrying capacity, ductility and energy absorbing capacity of RC beams (Banthia et al. 2002; Lee and Hausmann 2004; Lee et al. 2008). Only limited research has been carried out on the seismic behaviour of sprayed-FRP retrofitted columns. Available research is mostly on square columns while circular columns can provide more promising outcomes. Under seismic load the FRP confinement in rehabilitated square and rectangular columns has to resist higher stresses near the corners whereas in circular columns the external confinement experience uniform stress in all direction. In-depth research is required on the seismic performance of sprayed-FRP retrofitted circular columns with inadequate lap splice under different service loading conditions. It is also important to determine the potential of this new retrofitting technique to satisfy new seismic design requirements and to restore structures for intended performance. Until now, glass (G) fibre is the most used type in construction industry because of satisfactory material property and economy. Hence, the proposed research primarily focuses on retrofitting of seismically-deficient RC circular columns subjected to seismic load using sprayed-GFRP composites.

1.3 Research Objective

The main objectives of this study were to:

- Investigate the behaviour of deficient RC circular columns retrofitted with sprayed-GFRP composites under seismic loading.
- Provide recommendations and design guidelines on retrofitting of seismically deficient circular RC columns by sprayed-GFRP composites.

The following parameters were included in this study to evaluate the seismic response of deficient RC circular columns retrofitted with sprayed-GFRP technique.

- Degree of Damage (Intact, Partially-Damaged and Fully-Damaged)
- Sprayed-GFRP composite thickness (3.0 and 6.0 mm)

1.4 Scope of Work

Steel-RC circular columns with continuous spiral as transverse reinforcement were considered in this study. The columns were designed to fail in flexure. Longitudinal bars were spliced at the footing-column interface; effects of bar splice at mid-height of the column were not studied. In strengthening, only sprayed glass fibres with vinyl ester resin were used. The specimens represent a portion of a column in buildings and bridges located between foundation and point of inflection. Normally, this region experiences inelastic stress reversals and higher moment than other portions of the structure during an earthquake event. Therefore, the development of a plastic hinge is required in this region to dissipate energy induced from the inelastic stress reversals. To simulate a seismic loading condition, the specimens were subjected to simultaneous reversed-cyclic lateral loads and monotonic axial loads.

1.5 Methodology

The seismic performance of steel-RC circular columns rehabilitated with sprayed-GFRP composites was analyzed in this study. Six large-scale circular columns reinforced with steel bars and spirals were constructed, rehabilitated with sprayed-GFRP and tested under simulated seismic

loading. The column specimen had 305-mm diameter and 1,725-mm cantilever height (1,525-mm shear span). A column head measuring 550 × 350 × 400 mm was used to facilitate the application of simultaneous axial and lateral loads. The fixity of the specimens was ensured by a 1,400 × 900 × 600 mm footing, which was stressed to the laboratory strong floor with four dywidag bars. The footing with the dowel/starter bars was cast one week before the column to simulate field condition. The specimen represents a portion of a column between the foundation and point of inflection located in the first storey of a building. Two specimens were tested up to 2.5% drift ratio (drift limit according to National Building Code of Canada (NBC 2015)) and two specimens were tested up to failure before the application of sprayed-GFRP coat to serve as references. These four specimens were rehabilitated and then retested to failure. Two specimens were first strengthened and then tested under seismic load up to failure. A spraying unit was used to spray glass fibres along with vinyl ester resin and catalyst on the specimen surface up to the specified thickness. A 1000-kN capacity actuator with ±250 mm stroke was used to apply quasi-static reversed-cyclic load laterally at the column head. This actuator was mounted on a stiff steel frame and aligned with the center line of the column. The vertical load was applied using a hydraulic jack that was attached to a steel rigid beam linked to the laboratory strong floor. A data acquisition system (DAQ) was used to record the response of the specimen during testing. Specimen load carrying capacity, ductility and energy absorption capability are analyzed to achieve research objectives. During column rehabilitation process, three concrete cylinders were strengthened with sprayed-GFRP of 6-mm thickness, cured for 4-days then tested under compression to determine the ultimate tensile strength of the system. Sprayed-GFRP samples were collected from rehabilitated columns and tested following burn-off method (ASTM D2584) to determine the fibre content in composite.

1.6 Thesis Outline

This thesis comprises five chapters as follows:

Chapter 1 introduces problem definition, research objectives, specific scopes and the methodology that was followed to achieve the research objectives.

Chapter 2 contains information about sprayed-FRP composites, the effect of structural characteristics on the seismic response of steel-RC columns and review and summary of the previous researches on existing rehabilitation techniques as well as on sprayed-FRP composites technique.

Chapter 3 illustrates the experimental program with schematic drawings and reinforcement details of the test columns, the material properties, construction steps, and strengthening process. It also gives a description of the instrumentation, test set up, and the testing procedure.

Chapter 4 presents the analysis and discussion of the experimental results of the test columns. The structural performance based on crack pattern, mode of failure, hysteretic behaviour, energy dissipation, lateral drift-strain relationship and drift components of each column is evaluated and compared with one another to understand the effect of the variables on the performance of test specimens.

Chapter 5 provides work summary and the major findings and conclusions regarding the test results. In addition, recommendations for future works are included in this chapter.

Both flexural and shear design of the test columns along with design of rehabilitation system using the available design provisions are demonstrated in Appendix A and Appendix B.

CAHPTER 2 – LITERATURE REVIEW

2.1 General

Rehabilitation of RC structures has become a common issue in construction industry now-a-days. For example, approximately 56,000 existing bridges in USA are structurally deficient as reported by the federal highway administration (FHWA 2017). Most of these bridges were built around early or mid-19th century. Since then, there has been continuous upgrade in design codes and guidelines, therefore, these bridges have now become structurally deficient to meet the increased traffic demands. Also, recent advancement in seismic design has created some doubt about the seismic performance of the existing structures. Building new structures to serve the increased structural requirements is not only uneconomical but also time and labour consuming. Rehabilitation of existing structures was found to be the most suitable way to solve this problem. Strengthening using steel plating technique was used; however, some concern arose regarding the efficiency of this method due to corrosiveness and heavy weight of steel. Also, the application process was found substantially complicated. To overcome these complications, the more lightweight and durable fibre reinforced polymer (FRP) material was implemented in RC rehabilitation. Recently, rehabilitation with FRP sheet technique became very popular due to its high corrosion and fatigue resistance, electromagnetic neutrality, low thermal expansion, high strength and comparatively easy application method (Chajes et al. 1994; Ehsani 1994). However, researchers were still ungratified with the high cost and labour-intensive surface preparation process in FRP sheet rehabilitation technique. In addition, researchers found some limitations while applying the FRP sheets at structural joints and corners. As such, a more convenient and economic rehabilitation technique is required. Recently, sprayed-FRP composites technique was developed to overcome the limitations of existing techniques. Few studies reported its propitious

performance in RC beam rehabilitation but further research is required to establish a proper design guideline (Banthia and Boyd 2000; Ha et al. 2014; lee 2012).

Lap splice is a very common practice in RC construction and considered a prime issue for structures in seismic region. Several studies reported the adverse effect of inadequate lap splice in RC structure under seismic load (Paulay et al. 1981; Lukose et al. 1982). Furthermore, magnitude of service load prevalently governs the seismic performance of RC columns (Rabbat et al. 1986; Sheikh and Yau 2002). Rehabilitated structures also need to satisfy the performance requirement specified by recent codes and design guidelines. Therefore, research is required on sprayed-FRP composites rehabilitation technique considering lap splice length and service load for better understanding.

2.2 Concrete Confined with Steel Reinforcement

Steel bars have been very popular for reinforcing concrete for many years due to good bonding and satisfactory combined behaviour. The contribution of steel transverse reinforcement in concrete confinement was first studied by Considere (1903**)**. Since then, transverse reinforcement of different size and shape has been developed by researchers depending on structural requirements. Continuous spirals or hoops are generally used for circular columns and rectangular ties or combination of C-shaped ties are used for rectangular column core confinement. The efficiency of confinement largely depends on the material properties and configuration of the transverse reinforcement. Moreover, due to discontinuity of transverse reinforcement, the effective area differs along the line between two successive ties or hoops. A general conceptual model was developed by Sheikh and Uzumeri (1982) for tied columns under concentric loading and it was widely accepted by other researchers. Later, Mander et al. (1988) modified the model for rectangular and circular columns with normal strength concrete under static, dynamic and cyclic

loading as shown in Fig. 2.1. According to this model, the effective transverse confining stress can be calculated as,

$$f_1 = k_{ef}\left(\frac{A_{sh} f_{yh}}{d_s\, s}\right) \qquad \text{Equation 2.1}$$

Where,

k_{ef} : Confinement efficiency coefficient;

A_{sh} : Total effective cross-sectional area of transverse reinforcing steels in the direction under consideration;

f_{yh} : Yield strength of transverse reinforcing steel;

d_s : Diameter of spiral between bar centers;

s : Center-to-center spacing of adjacent transverse confining steels.

For column with circular hoops,

$$k_e = \frac{\left(1 - \frac{s'}{2\, d_s}\right)^2}{1 - \rho_{cc}} \qquad \text{Equation 2.2}$$

For column with circular spirals,

$$k_e = \frac{1 - \frac{s'}{2\, d_s}}{1 - \rho_{cc}} \qquad \text{Equation 2.3}$$

For rectangular column,

$$k_e = \frac{\left(1 - \sum_{i=1}^{n} \frac{(w_i')^2}{6 b_c d_c}\right)\left(1 - \frac{s'}{2\, b_c}\right)\left(1 - \frac{s'}{2\, d_c}\right)}{1 - \rho_{cc}} \qquad \text{Equation 2.4}$$

Where,

b_c : Core dimensions to centerlines of peripheral hoop in X-direction of rectangular cross sections;

d_c : Core dimensions to centerlines of peripheral hoop in Y-direction of rectangular cross sections;

s': Clear spacing between adjacent transverse confining steel;

w_i' : Distance between adjacent longitudinal steel in rectangular cross-sections;

ρ_{cc} : Area ratio of total longitudinal steel to concrete core.

Columns with circular cross section were reported superior over rectangular section in the strength, deformability and aesthetic appearance. Improvement in column ductility against seismic loading was observed when the sharp corners in a rectangular section were replaced by round corners. Also, increase in the radius of round corners resulted in enhanced strength and ductility of columns (Hasegawa et al. 1992).

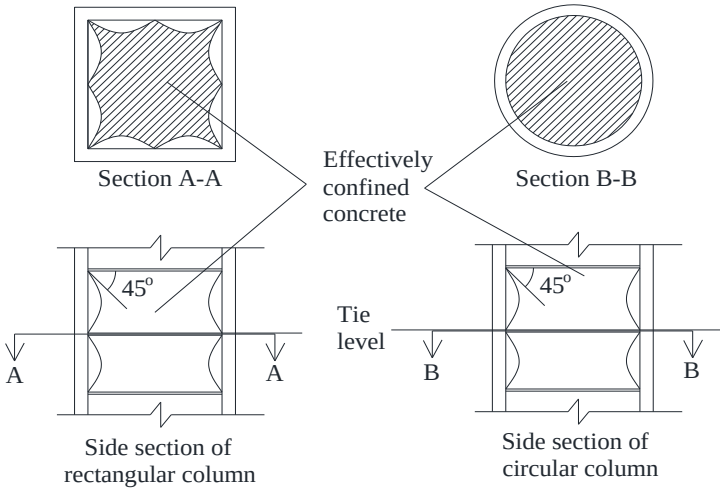

Figure 2.1: Effective confined area in rectangular and circular column transversely reinforced with steel ties and hoops (reproduced from Mander et al. 1988)

2.3 Steel-RC Columns under Seismic Loading

Since last century, considerable number of research studies has been carried out to determine the seismic behaviour of concrete columns reinforced with steel. The strength of a column section is considered as the combined strength of concrete and reinforcing element in which their

contribution is calculated separately. The axial load-moment interaction diagram for RC column cross section is developed on the basis of the following assumptions:

- Plane sections remain plane under bending. Thus, the strain in the concrete and reinforcement are proportional to the distance from the neutral axis,
- Perfect bond exists between the reinforcement and concrete,
- The tensile strength of concrete can be neglected,
- The area of the concrete displaced by reinforcement in compression will be subtracted.

The interaction diagram consists of two regions based on the failure mode, compression-controlled and tension-controlled region. Compression-controlled region indicates the state when the extreme compression fibres of the concrete reach their ultimate strain before yielding of steel. The condition when yielding of steel occurs before concrete fibres reach their ultimate compressive strain is referred to the tension-controlled region. The point between these two regions are termed as balance point. Balance point indicates the situation when steel and concrete reach their ultimate tensile and compressive strain simultaneously. Figure 2.2 shows a typical strength interaction diagram for steel-RC column. To avoid bar congestion in a column section, the maximum reinforcement ratio was limited to 8% by the design guidelines although many studies suggested not use more than 6%. The ACI committee 318 (2014) recommended a minimum longitudinal reinforcement of 1% in a column section to prevent yielding of steel under service load. Although several studies reported that column with longitudinal reinforcement ratio less than 1% and above 0.25 % did not show yielding at service loading (Choo 2005*;* Tavassoli 2013).

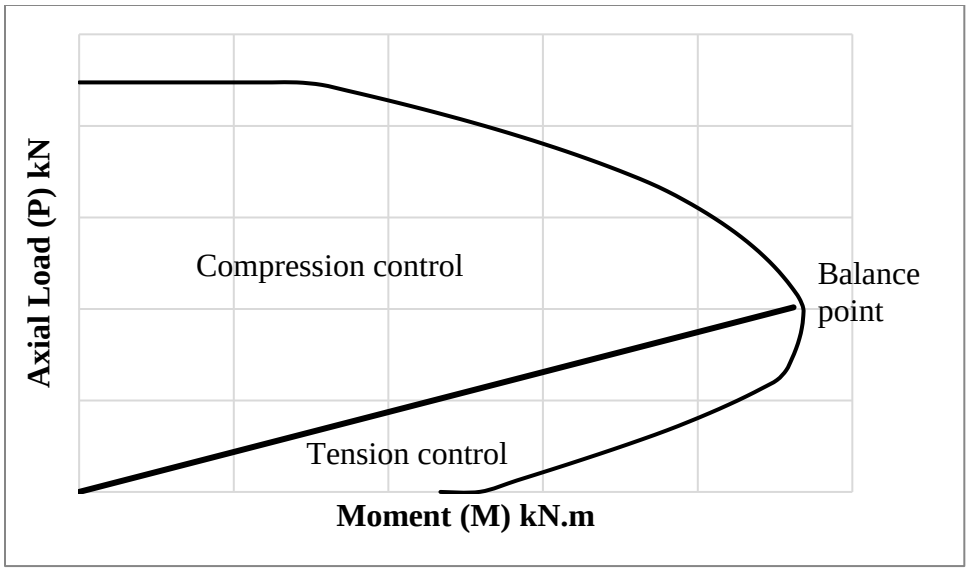

Figure 2.2: Typical strength interaction diagram for steel-RC column

2.3.1. Effect of lap splice length

In any moment resisting frame, lap splicing is a common practice due to the limited length of reinforcing bars. It also helps in concrete scheduling and facilitates reduction in bar size in the columns of upper stories of a building. Usually, bars are lapped together side way or one over another to maintain continuity of the structure. The bond strength between two lapped bars is typically lower than the tensile strength of a monolithic bar. Also, in an earthquake event, the developed moments lead to significant increase in tensile stresses in the longitudinal reinforcement in the splice region (Melek and Wallace 2004). Therefore, the lap splice regions are considered the most vulnerable portion of a column under seismic loads. In practice lap-splice is also used immediately above the footing to make connection between footing and column reinforcement. This region carries the maximum moment resulting from structural loads and ground motion. Therefore, codes suggested assuming plastic hinge formation at the end of the column while designing the structure to facilitate energy dissipation. However, this increases the possibility of

bond failure of lap-splice due to yielding of bars in both tension and compression. As such, adequate lap-splice length should be provided to ensure structural stability and performance.

Paulay et al. (1981) investigated the feasibility of allowing lap splice for columns in seismic regions. Ten column specimens of octagonal and square cross section were constructed and tested. These specimens represented the high moment region of a lower storey column in a multistory frame structure. New Zealand Code for the Design of Reinforced Concrete Structure (DZ 3101-1980) was followed in designing the specimens. The length of lap-splice varied from 22.5 to 32 times the diameter of longitudinal bars. All specimens were tested under simultaneous axial and quasi-static lateral load up to failure. Satisfactory performance was observed for column specimens with lap splice under reversed cyclic load. It was concluded that column having a bar splice length satisfying New Zealand Code requirement can be used in the region of maximum moment in a multi-storey building subjected to seismic loading.

Goksu et al. (2014) studied the effect of lap splice length on the behaviour of low strength concrete columns reinforced with plain steel bars. A total of five specimens (200 × 300 × 1,950 mm) were constructed with geometric longitudinal reinforcement ratio and volumetric transverse reinforcement ratio of 1% and 0.8%, respectively. In order to represent the column portion of an old frame structure, the specimens were reinforced with low strength plain steel bars. Four specimens had lap splice length equal to 25, 35, 44 and 55 times longitudinal bar diameter and one specimen was reinforced with continuous bars to serve as reference. The longitudinal bars were lapped at the connecting portion between column and stub with 180-degree hook at both ends. All specimens were tested in a displacement-controlled quasi-static manner under reversed-cyclic lateral loads. No axial load was applied to represent the actual columns in the field under low axial loads. Insignificant strength degradation was recorded for each specimen prior to reaching higher

drift levels. All specimens failed after attaining the design flexural strength. Despite of having inadequate lap splice length compared to code requirement, the presence of 180-degree hook enabled the specimens to behave in a ductile manner by dissipating high amount of energy under large lateral load levels. Satisfactory seismic response was recorded for all specimens.

2.3.2. Effect of axial load

Several studies have been carried out to determine the behaviour of RC-columns in seismic region under constant axial load. Typically, researchers have applied 10 to 30% of column axial capacity as service load while testing (Melek and Wallace 2004; Choi 2008; Pam and Ho 2010; Ibrahim et al. 2016).

Rabbat et al. (1986) conducted an investigation to determine the influence of axial load on the seismic performance of RC columns. Sixteen full scale specimens were constructed and tested under simulated seismic loads up to failure. Initially a constant axial load was applied to each specimen without any cyclic load. Later, the specimens were subjected to combined cyclic load and increased axial load based on their response at the initial stage of loading. At the primary stage of loading (10% of the column axial capacity) each specimen showed high ductility and energy dissipation Also, specimens behaved in a satisfactory ductile manner with adequate energy dissipation when the axial load increased to 20% of the column axial capacity. However, the energy dissipation capacity decreased with further increase in the applied axial load. At an axial load equal to 30% of column axial capacity, an increase in flexural capacity was observed while the dissipated energy decreased.

Melek and Wallace (2004) studied the cyclic behaviour of columns with short lap splice under different axial load. Six column specimens of 457 mm square cross section were constructed having lap splice of $20d_b$ (d_b is the diameter of longitudinal reinforcement) at the base. All the

specimens were tested under combined cyclic lateral load and axial load up to failure. The axial loads (10, 20 and 30% of the column axial capacity, $f_c' A_g$) were kept constant throughout the entire test. Specimens subjected to lesser axial load showed higher energy dissipation compared to that of specimens tested under high axial load. At lower axial load (10% of column axial capacity) specimens maintained their axial load carrying capacity up to higher drift ratio (typically about 10%). However, specimens lost their axial load resistance capacity at a lower drift ratio when the axial load increased to 20% and 30% of column axial capacity. Test results showed that the axial load level had no significant impact on the strength degradation rate of the specimens resulting from the bond slippage of reinforcing bars.

2.4 Fibre-Reinforced Polymers (FRP)

Fibre reinforced polymer (FRP) is a composite material composed of matrix, reinforcing fibres, curing agent, core material and additive or fillers. Most FRP composites are non-corrosive, non-conducive and non-magnetic. In addition, FRP composites have high strength-to-weight ratio compared to conventional steel used in construction. The mechanical properties of the FRP materials largely depend on fibre quality, orientation, shape, volumetric ratio, adhesion to the matrix and manufacturing process. The fibres are mainly responsible for strength. Four types of fibres are available namely carbon (C) fibre, glass (G) fibre, aramid (A) fibre and basalt (B) fibre. Carbon fibres show higher strength and modulus of elasticity. However, they are very expensive and have lower impact resistance along with high electrical conductivity. Glass fibres are comparatively inexpensive, shows reasonable physical and mechanical properties. Aramid fibres have good strength, impact resistance, fatigue performance and insulation property. Nevertheless, they show higher creep and susceptibly to corrosion in moist environment. Basalt fibre is a relatively new material. It has similar chemical composition as glass fibre but shows better strength

characteristics. Thermosetting and thermoplastic resin are commonly used in FRP production to achieve weatherability as well as corrosion resistance and to reduce combustibility. Thermosetting resins are more popular because those cannot be altered by heat or pressure after curing. Epoxy, vinyl ester and polyester are provided as coating on FRP composites to protect it from adverse environment. FRP composites have higher tensile strength than conventional steel. However, they have lower modulus of elasticity. So, the higher strength is quite complicated to fully utilize. The FRP composites are one sixth times lighter than steel which helps in reducing the construction cost by minimizing structural self-weight and enabling easy handling during construction (CSA/S806-12).

2.5 Existing Rehabilitation Techniques

Several rehabilitation methods are available for RC columns such as concrete cladding, steel caging, steel lining and FRP fabric wrapping. Concrete cladding is used when the column is seriously damaged or has inadequate seismic resistance. In this method, an RC sheath is provided along the full or certain portion of the perimeter of the column. This sheath contains longitudinal and transverse reinforcement which is designed based on capacity requirements. To ensure proper load transmission, the reinforcements are continued through beam-column joints on both sides. Special types of concrete such as self-compacting and non-shrinking concrete are used for better workability and performance. This method gained high acceptance as the engineers and the construction industry were already familiar with the field application of structural concrete. Moreover, its versatile appositeness and shape-adaptability made it more popular especially in seismic-prone countries (Bousias et al. 2007).

In steel caging rehabilitation method, steel plates are glued on the concrete surface around the column as external confinement. Sometimes steel channels, angles or built-up members are also

used in place of steel plates. Epoxy adhesives are commonly used as glue. Moreover, screw or anchor bolts are used to transfer load from column to rehabilitation system if adhesion fails. Some additional protective measures are considered since the steel used in rehabilitation is susceptible to environmental corrosion. Steel lining is quite similar to steel caging; however, in the steel lining method, the column is wrapped with thin steel sheet rather than steel plate (Chail et al. 1990).

The FRP sheet wrapping technique strengthening is carried out by wrapping an FRP fabric around the column. An epoxy resin is used on concrete surface for bonding between FRP sheets and column. Significant increase in column compressive strength was recorded in case of FRP sheet rehabilitation compared to other conventional methods. The FRP sheets resist the lateral pressure as well as deformation of column under compressive force and thus increase the confinement capacity (Xiao and Ma 1997; Haroun & Elsanadedy 2005).

2.5.1. Rehabilitation with concrete and steel

Rodriguez and Park (l994) analyzed the effect of RC jacketing on the seismic performance of structurally deficient columns. A total of four column specimens, 350 × 350 mm cross section, were constructed. Two specimens were retrofitted with RC jacketing before being subjected to any kind of loading. The other two specimens were tested both before and after strengthening to determine the effect of RC jacketing on damaged columns. Each specimen represented the mid-height portion of beam-column joint between two successive stories of a building. Specimens were designed with low quantity transverse reinforcement to characterize typical building columns constructed prior to 1970. The strengthening system consisted of 100-mm thick concrete jacket reinforced with longitudinal bars and ties. Two types of tie arrangement were used to reinforce the concrete jacket. All the specimens were tested under simulated seismic load up to failure. The as-built column showed insufficient ductility and high strength degradation whereas satisfactory

seismic resistance was recorded in case of retrofitted columns with RC jacket. The damaged as-built columns were then again tested under combined axial and reversed cyclic load after being strengthened with RC jacket. Pronounced increase in column strength and stiffness was recorded due to the application of strengthening system. These strengthened columns also showed reasonable energy dissipation capacity with slower strength degradation. Overall, the study concluded that RC jacket retrofitting successfully enhanced the seismic performance of structurally deficient RC columns even when the column was partially damaged. However, this method was also reported as labor-intensive which may lead to higher cost and less efficiency.

Chail et al. (1990) tested six rectangular columns with lap splice retrofitted with steel plates under seismic loading. All specimens had a cross section of 490 × 730 mm and height of 3,657 mm. The lap splice length was equal to 20 times the diameter of longitudinal bar. Three types of steel jacketing scheme were investigated: elliptical, rectangular and build-up channels. Based on the test results, it was evident that the elliptical steel jacket scheme provided the best performance compared to the other two schemes. It satisfactorily increased the load carrying capacity and ductility of the columns. Moreover, it prevented sudden failure of specimens generating from the debonding of lap splices. Lin et al. (2010) also examined the lap splice failure prevention capacity of steel plate retrofitting technique with octagonal scheme. Three rectangular column specimens (750 × 600 mm cross section) were constructed including one control specimen. Other two specimens were retrofitted using octagonal and elliptical scheme. Specimens were tested up to failure under combined axial and reversed cyclic load. Both retrofitting scheme showed satisfactory performance. However, the octagonal arrangement required less area and provided slightly better strength and energy dissipation capacity compared to the elliptical one.

Choi (2008) conducted a study on the seismic behaviour of circular concrete columns with lap splice retrofitted with stainless steel wire mesh (SSWM) composite. The SSWM is composed of stainless steel wire and permeable polymer concrete which creates a light-weight and corrosion-resistant composite with versatile application possibility. This study included mainly two parameters: lap splice length and retrofitting height. The specimens had a 400-mm diameter and 2,000-mm shear span. One specimen had no lap while two specimens had different lap splice lengths (20 and 30d_b; d_b is diameter of longitudinal bar) were constructed and tested in as-built condition. In addition, three specimens having lap splice length of 20d_b were retrofitted at potential plastic hinge region with SSWM before load application. All specimens were tested under combined axial and lateral reversed-cyclic load. Specimens without strengthening system failed in a brittle manner with rapid degradation in column capacity in specimens with lap splice due to bond failure between lapped bars. However, slight increase in strength and ductility was recorded as the lap length increased. On the other hand, retrofitted specimens showed gradual strength degradation with potential hysteresis response. Comparatively, higher load resisting capacity and ductility was observed due to strengthening. Nevertheless, increase in retrofit height did not significantly contribute in improving the seismic performance. Based on test results, it was suggested that SSWM retrofitting can be used for seismic strengthening of circular bridge columns.

2.5.2. FRP sheet rehabilitation

Carbon (C) FRP and glass (G) FRP sheets have been largely used for structural rehabilitation due to their superior characteristics. Usually, 0.5 – 2 mm unidirectional FRP laminates are used as continuous wrap or strip with specific spacing. The sheets provide high strength in the direction parallel to the fibre orientation but weaker in the perpendicular direction. Under tensile forces, the

stress-strain response of the FRP sheets is almost linear-elastic up to failure and does not show any yielding. FRP sheets can be produced to any desired length which eliminates the requirement of joints in rehabilitation. Several steps are followed in the application of FRP sheets. First, the concrete area, on which the rehabilitation will be applied, is prepared to get a clean and even surface. A prime coat is applied on the prepared surface followed by a layer of resin. The resin works as a binder between the concrete surface and FRP wrap. Then, FPR sheets or fabrics are wrapped over that surface covering the whole area to be rehabilitated. At last, a resin top coat and a finish coat is applied on the FRP wrap to prevent environmental deterioration.

Xiao and Ma (1997) theoretically and experimentally studied the effect of prefabricated GFRP sheet retrofitting on the seismic performance of RC columns with poor lap splice. Three circular columns of 610-mm diameter and 2,642-mm height was constructed. Two columns were retrofitted using unidirectional GFRP sheets. The control specimens were retrofitted after being damaged up to failure. All the specimens were tested under constant axial load and reversed cyclic lateral load. Rapid degradation in load carrying capacity was observed for the control specimen due to lap splice failure. It failed in brittle manner without showing enough ductility. On the other hand, the retrofitted specimens and the control specimen being strengthened showed satisfactory seismic performance with improved ductility and load resistance. The strengthening system lowered the rate of reduction in column capacity and prevented the sudden failure of longitudinal bars in rupture.

Haroun & Elsanadedy (2005) evaluated the performance of carbon and e-glass fibre jacketing in strengthening circular and rectangular column with inadequate lap splice ($20d_b$). Eight circular and five square small-scale columns were built and ten of them were retrofitted using different composite-jacket systems. All the specimens were tested under combination of axial and lateral

cyclic load up to complete failure. Specimens without jacketing failed in a brittle manner without satisfying the ductility requirement stated in Caltrans Seismic Design Criteria (Caltrans 1999). Failure occurred at the lap-spliced zone due to premature spalling of concrete cover followed by rapid reduction in bond strength between spliced longitudinal bars. On the other hand, jacketed specimen failed in a ductile manner with improved cyclic performance. However, retrofitted specimens with square cross section failed before reaching the required ductility level mentioned in design guideline (Caltrans 1999). This occurred as the confining retrofit had weaker bond at the corners of the square specimens. In case of circular specimens, the resisting stress was uniform throughout the perimeter of the specimens and they showed adequate ductility before failure. No variation in column lateral stiffness was observed due to the application of composite jacket. In conclusion, the dynamic characteristics of bridge column remained unaffected even after retrofitting. To predict the seismic performance of retrofitted column, a numerical model was developed based on moment curvature analysis. Using this model, some design guidelines were proposed for bridge column with inadequate splice length.

Bousias et al. (2007) experimentally compared the seismic performance of columns strengthened with RC jacketing system or FRP wrapping technique. Test results showed that the latter method was more effective in increasing deformation and energy dissipation capacity than the former one. A total of 22 square column specimens with 250 × 250 × 1,600 mm dimension were constructed. Thirteen specimens had a lap splice at the column base region. All the specimens were tested under seismic loading until failure. Three specimens were tested up to almost ultimate strength before retrofitting to evaluate the effect of retrofit on damaged columns. In case of FRP wrapping rehabilitation, four columns were wrapped with 2 layers and the rest were wrapped with 4 layers of fibre CFRP sheets. The parameters included in this study were lap splice length, number of FRP

layers and height of the FRP wrap. Test results showed that the energy dissipation and deformation capacity do not necessarily depend on the lap splice length when the column has a lap splice length of at least $15d_b$. The RC jacketing satisfactorily increased the deformation capacity and enhanced the seismic performance even for the damaged column. Slippage of retrofit was observed due to lack of bonding provision between old column and new jacket; however, it did not significantly affect the seismic load resistance of the retrofitted column. CFRP sheet wrapping technique showed satisfactory performance despite it was applied only in plastic hinge and lap splice region. However, this method did not prevent formation of plastic hinge and failure outside the wrap.

Gu et al. (2010) evaluated the confinement effectiveness of circular RC columns retrofitted with different type and amount of fibre-reinforced polymer (FRP). A total of 17 column specimens were tested under combined constant axial and lateral-cyclic load. Each specimen represented the part of a bridge column or a building column between the section of maximum moment and the point of contraflexure. Specimens were divided into two groups. In first group, nine specimens were constructed with a diameter of 300-mm and a cantilever height (lateral load application point to footing face) of 850-mm (aspect ratio 2.8). These columns were subjected to a constant axial load equal to 5% of the column axial capacity. Among them, one specimen was tested in as-built condition while the other eight specimens were tested after being retrofitted by FRP wrapping. In the second group, eight specimens had a diameter of 360-mm and a cantilever height of 1,100-mm (aspect ratio3.1) or 800-mm (aspect ratio 2.2). These columns were tested under a constant axial load equal to 36% of column axial capacity. Two columns in this group were tested in as-built condition. Carbon FRP and Dyneema FRP (FRP with polyethylene fibers) sheets with different number of layer combination ranging from 1 to 3.5 were used in strengthening. Test results showed that increase in the axial load ratio ($P/A_g f_c'$) from 0.05 to 0.36 decreased the ultimate drift ratio by

7%. Again, increasing the axial load level, increased the requirement of FRP jacket confinement stiffness or number of layers for satisfactory energy dissipation. The ultimate fracture strain of FRP material showed no impact on the drift capacity of the specimens. For the specimens in first group, the ultimate drift capacity increased from 2.8% to 15.6% as the confinement ratio (confinement pressure over unconfined concrete strength) increased from 0 to 0.223. Although, as the confinement ratio increase further to 0.336, the deformation capacity reduced to 12.5%. Similar behaviour was also observed for the specimens in the second group.

Raval and Dave (2013) studied the efficacy of external GFRP wrapping system in strengthening RC columns of circular, square and rectangular cross sections. Fifteen RC column specimens were constructed with 1,000-mm cantilever height. Five circular columns had a diameter of 170-mm. Five square and five rectangular columns were constructed with 150 × 150 mm and 110 × 210 mm cross section, respectively. Nine specimens were tested as control specimens and the other six were strengthened using one layer of GFRP wrap before testing. The ACI Committee 440.2R (2008) provisions were followed to design the GFRP wrapping system. All the specimens were tested to failure under a constant axial load. The control columns failed in a brittle manner with blasting effect while GFRP wrapped circular column failed without any sign of debonding. Although release of high amount of energy was observed in form of explosion during the failure of GFRP wrapped circular columns. Square columns failed by tearing of GFRP layers at one of the corners due to high stress concentration at these corners. Failure of rectangular columns occurred by simultaneous debonding and rupture of the GFRP sheets. The failure zone was shifted from corners to the sides as the column shape changed from square to rectangular. Considerable increase in load carrying capacity and ductility was observed for all the specimens strengthened with GFRP sheets; however, the increment was different for different shapes. Column with circular cross section

showed highest increase in load carrying capacity which was 159% while in case of square and rectangular column it was approximately 79% and 76%, respectively. Due to superiority in slenderness resulting from the shape, strengthened circular columns showed higher deformation capacity compared to the square and rectangular ones.

Hassan et al. (2017) experimentally investigated the performance of high-strength concrete (HSC) columns subjected to uniaxial eccentricity and strengthened by GFRP fabrics. Seven 200 × 200 × 1,050 mm columns were constructed, strengthened by external GFRP fabrics and tested under single eccentric load. The main objective was to determine the effect of arrangement and the amount of GFRP laminates on the performance of steel-RC column. The test parameters included the number (0, 1 and 2) and arrangement (partial and full wrapping in longitudinal and transverse orientation) of fabric layers and the value of load eccentricity (25 and 125 mm). Columns tested under small eccentricity loading were strengthened in partial or full wrapping by single or double layers of GFRP laminates. On the other hand, columns tested under large eccentricity loading were strengthened using longitudinal laminates in the tension side along with a partial overlaying wrap of GFRP laminate in the transverse direction. Results showed that single and double layers of GFRP laminates increased the strength of HSC columns loaded under smaller eccentricity by 12.5 and 23%, respectively. For columns loaded under larger eccentricity, 41 and 53% increase in load carrying capacity as well as 54% and 60% increase in flexural capacity was recorded due to single and double layer of vertical GFRP laminates, respectively. Strengthening decelerated the stiffness degradation of HSC short columns. A further decrease in stiffness degradation rate was observed as the number of layers and area of wrapping increased. A significant improvement in ductility was recorded for the specimens loaded with large eccentricity due to GFRP wrapping. The longitudinal strains increased by 153 and 111% due to single and double layers of GFRP wrap,

respectively. For specimens tested under small eccentricity load, GFRP wrap changed the failure mode from a brittle to a more ductile one.

2.6 Sprayed-FRP Composites Rehabilitation System

The sprayed FRP rehabilitation system composed of resin, catalyst, coupling agent and fibres. A special type of gun sprays chopped fibres and other components simultaneously on the concrete surface with a high speed. The final composite consists of randomly oriented chopped fibres of controlled length in a polymer matrix. The physical and mechanical properties of resin have a great influence on spraying process as well as on the performance of final composite. Two types of resin are commonly used worldwide, epoxy resin and vinyl ester resin. Both are thermosetting resin, i.e. once cured, they cannot be reshaped using heat or pressure. The type of resin that would be used in matrix is mainly selected based on workability requirement while spraying. Several studies showed that vinyl ester resin get hardened faster than epoxy resin after application. Catalyst is used for curing of resin and it is selected based on required gel time. Coupling agent is applied using brush or roller to ensure good chemical bonding between FRP and concrete surface. Fibres are mainly responsible for the strength of the composite. A bundle of continuous glass or carbon filament is fed in the chopper gun to get fibres of desired length. The performance of overall retrofitting work largely depends on the characteristics of FRP filament used in the process. Sprayed-FRP composites does not show similar strength or stiffness as unidirectional continuous fibre laminates but exhibit higher strain at rupture and a nonlinear response before reaching ultimate capacity (Fig. 2.3). This partial ductile response originates form a combined failure of fibre pullout and fibre rupture which enables the rehabilitated structure to provided ample warning before failure. Sprayed-FRP rehabilitation technique can be applied to increase service capacity of existing structures, restore historical structures, reinforce masonry structure and stabilize structural

deterioration. Studies reported higher workability of this technique while applying on structures with complex shape under adverse environmental and accessibility condition (Harries and Young 2003).

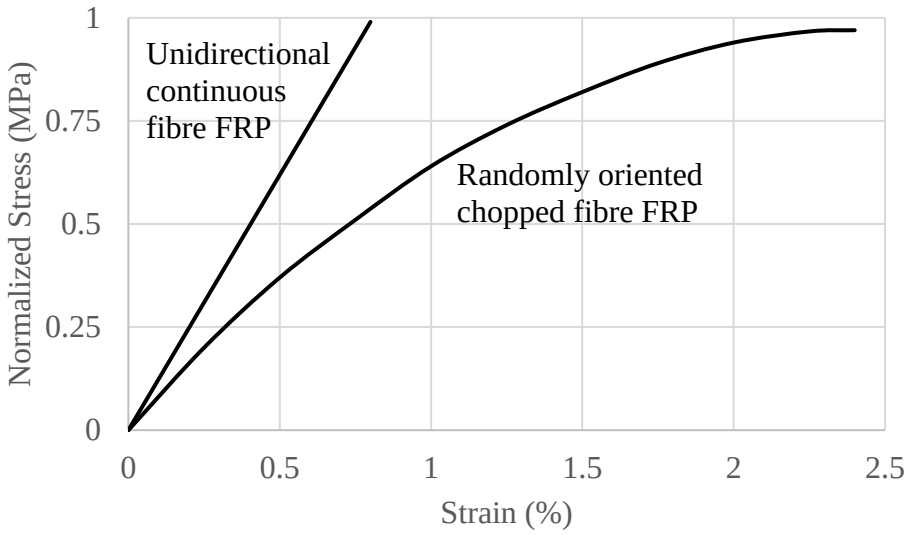

Figure 2.3: Normalized stress versus strain behaviour of FRP materials (reproduced from Harries and Young 2003)

2.7 Sprayed-FRP Material Property

The properties of the sprayed FRP composite play an important role in the overall performance of the retrofitting work. Several studies have been carried out to determine the tensile property, elastic modulus, density, fibre volume fraction, etc. This section summaries the main properties of the sprayed FRP composites found in the literature.

2.7.1. Tensile strength and modulus of elasticity

The tensile strength of sprayed-FRP composite largely depends on the tensile strength of the FRP fibres. Several studies reported increase in tensile strength of sprayed-FRP composite with increasing the fibre length (Lee et al. 2008; Lee et al. 2016). Also, increase in fibre length led to more linear stress-strain response as a result of improved stress transfer between the fibres and the

matrix. Decrease in the fibre length made the stress transfer more reliable on the matrix and consequently, the composite with shorter fibre length showed comparatively less linear stress-strain response under tensile forces. The ultimate tensile strength ranged between 35 to 108 MPa when the fibre length increased from 8 to 48 mm. Besides, the modulus of elasticity was found varying from 5.8 to 11.8 GPa for the same range of fibre length. Figure 2.4 shows the stress-strain response of sprayed-FRP composites under tensile force for different fibre lengths (Boyd 2000).

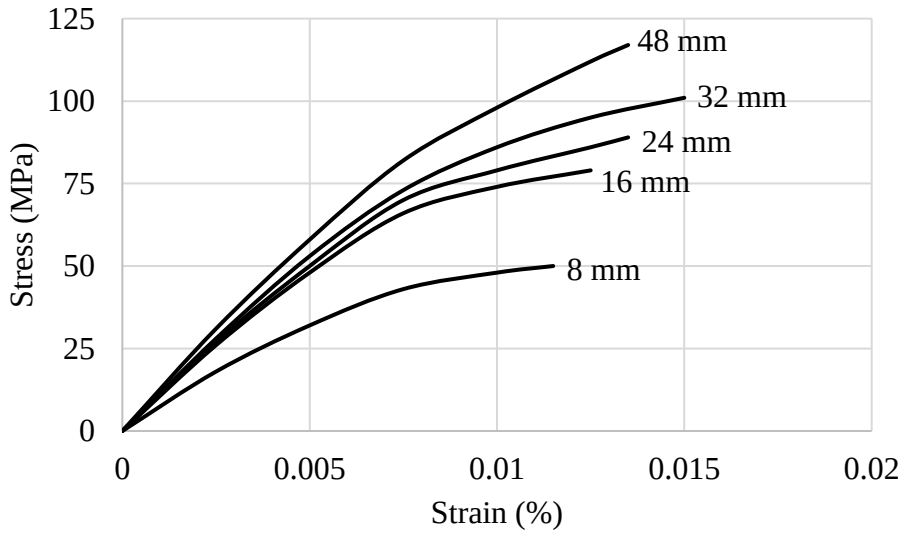

Figure 2.4: Typical stress-strain plot for sprayed-FRP composites under tension (reproduced from Boyd 2000)

2.7.2. Density

Boyd (2000) reported an increase in the density with the increase of fibre length in sprayed-FRP composite. The density varied from 1,263 to 1,394 kg/m^3 when the fibre length increased from 8 to 48 mm. Density of the sprayed composite was found dependent on the degree of compaction. Composite with shorter fibre length was found more influenced by the degree of compaction as those fibres can get easily displaced by the roller during compaction.

2.8 Research on Sprayed-FRP System

Banthia and Boyd (2000) performed a pioneer test to compare between the performance of existing FRP sheet wrapping technique and new sprayed-FRP technique in strengthening concrete cylinders under compression. Twenty-six small (height/diameter ratio of 2) and ten large cylinders (height/diameter ratio of 4) were cast. Among them twenty small and six large specimens were retrofitted using FRP sheet wrapping technique with single and double layer wrapping of 0-90˚ and ±45˚ fibre orientation. On the other hand, three small and two large specimens were strengthened using sprayed-FRP technique. Sand blasting was carried out for all specimens before the application of retrofit. Specimens to be retrofitted with sprayed-FRP technique were coated with a bonding agent before applying the spray. To remove the entrapped air voids and to ensure a uniform thickness, the sprayed fibre coating was compacted using a rigid aluminum roller at the end of the retrofitting process. A mixture of polyester resin and 48-mm long glass fibres were sprayed continuously over the treated surface targeting a constant thickness of 3.5-mm and 20% fibre concentration. The selection of fibre length was governed by the strength requirement while the fibre volume was selected to have reinforcement ratio equivalent to two layers of FRP sheet wrap. This used fibre concentration was found equivalent to one layer of FRP sheet in a previous research (Boyd 2000). Specimens retrofitted with sprayed-FRP technique mostly failed stridently by surface fracture accompanied by fibre pull-out. These specimens showed high variability in results due to non-uniformity in coating thickness and fibre concertation. Results showed also that both wrapping technique and sprayed-FRP technique increased the load capacity, ductility and energy absorption capacity significantly. In case of wrapping technique, 0-90˚ fibre orientation was found more effective than ±45˚ fibre orientation in enhancing performance of both large and small specimens. However, considerably higher increase in strength (55%) and energy absorption

capacity (555%) was recorded for sprayed-FRP technique compared to other technique due to random orientation of fibres. Moreover, higher toughness was observed for these specimens as the energy required for de-bonding increased. Nevertheless, the sprayed-FRP technique was found less effective than wrapping technique for large specimens. This occurred due to the generation of pure uniaxial compression in mid portion and vertical cracks. Considering placement method, cost effectiveness and workmanship requirement, it was concluded that sprayed-FRP technique could be used over other existing retrofitting techniques. Although further investigations were suggested to include more design parameters and loading conditions.

Furuta et al. (2001) briefly described the outline of sprayed-FRP technique and evaluated the bond strength between sprayed-FRP and concrete. Moreover, the performance of sprayed-FRP technique and FRP sheet technique in strengthening concrete structures was compared using tensile test. Carbon fibres, glass fibres, CFRP sheets and GFRP sheets were used in retrofitting 120 specimens. Length of the chopped fibres ranged from 38 to 50 mm (1.5 to 2 inch) and they were sprayed with vinyl ester resin instead of epoxy resin for better workability. Carbon and glass fibres were sprayed targeting a coating thickness of 3.0 mm and 4.5 mm, respectively. Figure 2.2.5 shows the stress-strain response of FRP sheets and FRP-sprayed composites. Specimens rehabilitated with CFRP and GFRP sheets showed ten and five times higher tensile strength than the corresponding specimens retrofitted by FRP-sprayed composites. In case of modulus of elasticity, CFRP sheet retrofitting showed the highest value compared to others. Later, four concrete column specimens with 300 mm × 300 mm cross section and 1.5 span-to-depth ratio were built and retrofitted with sprayed-FRP as well as FRP sheet wrapping techniques. These specimens were tested under asymmetrical bending moment in a cyclic manner and comparison was made between the performances of different techniques based on the test results. All specimens showed

yielding and sprayed-FRP strengthened specimens finally failed in fracture. Similar performance was observed for all specimens; however, specimens retrofitted with GFRP sheets showed better deformability compared to others. Moreover, several bonding and anchorage technique between FRP and concrete was examined to determine their comparative strength. Sprayed-FRP retrofitted specimens showed similar or a slightly higher bond strength than FRP sheet wrapped specimens. Also, increase in bond capacity was observed due to provision of slit on concrete surface. It was concluded that sprayed-FRP retrofit can offer comparable strength to that of FRP sheets while strengthening concrete structures.

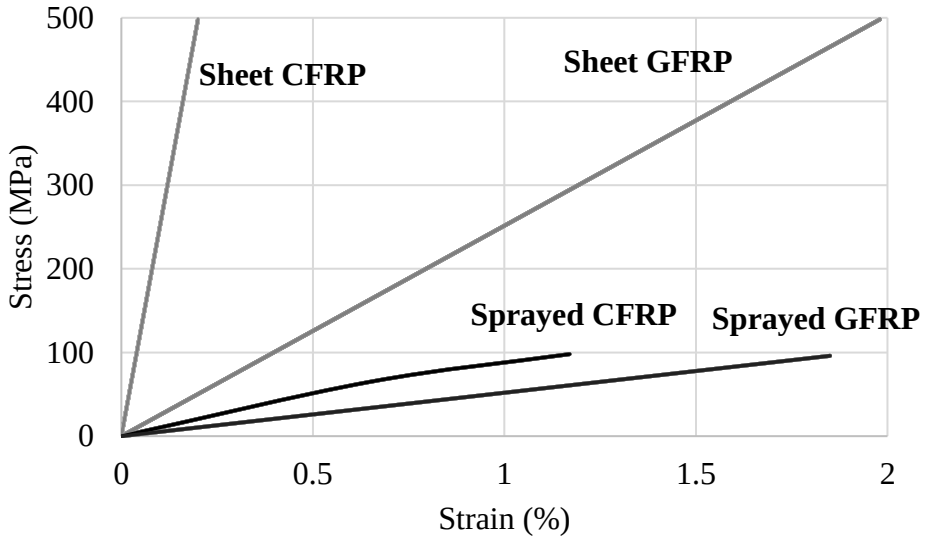

Figure 2.5: Stress-strain response of FRP sheets and sprayed composite (reproduced from Furuta et al. 2001)

Banthia et al. (2002) studied the performance of sprayed-FRP technique in strengthening of deteriorated structures. This study included experimental testing of beam specimens retrofitted with sprayed-GFRP and analysis of the response of actual bridge girders rehabilitated by sprayed-GFRP. Three replaced girders from an old bridge structure were collected among which one girder was used as control specimens. The second and the third girder were rehabilitated using fibre

wrapping composed of E-glass fibres and sprayed-GFRP technique, respectively. All three beams were selected to have similar design configuration with the actual bridge girders. Three-point loading test was used for all the specimens. Results showed increase in stiffness of beams strengthened with both types of retrofitting techniques. The ultimate load and the energy absorption capacity increased by 33 and 174 %, respectively, in FRP sheet rehabilitated beam. In case of sprayed-GFRP technique, the increment in load capacity was 96% and the energy absorption capacity increased by 195%. Later, a 7.2-meter single span bridge, constructed in1955, was strengthened using sprayed GFRP technique to investigate the effectiveness of this technique in field application. Several strain gauges were attached at the mid-span of the bridge girder and calibration was done for different loading conditions. The response of rehabilitated bridge was evaluated through static and roll tests. Retrofitted bridge girder showed decrease in maximum rebar strain as well as in deflection. It was concluded that the sprayed-GFRP technique was more cost-effective than other available rehabilitation methods and it had wider applicability in practical field. It was also stated that the sprayed-GFRP technique can be used to provide protective coating on the structures to prevent corrosion in adverse environment.

Harries and Young (2003) carried out an experimental study comparing the performance of epoxy-only sprayed technique and sprayed-FRP technique in strengthening concrete beams. Parameters affecting their performance and the potentiality of applying these techniques on actual structures were also investigated. Fibre content (5, 10, and 15% by volume) and coating thickness (3, 6, and 13 mm) were considered as study parameters. All specimens were tested under three-point loading according to American Society for Testing Materials (ASTM C78 and ASTM C1018) requirements. Increase in the load carrying capacity and the energy absorption capacity was observed for all rehabilitated specimens. Specimens covered with only-epoxy of 3-mm and 6-mm

thickness showed 30% and 40% increase in load carrying capacity, respectively, while in case of 13-mm thick coating, the improvement was insignificant. Therefore, the optimum coating thickness for maximum performance was defined as 6-mm. Minor increases in load capacity was obtained when fibres were introduced with resin due inadequate bonding at their interface. However, presence of fibres enhanced the ductile behaviour of beams. Consequently, energy absorption capacity increased. Sprayed-FRP rehabilitated specimens failed in a more ductile manner than the plane concrete specimens by the combination of fibre rupture and fibre pull-out. Adverse acidic environment had negligible effect on rehabilitated specimens. It was concluded that the quality of rehabilitation work, temperature of epoxy and type of fibres had greater effect on the response of rehabilitated structure. It was recommended that the upper limit of fibre volume ratio is 30% and fibre length is 50-mm.

Lee and Hausmann (2004) conducted a research study to determine the feasibility of using sprayed-FRP technique in concrete beam rehabilitation. Also, the effect of different fibre characteristics on the performance of rehabilitated beams was evaluated. Pre-cracked and undamaged RC beams of 100 × 100 × 450 mm dimension were retrofitted with E-glass fibres and carbon fibres. Parameters included in this study were: type of fibre (E-glass & carbon), coating thickness (3.2 mm & 6.4 mm), fibre length (13 mm & 26 mm) and fibre concentration (15% & 30%). All specimens were tested up to failure under three-point loading. Test result showed that both E-glass fibres and carbon fibres coating increased the maximum load and energy absorption capacity for all the specimens. Carbon fibres coating was found more effective in increasing energy absorption capacity rather than increasing load carrying capacity due to its higher brittleness than glass fibres. Specimens strengthened with thicker coating (6.4 mm) performed better than beams strengthened with thinner coating (3.2 mm). An optimum fibre length of 23 mm was suggested for

maximum load capacity and energy absorption capacity. Increase in fibre volume caused increase in load capacity for almost all specimens. A 30 % fibre concentration was found most effective in achieving satisfactory performance from sprayed-FRP system.

Lee et al. (2008) suggested considering sprayed-GFRP technique over using fibre reinforced mortar in rehabilitating plain concrete beams. This study also aimed to determine the optimum fibre formulation and coating thickness for retrofitting beams with sprayed-GFRP system. A total of 48 rectangular beams of 100 × 100 × 450 mm dimension, rehabilitated with different coating thickness (3 mm & 6 mm), fibre length (13 mm & 26 mm) and fibre concentration (15% & 30%) were tested under 3-point bending loading. Some specimens were notched at mid-length according to American Concrete Institute (ACI 446-01) requirements to represent damaged beams. Mostly, pull-out failure with loud noise was observed for specimens rehabilitated with sprayed-GFRP due to incomplete wet-out of fibres by epoxy resin. On the other hand, specimens retrofitted with fibre reinforced mortar failed so quietly that it was hard to determine the failure point. Sprayed-GFRP retrofit was found more effective in increasing ductility, load and energy absorption capacities. Also, it had better bonding to beam surface than fibre reinforced mortar covering. Increase in coating thickness and fibre concentration caused significant increase in maximum load, load at failure and energy absorption capacity for un-notched specimens. However, both notched and un-notched specimens showed minor improvement in performance as the fibre length increased. Noticeably, the energy absorption capacity of un-notched specimens almost doubled due to increase in fibre length.

Lee (2012) determined the optimum configuration of materials used in sprayed-FRP technique to attain maximum performance. Initially, a research was carried out to specify the composition of sprayed-FRP materials which are equivalent to one layer of FRP sheet in case of developing almost

equal structural strength after rehabilitation. These configurations were later used in strengthening beam specimens by sprayed-FRP technique. From the preliminary test data, the optimum fibre length and fibre-resin mix ratio was found 38-mm and 1:2, respectively. Moreover, sprayed-FRP coating of 4.2-mm was selected as optimal thickness based on specimen performance. Several beam specimens were constructed and rehabilitated with sprayed-FRP and FRP sheets. The selected material configuration from the preliminary study was used in this rehabilitation work. To investigate the efficiency of these retrofitting techniques on damaged structure, few specimens were damaged prior to strengthening. All specimens were tested under three-point loading until failure. Sprayed-FRP and FRP sheet strengthened specimens behaved in a similar manner throughout the test. Results showed that the design equation for FRP sheet wrapping method can be used for sprayed-FRP technique. However, a new design equation was also proposed for beam rehabilitation using sprayed-FRP method.

Ha et al. (2014) proposed a new spraying method for sprayed-FRP technique to overcome the drawbacks in existing method such as inconsistent fibre load, non-uniform thickness of coating and incomplete wet out of reinforcing fibres. This advanced multiple layup process was developed based on technical skills specified by American Composites Manufactures Association (ACMA 2004) for spray work and modified spray-gun calibration technique. Several material parameters (fibre length, number of strands processed simultaneously, fibre volume), spraying equipment parameters (heating unit), spraying process parameters (spray operations of the materials i.e., chopped glass fibres, resin and mixed stream with the fibres and resin) and gun-motion parameters (moving gun speed, height of the chopper and spray gun above the substrate, offset distance and spray-fan pattern of the materials, and the stroke as a lay-down strategy) were considered in developing this new spraying method. The performance of sprayed-FRP retrofit was assessed

considering coating thickness, volume fraction of the fibres, and mechanical properties. A constant thickness of spray was maintained following ACMA (2004) recommendations. The spray fan width for epoxy resin was recorded as 300 mm. But for chopped fibres with different fibre lengths and different numbers of strands, the spray fan width ranged from 197 to 310 mm. A spray-line offset distance of 100 mm was found capable of satisfying the basic requirements for overlapping spray length stated in ACMA (2004). To ensure a consistent fibre volume throughout the sprayed-FRP and resin coat, a modified gun-calibration technique was proposed in this study. First the required fibre weight (fibre and resin mix) was determined from targeted fibre loading. Then the fibre-resin mix was sprayed for a certain period of time and the fibre volume deposited for a unit time of spray was calculated by linear regression analysis. An equation was developed relating the targeted fibre loading to the estimated fibre deposited over unit time. Finally, the equation gave the number of required spray layup for targeted fibre volume concentration. A coefficient of variation of 8.6 to 14.4% was obtained from the qualitative analysis of the thickness of final sprayed FRP product. Study concluded that the final coating thickness could be reduced by 46 to 53% with respect to targeted thickness since the compaction factor of the fibre-resin composite found varying between 0.4 and 0.53. Advanced spray multiple layup process and matrix digestion method showed quite similarity while predicting volume fraction of the fibres. The final laminates showed coefficient of variation of 5.9 to 11.3% and 0.3 to 12.7% for tensile strength and modulus of elasticity, respectively. Further study was recommended considering long term behaviour of fibres and resins under alkaline environment.

Peng et al. (2014) studied the performance of sprayed-FRP technique in rehabilitating pre-damaged RC column. Four square columns of 250 × 250 × 1,000 mm dimension were constructed. Three of them were first damaged up to yielding of longitudinal reinforcement and then

strengthened using sprayed BFRP (4.5 mm and 7 mm thickness) and sprayed BF-CFRP (7:3) hybrid composite (4.5 mm thickness). One column was tested up to failure and used as control specimen. A combined quasi-static cyclic shear load and constant gravity loads were used to test all the specimens. Specimens rehabilitated with hybrid BF-CFRP polymer resulted in 30% and 33.9% higher ductility and energy absorption capacity, respectively than the specimens rehabilitated with only sprayed BFRP. Again 5% and 34.8% increase in ductility factor and energy dissipation capacity was observed, respectively as the thickness of sprayed BFRP increased from 4.5 to 7 mm. However, the peak load was recorded decreased on average by 6.16%, 11% and 5% for specimens rehabilitated with 4.5 mm and 7 mm thick sprayed BFRP and 4.5 mm thick sprayed BF-CFRP hybrid, respectively compared to the original column. Overall, study concluded that, hybrid sprayed BF-CFRP rehabilitation technique can be used to satisfactorily regain the ductility and energy absorption capacity of damaged RC columns.

Lee et al. (2016) investigated the seismic performance of rectangular column retrofitted with sprayed-FRP technique. Initially 160 specimens with different combination of fibre length and mix ratio of fibre, epoxy and vinyl ester were cast and tested under tensile loading. Based on these test results, an optimum matrix with fibre length of 38 mm and fibre-resin mix ratio of 1:2 by weight was selected which can replace one layer of FRP sheet while retrofitting. This matrix was used to retrofit steel-RC columns using sprayed-FRP technique. Five column specimens of 400 × 400 × 1,400 mm dimension were constructed and tested. The specimens were critical in in shear and four of them were retrofitted with different combinations of carbon or glass fibres and epoxy or vinyl ester resins. To increase the workability of spray, a mixture of stronger epoxy resin and vinyl ester resin was used in place of conventional vinyl ester resin. All five specimens were tested under seismic loading following a test method developed by the Japan Concrete Institute (2004).

Although, both control and retrofitted specimens failed in shear, significant difference was recorded in their performance. On average 31% increase in shear strength and 43% increase in deformation capacity was observed for retrofitted specimens compared to those of control specimen. It was concluded that, the newly developed sprayed-FRP technique is feasible for strengthening columns of low to medium rise RC buildings in seismic region. Moreover, seismic strengthening design equation for sprayed-FRP reinforcement was proposed. Further studies were recommended to determine optimum thickness of the sprayed coating and to evaluate the de-bonding mechanism between strengthening material and concrete.

2.9 Design Guidelines

2.9.1 Canadian Standards Association (CSA/A23.3-14a)

The following assumptions are considered during the analysis of a cross-section,

- Plane sections, which are perpendicular to the axis of bending, when subjected to bending remains plane after bending,
- There is a perfect bond between concrete and steel so that strains in steel and concrete at the same location are equal,
- Stress-strain diagram may predict the stresses in the concrete and steel,
- The tensile strength of concrete is ignored when the flexural capacity is calculated.

Several recommendations are provided in the CSA/A23.3-14a for flexural design. According to Clause 10.5.2, yielding of steel at the tension side should occur prior to crushing of concrete to avoid brittle failure. The maximum compressive strain of concrete is limited to 0.0035 (Clause 10.1.3).

Clause 10.9.1 states that minimum longitudinal reinforcement should be larger than 1% of the gross area to avoid sudden failure of the column and should be less than 6% to avoid congestion of steel. Code recommends not to use less than 6 bars in the circular section of a compression member (Clause 10.9.3).

The maximum factored axial load resistance for spirally reinforced column, $P_{r,max}$, is given by (Clause 10.10.4),

$$P_{r,max} = 0.90P_{ro} \qquad \text{Equation 2.5}$$

P_{ro} is the factored axial load resistance at zero eccentricity which can be calculated as,

$$P_{ro} = \alpha_1\phi_c f_c' \left(A_g - A_{st} - A_t - A_p\right) + \phi_s f_y A_{st} + \phi_a f_y A_t - f_{pr}A_p \qquad \text{Equation 2.6}$$

Where,

α_1 : Ratio of average stress in rectangular compression block to the specified concrete strength $(0.85 - 0.0015f_c' \geq 0.67)$;

ϕ_c : Resistance factor for concrete;

ϕ_s : Resistance factor for non-pre-stressed reinforcing bars;

ϕ_a : Resistance factor for structural steel;

A_g: Gross area of section;

A_t : Area of one leg of closed transverse torsion reinforcement;

A_p : Area of prestressing tendons;

A_{st} : Total area of longitudinal reinforcement;

f_{pr} : Stress in prestressing tendons at factored resistance;

f_c' : Specified compressive strength of concrete;

f_y : Specified yield strength of non-prestressed reinforcement or anchor steel.

Factored shear resistance can be calculated as follows (Clause 11.3.3):

$$V_r = V_c + V_s \qquad \text{Equation 2.7}$$

Provided that V_r should be less then V_{rmax}

Where,

V_c : Shear resistance attributed to the concrete factored by ϕ_c;

V_s : Shear resistance provided by shear reinforcement factored by ϕ_s.

$$V_{rmax} = 0.25\phi_c f_c' b_w d_v \qquad \text{Equation 2.8}$$

b_w is the diameter in case of circular section and d_v is the effective shear depth taken as the greater of 0.9*d* or 72*h.*

For shear and torsion, code recommended that maximum spacing of transverse reinforcement should be less than $0.7d_v$, or 600 mm (Clause 11.3.8.1). However, when V_r exceeds $0.125\lambda\varphi_c f_c' b_w d_v$, the maximum spacing shall be reduced by one-half (Clause 11.3.8.3).

According to Clause 11.2.8.2, minimum shear reinforcement can be calculated as,

$$\mathrm{A_{v,min}} = 0.06\sqrt{\mathrm{f_c'}}\frac{\mathrm{b_w s}}{\mathrm{f_y}} \qquad \text{Equation 2.9}$$

Where;

s : Spacing of shear reinforcement, measured parallel to the longitudinal axis of the member,

$A_{v,min}$: Area of shear reinforcement perpendicular to the axis of a member within the distance *s*.

According to Clause 7.6.4.2, spiral reinforcement shall have a minimum diameter of 10 mm. The clear spacing between successive turns of a spiral shall not be less than 25 mm or greater than 75

mm (Clause 7.6.4.3). Clause 10.9.4 states the allowed minimum spiral reinforcement ratio as given below,

$$\rho_s = 0.50\left[\frac{A_g}{A_c} - 1\right]^{1.4}\frac{f_c'}{f_y} \qquad \text{Equation 2.10}$$

Where,

A_c : Area of core of spirally reinforced compression member measured to outside diameter of spiral.

Clause 12.17.3.5 states that, in spirally reinforced compression members, the lap splice length of bars within a spiral, computed as specified in Clauses 12.16.1 (Minimum lap length: The minimum lap length for compression lap splices shall be $0.073f_y d_b$ for f_y less than or equal to 400 MPa or $(0.133f_y - 24)db$ for f_y greater than 400 MPa, but shall not be taken less than 300 mm) and Clause 12.16.2 (Lap length for bars of different sizes: When bars of different sizes are lap spliced in compression, the splice length shall be the larger of the development length of the larger bar or the splice length of the smaller bar. Bar sizes 45M and 55M may be lap spliced to 35M and smaller bars), may be multiplied by 0.75, but the lap splice length shall be not less than 300 mm.

Anchorage of spiral reinforcement shall be provided by 1-1/2 extra turns of spiral rod or wire at each end of the spiral unit (Clause 6.6.3.5). Splices in spirals shall have a minimum 50 bar diameter lap plus a 90° hook around a longitudinal bar at the free end or shall be welded in accordance with Clause 6.6.3.6 of CSA/W186 (2016). The reinforcing spiral shall extend from the floor level in any storey or from the top of the footing to the level of the lowest horizontal reinforcement in the slab, drop panel, or beam above (Clause 6.6.3.7).

2.9.2 American Concrete Institute (ACI 318-14)

The ACI 318-14 (ACI Committee 318 2014) has the same assumptions for analyzing the cross-section expect for the maximum compressive strain of concrete, which is assumed to be 0.003. The equation to determine maximum nominal load capacity, P_r, of a concrete column reinforced with steel according to ACI 318-14 is as below:

For spiral columns ($\emptyset$ = 0.75) (Clause 10.3.6.1)

$$\mathrm{P_r = \emptyset P_o = 0.85\emptyset[0.85f'_c\left(A_g - A_{st}\right) + f_y A_{st}]} \qquad \text{Equation 2.11}$$

For hopped columns ($\emptyset$ = 0.65) (Clause 10.3.6.2)

$$\mathrm{P_r = \emptyset P_o = 0.80\emptyset[0.85f'_c\left(A_g - A_{st}\right) + f_y A_{st}]} \qquad \text{Equation 2.12}$$

Where,

A_g : Gross area of concrete section;

A_{st} : Total area of non-prestressed longitudinal reinforcement;

f'_c : Specified compressive strength of concrete;

f_y : Specified yield strength of reinforcement.

The reduction factors (15% for spiral and 20% for hooped column) in the maximum nominal load capacity were considered assuming that there is no perfect axially loaded column. Unintended eccentricity arises in the column section due to the end condition, inaccuracy of construction, and normal variation in material properties which affects the column capacity.

Design of shear according to ACI 318-14 has the following requirements:

Factored shear resistance should be computed as follows:

$$V_r = V_c + V_s \qquad \text{Equation 2.13}$$

Where,

V_c : Nominal shear strength provided by concrete;

V_s : Nominal shear strength provided by shear reinforcement.

Minimum shear reinforcement should be such that (Clause 11.5.6.3),

$$A_{v,min} = 0.75\sqrt{f'_c}\frac{b_w s}{f_y} > \frac{50 b_w s}{f_y} \qquad \text{Equation 2.14}$$

Where,

s : Spacing of shear reinforcement, measured parallel to the longitudinal axis of the member;

$A_{v,min}$: Area of shear reinforcement perpendicular to the axis of a member within the distance s.

According to Clause 10.9.3, the volumetric ratio of spiral reinforcement, ρ_s, should not be less than the value given by:

$$\rho_s = 0.45\left[\frac{A_g}{A_{ch}} - 1\right]\frac{f'_c}{f_{yt}} \geq 0.12\frac{f'_c}{f_{yt}} \qquad \text{Equation 2.15}$$

Where,

ρ_s : Ratio of volume of spiral reinforcement to total volume of core confined by the spiral (measured out-to-out of spirals);

A_{ch} : Cross-sectional area of a structural member measured to outside edges of transverse reinforcement;

f_{yt} : Specified yield strength of transverse reinforcement.

Code limits the value of f_{yt} to 690 MPa and lap splice of spirals were discouraged if the value of f_{yt} exceeds 400 MPa. In spirally reinforced or tied reinforced compression members, clear distance between longitudinal bars shall be neither less than 1.5d_b nor less than 38 mm (Clause 7.6.3). For cast-in-place construction, size of spirals shall not be less than 10 mm. diameter. Clear

spacing between spirals shall not exceed 75 mm., nor be less than 25 mm. Anchorage of spiral reinforcement shall be provided by 1.5 extra turns of spiral bar or wire at each end of a spiral unit. Spirals shall extend from top of footing or slab in any story to level of lowest horizontal reinforcement in members supported above. Where beams or brackets do not frame into all sides of a column, ties shall extend above termination of spiral to bottom of slab or drop panel (Clause 7.10.4).

In spirally reinforced compression members, lap splice length of bars within a spiral shall be permitted to be multiplied by 0.75, but lap length shall not be less than 300 mm. (Clause 12.17.2.5). The volumetric ratio of spiral or circular hoop reinforcement, ρ_s, shall not be less than required by (Clause 21.4.4)

$$\rho_s = 0.12 \frac{f'_c}{f_{yt}} \qquad \text{Equation 2.16}$$

2.9.3 FRP sheet design (CSA/S806-12; CSA/S6-14; ISIS-08)

FRP rehabilitation system for columns is usually designed as a confinement around compression element. The confinement design aims not only to increasing compression capacity of the column but also improving column ductility (ability to undertake inelastic deformation without adversely affecting the load carrying capacity) to resist seismic loads (Fig. 2.6).

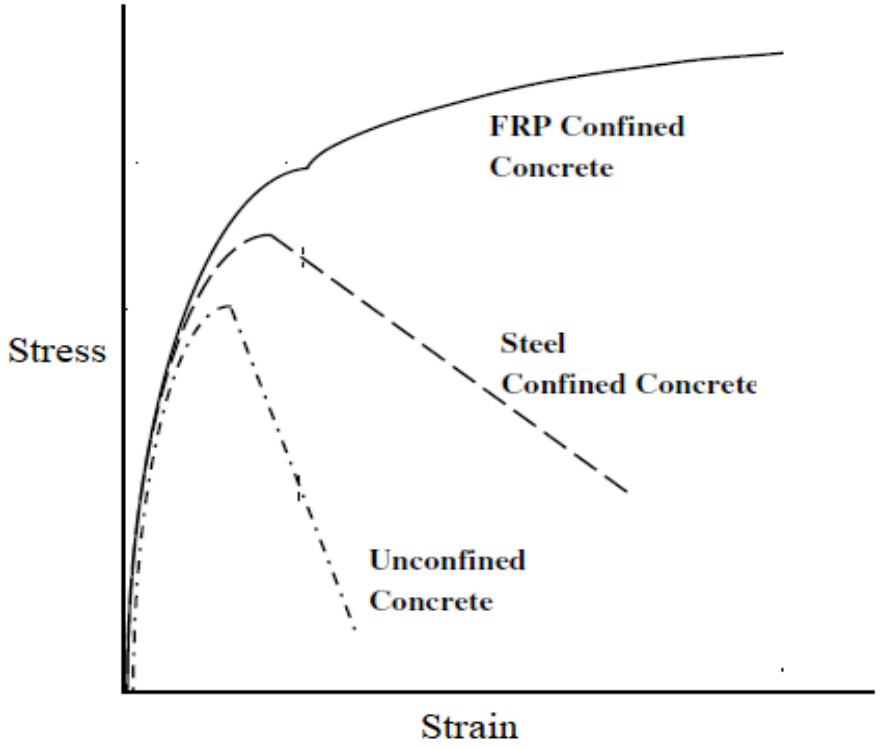

Figure 2.6: Stress-strain response of unconfined concrete, steel confined concrete and FRP wrapped concrete (reproduced from Harajli 2006)

Both CSA/S806-12 and CSA/S6-14 provided design guidelines for FRP sheet confinement considering good bonding with concrete surface. When good bonding exists between FRP confinement and column surface, the rehabilitation system also contributes in increasing flexural capacity. Moreover, the FRP confinement can effectively increase shear capacity of column by hoop action. In most cases the FRP rehabilitation system is designed as a passive confinement (start working after concrete being significantly damaged). This confinement action was found more efficient in case of circular column compared to rectangular column. Because in circular column the stress on confinement is uniform in all direction. In rectangular column the stress on confinement is higher near the corners and lower along the sides (Fig. 2.7). Therefore, it is recommended to round up the corners for rectangular column before applying FRP. Even the

section can be made circular or elliptical to increase the effective confinement area (CSA/S806-12, CSA/S6-14).

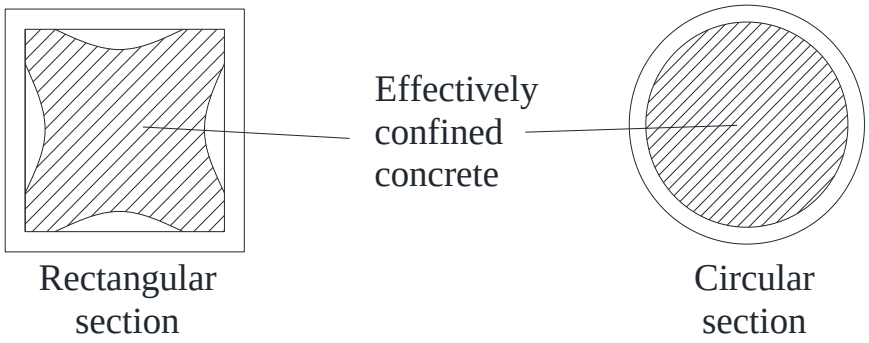

Figure 2.7: Effective confined area in rectangular and circular column for FRP (reproduced from ISIS 2008)

The manufacturer supplies the material properties used in design. However, specified lab tests can be performed following existing standards to determine mechanical properties under specific condition. Again, property of FRP system can be estimated using equation 2.17 and equation 2.18 when the property of individual materials is known.

$$E_{frp} = V_f E_f + V_m E_m \qquad \text{Equation 2.17}$$

$$f_{frp} = V_f f_f + V_m f_m \qquad \text{Equation 2.18}$$

Where, E_{frp}, E_f, E_m are modulus of elasticity of FRP, fibre and resin respectively. f_{frp}, f_f, f_m are tensile strength of FRP, fibre and resin respectively. V_f, V_m are the volumetric ratio of fibres and resin/matrix and V_f+V_m=1.

Material resistance factors are used in design to consider uncertainties in material property and construction (ISIS 2008). This section is mainly focused on the design method when FRP is used to rehabilitate compression member.

In both CSA/S806-12 and CSA/S6-14, the equation for factored load resistance was developed assuming perfect bonding, material resistance factor, linear strain variation, strain compatibility, force equilibrium, equivalent concrete stress block and maximum usable strain (for FRP, CSA/S6-14 limits to 0.006 and CSA/S806-12 limits to 0.007; for concrete 0.0035). Also, shear deformation was neglected and fibres are assumed to be oriented at an angle 75º to 90º with the axis of the column. The equation for confinement pressure (f_{lfrp}) stated in both codes is given as follow,

$$f_{lfrp} = \frac{2t\phi f_{ufrp}}{D} \qquad \text{Equation 2.19}$$

Where,

t : Confinement thickness;

ϕ : Material resistance factor;

f_{ufrp} : Ultimate tensile strength of FRP;

D : Section diameter for circular column.

= Section dimension in loading direction for rectangular column (CSA/S806-12).

= Diagonal of cross section for rectangular column (CSA/S6-14).

However, CSA/S806-12 states that the hoop strain in FRP confinement should not be more than 0.004 times the modulus of elasticity of confining material. The equations to be applicable CSA/S6-14 and CSA/S806-12 requires minimum corner radius as 35-mm and 20-mm, respectively. CSA/S806-12 stated the equation for confined concrete strength (f'_{cc}) as follow,

$$f'_{cc} = 0.85f'_c + k_1 k_c f_{lfrp} \qquad \text{Equation 2.20}$$

Where,

f_c' : Concrete compressive strength, maximum limit 50 MPa to avoid abrupt failure;

k_1 : $6.7(k_c f_{lFRP})^{-0.17}$;

k_c = 1.0 for circular section.

= 0.25 for rectangular section.

CSA/S6-14 stated simpler equation for confined concrete strength as shown in equation 2.21. This equation usually provides conservative results close to the actual value (Teng et al. 2002, Bisby et al. 2005).

$$f_{cc}' = f_c' + 2f_{lfrp} \qquad \text{Equation 2.21}$$

This confined concrete strength is used in equation 2.22 for buildings or in equation 2.23 for bridges to determine axial load capacity.

$$P_r = 0.85\left[\alpha_1 \phi_c f_{cc}' \left(A_g - A_s\right) + \phi_s f_y A_s\right] \qquad \text{Equation 2.22}$$

$$P_r = 0.80\left[\alpha_1 \phi_c f_{cc}' \left(A_g - A_s\right) + \phi_s f_y A_s\right] \qquad \text{Equation 2.23}$$

Where,

α_1= 0.85 - 0.0015 $f_c' \geq$0.67,

ϕ_c = Resistance factor for concrete,

ϕ_s = Resistance factor for steel reinforcement

A_g = Gross area of concrete section,

A_s = Area of steel reinforcement,

f_y = Yielding stress of steel.

While designing to increase both axial compression and flexural moment capacity, both Canadian codes recommended analyzing the section based on stress and strain compatibility as shown in Fig. 2.8.

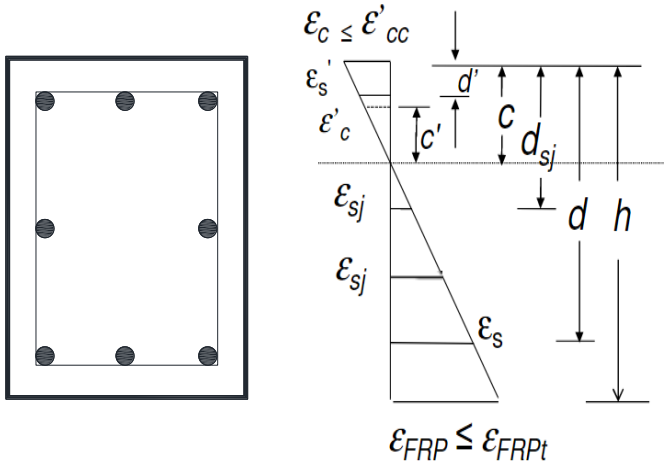

Figure 2.8: Strain diagram on rehabilitated column section (reproduced from ISIS, 2008)

While designing the rehabilitation system for columns under pure compression, first we have to check and assure that there is no slenderness and flexural effect on the column. Then from equation 2.22 or 2.23 we can determine the required confined compressive strength (f'_{cc}) assuming $P_r = P_f$. Corresponding required confinement pressure (f_{lfrp}) can be determined using equation 2.21 or 2.20. At last using the material properties provided by the supplier, the required confinement thickness (t) can be determined from equation 2.19. On the other hand, for column under compression and flexure, first we can assume the thickness of the confinement based on experience or previous calculations. Then we have to determine strain in each material using strain compatibility and assuming the failure strain limit mentioned in the codes. Then assuming equilibrium force condition, we have to determine position of neutral axis from resultant internal forces corresponding to calculated strain in each material. Based on this neutral axis we have to validate the assumptions of strain in each material. Upon validation of strain in each material, we can determine the axial and flexural resistance from cross sectional analysis and compare it with

required capacity. In both cases, the strain limit and confinement limit should be checked according to code provision. In case of lap splice region an extra confinement of thickness t_{frpex} can be provided. The thickness can be determined using equation 2.24.

$$t_{frpex} \geq 2D \frac{f_c'}{f_{lfrp}} \times \frac{P_f}{P_{ro}} \times \frac{\delta}{\sqrt{k_c}} \qquad \text{Equation 2.24}$$

Where, $f_{lfrp} = 0.004E_{frp} \leq \phi f_u$

$\frac{P_f}{P_{ro}} \geq 0.2$ where $P_{ro} =$ calculated axial capacity of unconfined section

δ = design lateral drift ratio$\geq$0.04

Available research data showed that column rehabilitated with FRP confinement are less susceptible to premature failure of concrete under creep and fatigue. However, ISIS 2008 limited the sustained load to prevent premature failure as follow,

$$P_{sus} \leq 0.85\left[\alpha_1 \phi_c 0.8 f_c' \left(A_g - A_s\right) + f_s A_s\right] \qquad \text{Equation 2.25}$$

Where, f_s should be less than $0.0015E_s$ and $0.8f_y$.

Initial strain in concrete and steel plays an important role in strengthening system design. Unfactored dead load and actual live load effects are considered while determining the initial strain. Higher initial strain yields higher requirement in confinement area. While designing, the initial strain in concrete and steel should be considered in design. So, for, no design guideline is available for designing sprayed-FRP rehabilitation system.

CHAPTER 3 – EXPERIMENTAL PROGRAM

3.1 GENERAL

The performance of sprayed-FRP technique in seismic retrofitting of RC circular columns is investigated in this study. Six large-scale column specimens were constructed, retrofitted and tested under seismic loading scheme. All specimens were constructed as deficient in lap splice length (20 d_b). The experimental program was conducted in two phases. In the first phase (Phase-1), the performance of 3-mm thick sprayed-GFRP in rehabilitation of circular RC columns was evaluated. The sprayed-GFRP thickness was increased to 6-mm in the second phase (Phase-2) based on the results in first phase. Each phase includes three columns; one column was tested up to 2.5% drift ratio before rehabilitation, another column was rehabilitated after being tested until failure and the other column was strengthened in intact condition. After rehabilitation, all columns were tested under simultaneous reversed-cyclic load and constant axial load of 500 kN (20% of column axial capacity) to study the effect of axial load on structurally deficient columns. In a moment-resisting frame structure, the inertia of forces generating from an earthquake event are transferred from one floor to another by columns. Therefore, columns are often subjected to nearly equal and opposite forces and moments. Hence, the column mid-height can be considered as the point of contra-flexure for earthquake analysis. In this study, each specimen stimulates a portion of a column between the foundation and the point of inflection in a moment-resisting frame structure as shown Fig. 3.1. Sprayed-GFRP samples were collected from each specimen and tested to determine the actual fibre content in cured composite. Three cylinders were rehabilitated along with column specimens and tested under uni-axial compression to determine the tensile strength of cured sprayed-GFRP composite.

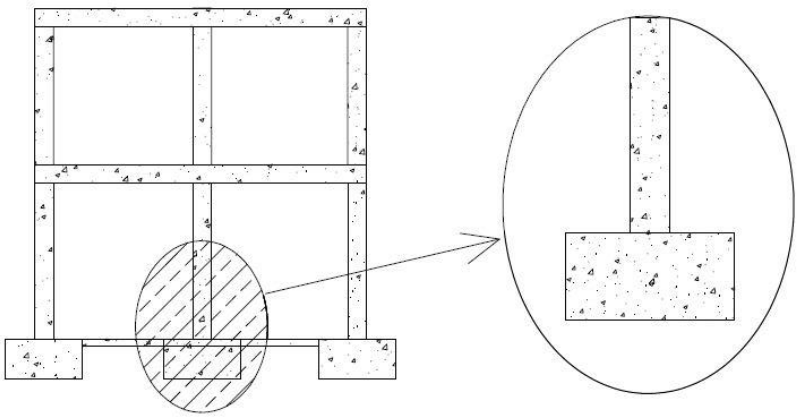

Figure 3.1: Simulated test specimen in moment resisting frame

3.2 Specimen Details

Six large-scale circular column specimens were designed and constructed to evaluate the efficiency of rehabilitation with sprayed-GFRP technique as shown in Fig. 3.2. These specimens represented a portion of a column between the foundation and point of inflection in buildings and bridges. All specimens had a diameter and a span length (distance between footing-column interface to the point of lateral load application) of 305-mm and 1,525-mm, respectively. A concrete block of 550 × 350 × 400 mm was constructed monolithically at the top of the column to facilitate the axial and lateral load transfer from the loading machines to the column. Six 15M steel bars were used in all columns as main reinforcement (reinforcement ratio of 1.64%) satisfying the minimum number of bar requirements according to CSA/A23.3-14a for circular column. Each column was transversely reinforced with size 10M spiral having a constant pitch of 75-mm. All column specimens had a massive footing (1,400 × 900 × 600 mm) to provide adequate fixity to the specimens while testing. The footing was reinforced with 15M bars at top and bottom in both directions. Six dowel bars of size 15M were cast with the footing. The embedded length of these dowel bars in footing was 575-mm satisfying the minimum required length specified in the

CSA/A23.3-14a. Moreover, this embedded length was reported to be adequate against slippage in previous studies (Ali and El-Salakawy 2016; Naqvi and El-Salakawy 2016).

Test parameters included degree of damage (Intact, Partially-Damaged and Fully-Damaged) and thickness of the sprayed-GFRP (3.0 and 6.0 mm). All the specimens were designated by three characters. First character represents the degree of damage of specimen at which the strengthening system was applied, "I" for intact, "PD" for partially damaged and "D" for fully damaged. Second character indicates the phase of experimental program, "1" for Phase-1 and "2" for phase-2. Third character refers to the thickness of the sprayed-GFRP composite, 3.0 and 6.0 mm. For example, I1-3 indicates that the specimen is from phase-1 which was strengthened in intact condition and the thickness of sprayed-GFRP was 3.0 mm. Test matrix of this study is summarized in table 3.1.

Table 3.1 Details of test matrix

Specimen	Remarks	Sprayed-GFRP thickness (mm)
PD1-0	Tested up to 2.5% drift ratio	0
D1-0	Tested up to failure	0
I1-3	Strengthened and tested up to failure	3
PD1-3	PD1-0 rehabilitated and tested up to failure	3
D1-3	D1-0 rehabilitated and tested up to failure	3
PD2-0	Tested up to 2.5% drift ratio	0
D2-0	Tested up to failure	0
I2-6	Strengthened and tested up to failure	6
PD2-6	PD2-0 rehabilitated and tested up to failure	6
D2-6	D2-0 rehabilitated and tested up to failure	6

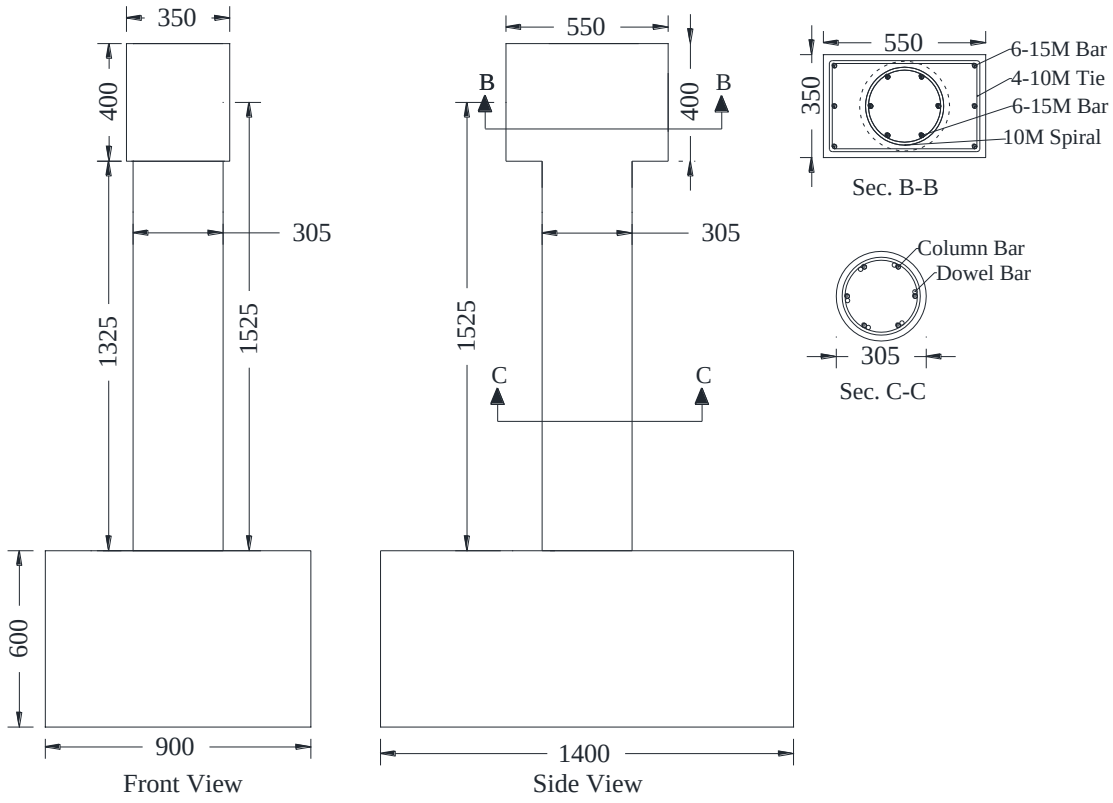

Figure 3.2: Typical dimensions of test specimen (all dimensions in mm)

3.3 Material Properties

All column specimens were constructed using ready-mixed normal strength concrete with a target 28-day compressive strength of 35 MPa. The maximum size of the aggregate in concrete was 20 mm and the slump was approximately 100-130 mm. Several concrete cylinders of 100-mm diameter and 200-mm height were tested following CSA/A23.2-14b guidelines to determine the average concrete compressive strength. In all specimens, grade 400 deformed steel bars were used as main and transverse reinforcement. Table 3.2 includes the mechanical properties of steel reinforcement used in constructing test specimens.

Table 3.2: Mechanical properties of reinforcing bars (Naqvi 2016)

Bar size	Nominal diameter (mm)	Area (mm^2)	Modulus of elasticity (GPa)	Yield strength (MPa)	Yield strain (%)
No. 15M	15.9	200	200	460	0.23
No. 10M	11.3	100	200	420	0.21

The resin solution used in strengthening was manufactured by Polynt Composites Canada Inc. It was an epoxy bi phenolic vinyl ester resin. Table 3.3 contains the physical properties of resin as per manufacturer's literature.

Table 3.3: Physical properties of resin (Polynt Composites Canada Inc., 2017)

Property	Value (unit)
Specific gravity	1.03-1.07 (g/cm3)
Viscosity	450-700 (cps)
Gel time	15-25 (minute)
Tensile strength	84 (MPa)
Tensile modulus	3750 (MPa)
Elongation	7.5 (%)
Flexural strength	151 (MPa)
Flexural modulus	3430 (MPa)

Hardener (United Initiators, Inc., 2017) used in rehabilitation was manufactured by United Initiators, Inc. Continuous roving glass fibers, manufactured by Owens Corning Composite Materials, LLC. was used in strengthening process. This type of glass fibre was developed to combine the electrical and mechanical properties of traditional E-glass with the acid corrosion

resistance of E-CR glass. Roving format prevents mechanical twist of continuous glass fiber gathered into a single bundle or yarn. Table 3.4 depicts physical properties of glass fiber according to manufacturer's literature.

Table 3.4: Physical properties of glass fiber (Owens Corning Composite Materials, 2015)

Property	Value (unit)
Diameter	11 (μm)
Density	2.6 (g/cm3)
Tensile Strength	3100-3800 (MPa)
Elastic modulus	80-81 (GPa)
Elongation	4.6 (%)

3.4 Specimen Construction

Plywood sheets were used to construct the formwork of the footing (Fig. 3.3a). Steel reinforcement cages designed for footing were placed inside the formwork along with four 20 mm diameter PVC pipes at designed locations. These locations of PVC pipes were selected based on the position of holes in the laboratory strong floor so that a dywidag bar can pass through both holes and provide fixity to the specimens while testing. The footing was cast with the starter bars embedded in it (Fig. 3.3b). Then the column reinforcement cage was tied with the rest portion of dowel bars at the top of cured footing. A sonotube of 305 mm diameter (inside) was used as formwork for the column specimens. Plywood was used to build the formwork of the column head (Fig 3.3c). A thin layer of form-oil was applied to the inner surface of the formwork to facilitate removing of formwork after casting. Additional, plywood strainers were used to restrain the lateral movement of the column during casting. The footing was cast one week before the column to simulate the

actual construction practice. The formwork was removed one week after casting and the specimens were cured for 28 days using burlap (Fig. 3.3d). Figure 3.3 shows the different stage of construction. Another two smaller footing (1,400 × 400 × 600 mm) was constructed to support the hinged frame facilitating the application of axial load.

(a) Steel cages for column footings

(b) Casting footing with column reinforcement

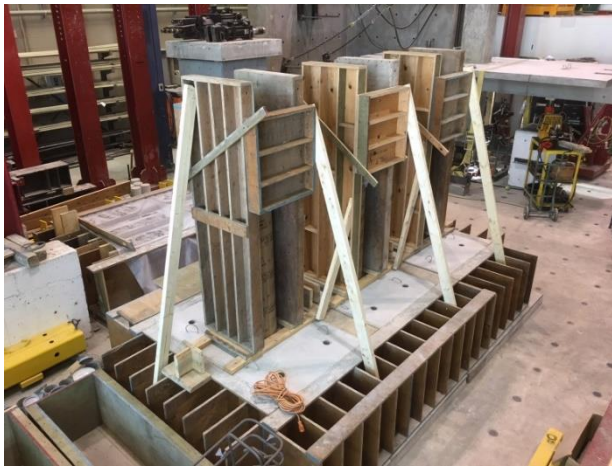

(c) Formwork for columns

(d) Completed column specimens

Figure 3.3: Stages of specimen construction

3.5 Patching and Strengthening Process

Several methods are available for the application of FRP materials in rehabilitation of RC columns. The most commonly used method is hand lay-up technique. However, application of FRP materials in strengthening of RC structures by spraying method is still limited. This section briefly presents the devices and techniques which were used in this research for repair and rehabilitation of RC column specimens.

3.5.1 Repair of damaged specimen

Recommendations stated in CSA/S6-14 and CSA/S806-12 were followed for concrete repair. First, all the loose, unsound and debris concrete was removed using hammer and chisel (Fig. 3.4 a). High air pressure was used to remove all dust and dirt from concrete surface (Fig 3.4b). Cement-based grout (mortar) prepared using non-shrinking cement, manufactured by CPD Construction Products (2017), and water was used in the repair work.. Table 3.5 shows the material properties of the non-shrinking grout as provided by the manufacturer.

Table 3.5: Properties of the non-shrinking grout

Property	Value (unit)
Specific gravity	2.2
Compressive strength (28 days)	60 (MPa)

The sonotube was adjusted along the length of damaged portion to restore original shape of the column specimens. Cement mortar was poured through a small hole at the top of sonotube and light hand vibration was applied to make sure the grout reached all the damaged area. Before applying the mortar, the concrete surface was made slightly wet to facilitate bonding between old concrete and new cement mortar. The sonotube was removed after one day as the non-shrinking

cement mortar hardens very quickly. Further patching was carried out to smoothen the surface (Fig 3.4c). Burlap was used for curing the concrete used in repair work (Fig. 3.4d).

(a) Removing loose and spalled concrete

(b) Dust removed by pressured air

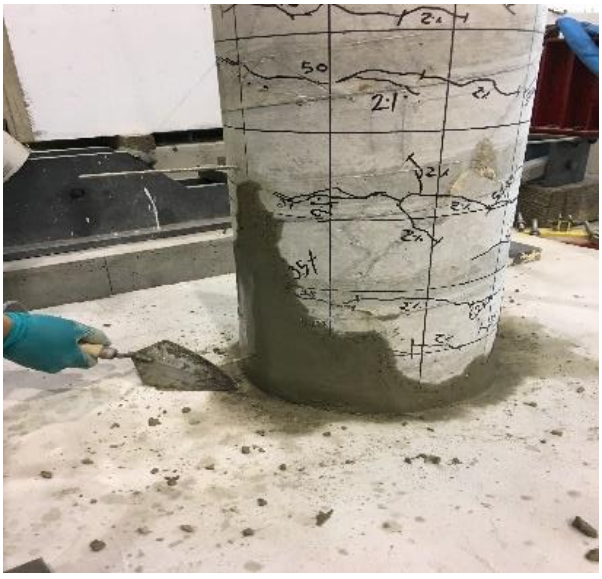

(c) Patching with mortar

(d) Curing with wet burlap

Figure 3.4: Stages of column repair/patching

3.5.2 Devices used in sprayed-FRP technique

Figure 3.5 shows different components of assembled spraying unit used in this study. Different types of system are available which can be used for sprayed-FRP rehabilitation work. But all these systems consist almost same components. The system used in this rehabilitation process was manufactured by Glass-Craft Inc. (Fig. 3.5a). The resin tank was bought separately which contains the promoted resin (Polynt Composites Canada Inc., 2017). A hose connects the resin tank to the resin pump. A perforated pipe screener attached at the end of the hose collects promoted resin from the tank and supplies it to the resin pump. Another tank contains the hardener (United Initiators, Inc., 2017) which is connected to the catalyst pump through a hose. Both the resin pump and catalyst pump are connected to a controller through separate hoses (Fig. 3.5b). The controller consists of several valves and dial gauges, allows the operator to control the mix proportion of resin with hardener and air pressure at the spray gun (Fig. 3.5c). An external compressed air supply unit provided all the required forces for pumping and spraying. Separate hoses of resin and hardener connects the controller to the spray gun. Another hose supplies air pressure from controller to the chopper unit mounted at the top of spray gun. These hoses are attached to a broom for easy operation. Resin and catalyst get mixed when they came out of the spray gun. The chopper unit cuts and throws fibre using two rollers. One roller has blades attached to its surface which cuts the fibres to a specific length based on the spacing of the blades. One bundle of glass fibre was fed between those rollers (Fig. 3.5d). The chopped fibres get mixed with resin-catalyst mixture in front of the spray gun. All these components are mounted on a wheeled cart for easy mobility.

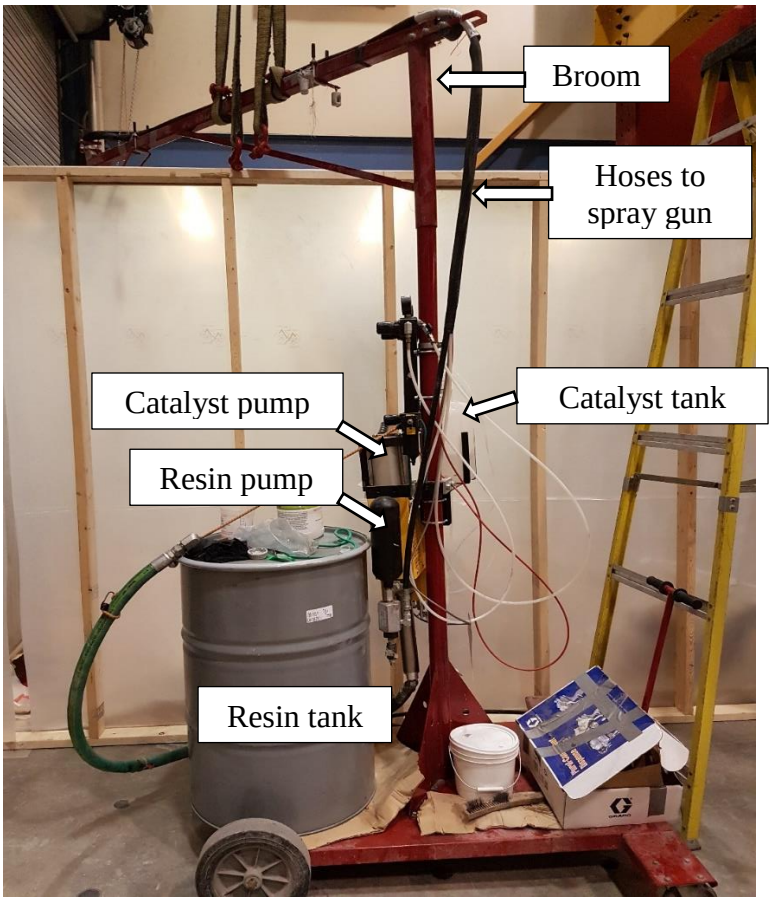

(a) Assembled spraying unit

(b) Controller

(c) Spray gun

(d) Glass fibre bundle

Figure 3.5: Spraying unit

3.5.3 Spraying process

Although sprayed-FRP technique was introduced in RC structural rehabilitation at the beginning of 20th century, still it is in research stage. No codes or guideline is available regarding surface preparation and application of sprayed-FRP system. In this research, the concrete surface was brought back to its original shape using cement mortar. The cured concrete surface was left to dry for one week before spraying. First the controller was connected to an air pressure source. The valves were to set spray a mix of 98% resin and 2% catalyst. Also, the pressure at the fibre chopper unit was set targeting a final product of 30% fibre and 70% resin. Trial spray was carried out before spraying finally on the specimens to make sure everything was working as planned. From the trial spray the average chopped fibre length was recorded as 26-mm (Fig. 3.6a). First, a primary layer of resin-catalyst mix was sprayed on concrete surface to create a sticky base for sprayed-GFRP. After waiting for few minutes, the bundle of fibre was fed at chopper unit. Then chopped glass fibres and resin-catalyst mixture was sprayed simultaneously until the thickness reached 3-mm all around the specimen (Fig. 3.6b). Later, an aluminum roller was rolled over the sprayed surface to achieve a uniform thickness by forcing out the entrapped air from sprayed-GFRP composites (Fig. 3.6c). The thickness of sprayed-GFRP layer was checked with a special device as shown in (Fig. 3.6d). In case of specimens with 6-mm targeted thickness, the same process was repeated after 30 minutes except no primary layer of resin-catalyst mix was applied. The spray produced a layer of GFRP composite which consists of two dimensional randomly distributed glass fibres embedded in resin-catalyst mix. Fibres and resin-catalyst mixture were sprayed from two separate levels of the spray gun. Chopper unit mounted on the spray gun sprayed the chopped fibres from an upper level which got mixed with resin and catalyst mixture after travelling a certain distance. This mixing distance was controlled by the alignment and air pressure of the chopper gun which was

set through trial spray and based on the experience of the operator. Similar procedure was followed in rehabilitating the cylinders with sprayed-GFRP.

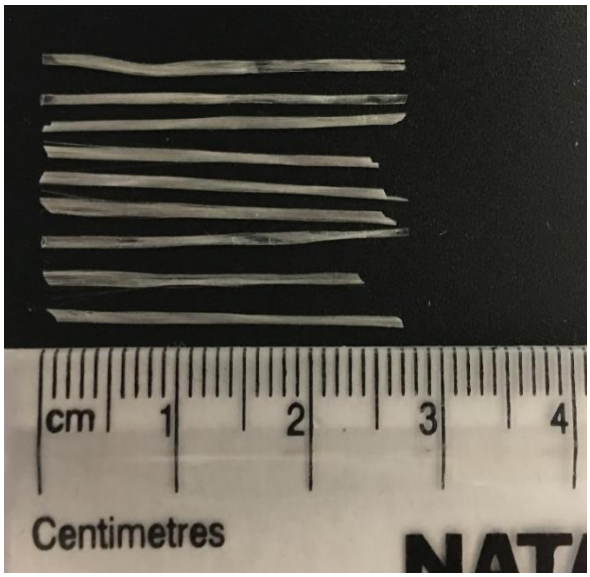

(a) Fibre length check

(b) Spraying

(c) Entrapped air removal

(d) Thickness check

Figure 3.6: Stages of spraying

3.6 Instrumentation

Instrumentation of the test specimens was designed to obtain strain, displacement, rotation and load during the test. All instruments were attached at suitable locations and were connected to a data acquisition system (DAQ). The DAQ collected readings of different instruments and recorded those in a practical unit system. However, the propagation of cracks while testing was monitored visually and marked carefully at the end of each loading cycle.

3.6.1 Load cells

The data of applied lateral load was collected directly from the load cell embedded in the dynamic actuator. Another load cell was placed between the hydraulic jack and column head to measure and record the data of axially applied load.

3.6.2 Linear variable displacement transducers (LVDTs)

Total of four LVDTs were used in this study to measure the rotation components of the column specimens (Fig. 3.7). Two LVDTs was attached vertically on both sides of the column in loading direction to measure the total flexural rotation relative to footing. Both of these LVDTs were placed directly on the footing surface having their top attached to a threaded rod mounted on column surface. The actual horizontal distance between these two LVDTs was measured for specimen. The total flexural rotation was calculated by dividing the difference in readings of the LVDTs by the measured horizontal distance. The other two LVDTs were also positioned in the same way except the bottom of those LVDTs were attached to a threaded rod at a distance 25 mm above the footing surface. Using the same calculation method as mentioned before, the data of these two LVDTs were used to calculate the rotation of hinging region.

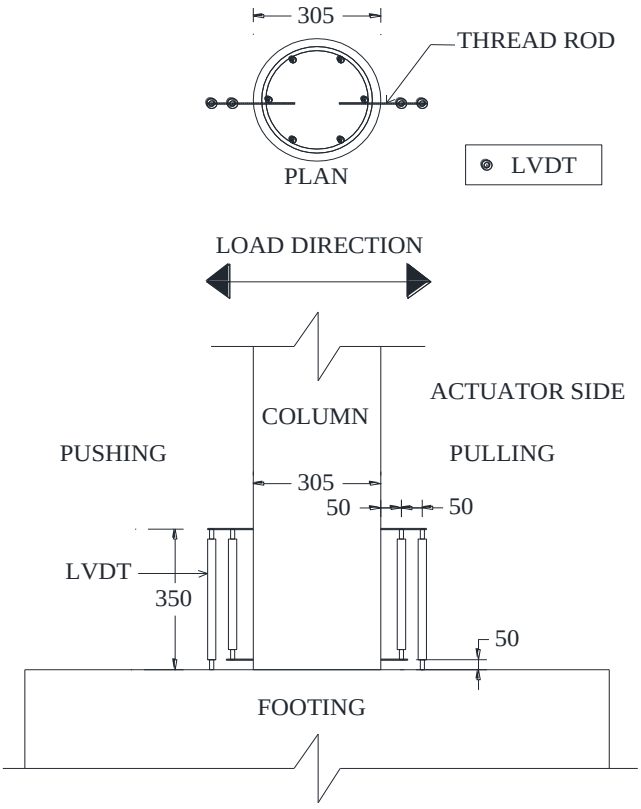

Figure 3.7: Location of LVDTs (all dimensions in mm)

3.6.3 Strain gauges

A total of eight strain gauges were used for each specimen to monitor the strain development in longitudinal reinforcement corresponding to the applied loads. In order to measure the force transfer and slippage between the lap spliced bars, these strain gauges were attached on the column and dowel bars "A" and "D" in the lap splice region. Figure 3.8 illustrates the locations of strain gauges.

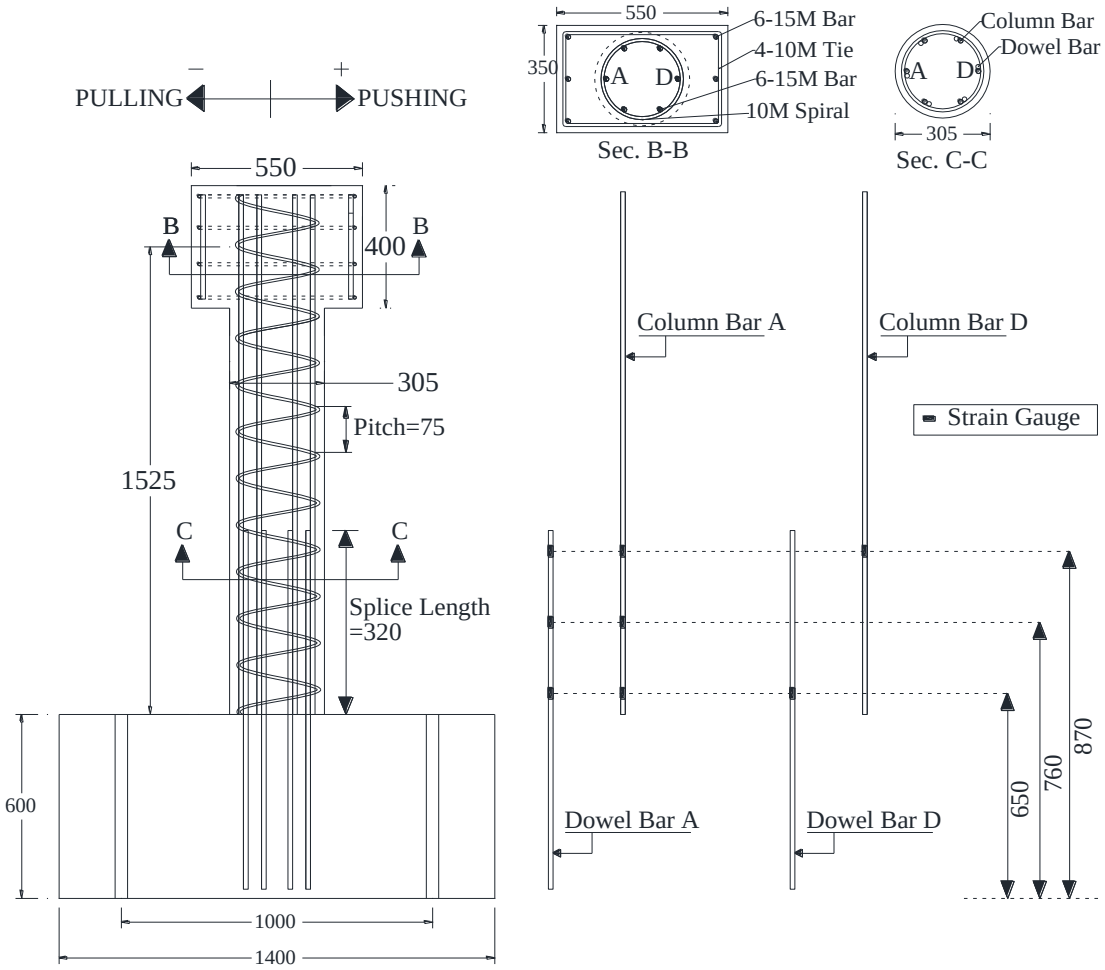

Figure 3.8: Details of test specimens and locations of strain gauges (all dimensions in mm)

3.7 Test Setup and Procedure

3.7.1. Column specimens

All specimens were tested in vertical position and were subjected to simultaneous constant axial load and lateral quasi-static reversed-cyclic load as shown in Fig. 3.9. A 1,000-kN load and 250-mm stroke capacity dynamic actuator was used to provide cyclic-reversed lateral load at the column head. The actuator was mounted on a massive steel column with its center line 2,125 mm above the laboratory floor level. The massive column was prestressed to laboratory strong floor with eight dywidag bars. A hydraulic jack supported on a hinged frame was used to apply the axial load. The hinged frame allowed the movement of the hydraulic jack with column head during testing and thus helped in keeping the axial load constant throughout the test. Two separate RC footings, prestressed to the laboratory strong floor, were used to support the hinged frame. Before testing, each specimen was aligned in such a way that the centerline of the column coincides with the line of action of both lateral and axial load. After ensuring proper alignment, each specimen footing was prestressed to the laboratory strong floor using four dywidag bars.

The load was simulated in the laboratory by dividing the loading scheme into two main phases; load-controlled phase and displacement-controlled phase (Fig. 3.10). The load control phase included two cycles; cracking and service cycle where the rate of applied lateral load was maintained at 20 kN/min. The cracking cycle was used to determine the cracking load and loading was continued until the first crack was observed visually. The second cycle represented the service loading condition which is 60% of the yield strain for steel bars (CSA/A23.3-14a). In the displacement control phase, the loads were applied in a quasi-static displacement control mode following the recommendation of ACI committee 374 report on the acceptance criteria for moment resisting frames based on structural testing (ACI 374.1-05). In practice, the RC buildings are

designed to have less applied seismic drift than the specified allowable drift mentioned in National Building Code of Canada (NBC 2015) i.e. 2.5%. However, the structures might experience higher drifts during an earthquake event than the designed one. For the displacement-controlled phase, quasi-static drift reversals were applied in a cyclic manner to ensure the gradual increment of applied displacement. Each drift step in displacement-control phase was applied in three identical cycles. To monitor the stiffness degradation of the specimens at different seismic loading stage, one load-controlled cycle with peak load equal to service load was applied after each drift step. Figure 3.11 shows an actual image of test setup.

Two specimens were damaged up to 2.5% drift ratio and then retested after rehabilitation; two specimens were tested up to failure before and after rehabilitation and two specimens were strengthened in as-built condition and then tested following the loading scheme discussed above.

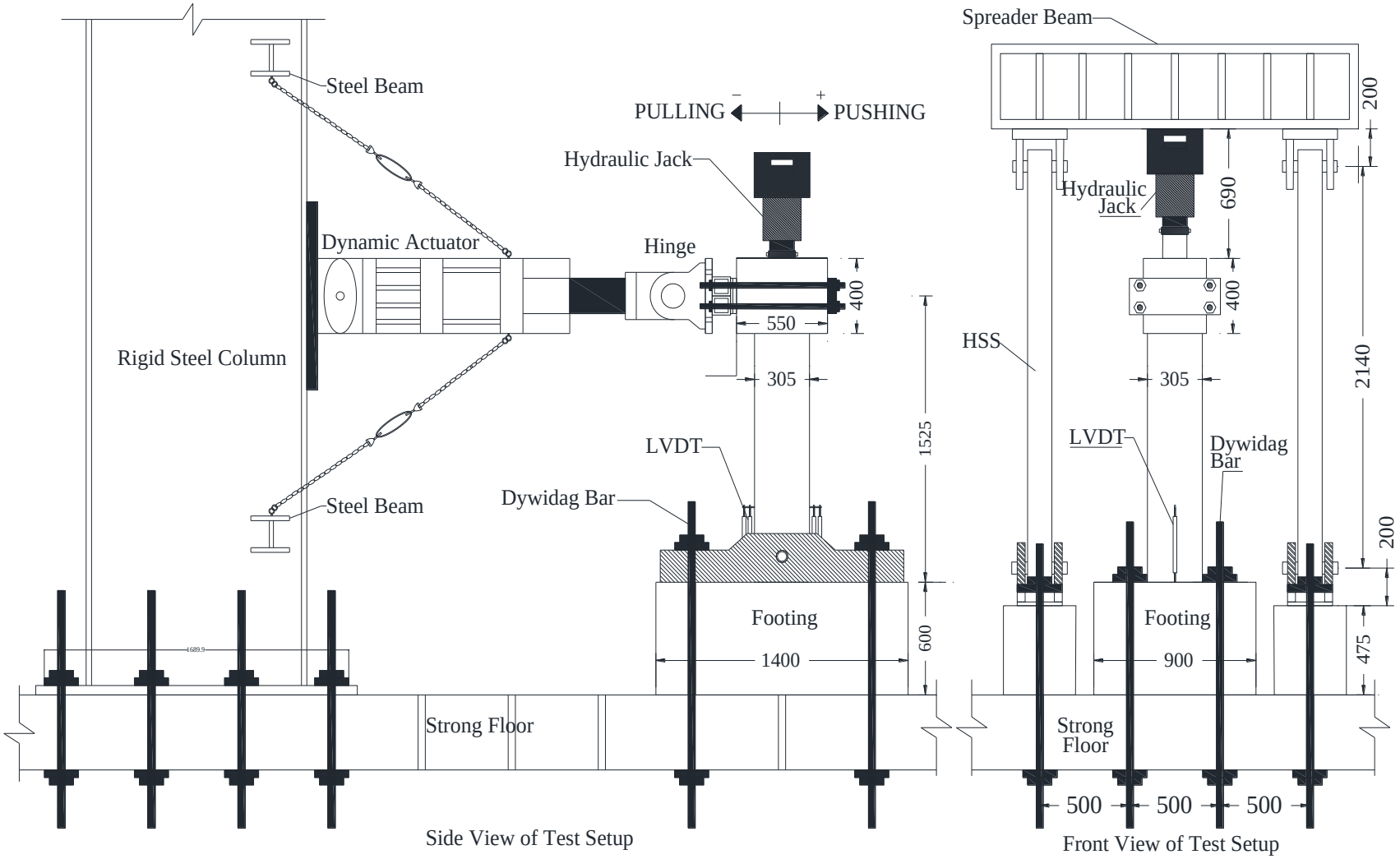

Figure 3.9: Test setup (all dimensions in mm)

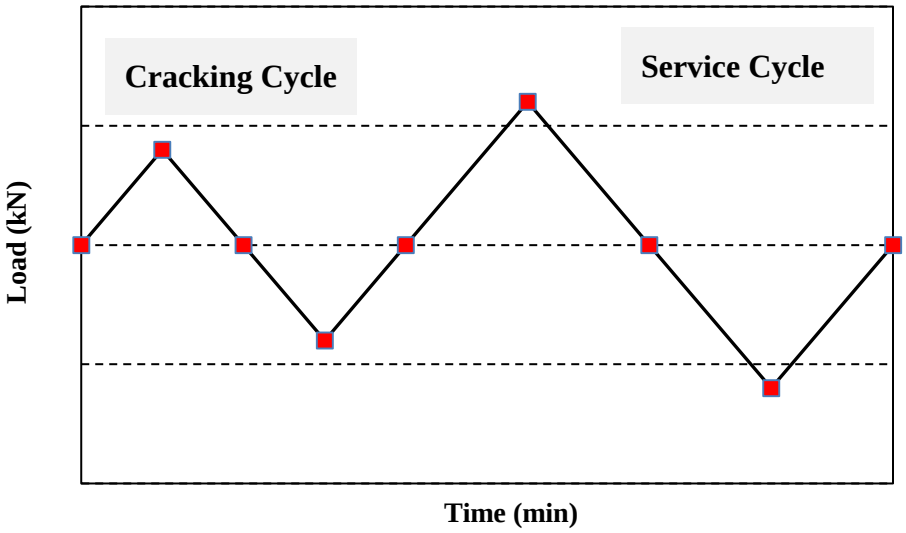

(a) Load-controlled phase (Phase 1)

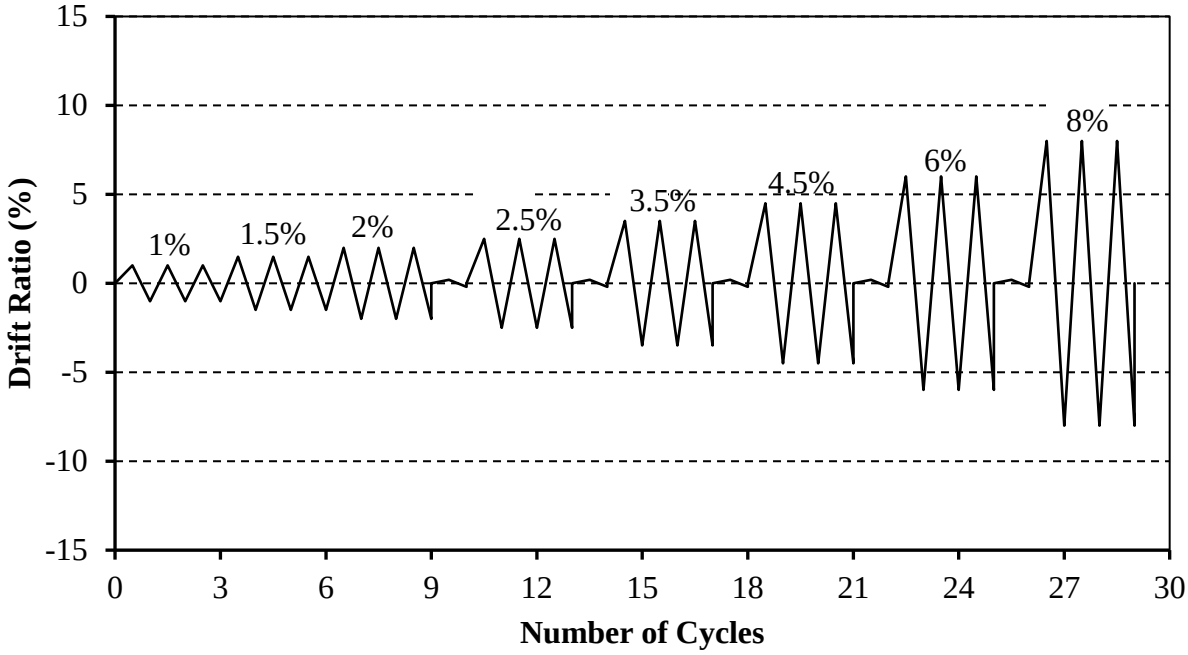

(b) Displacement-controlled phase (Phase 2)

Figure 3.10: Loading scheme

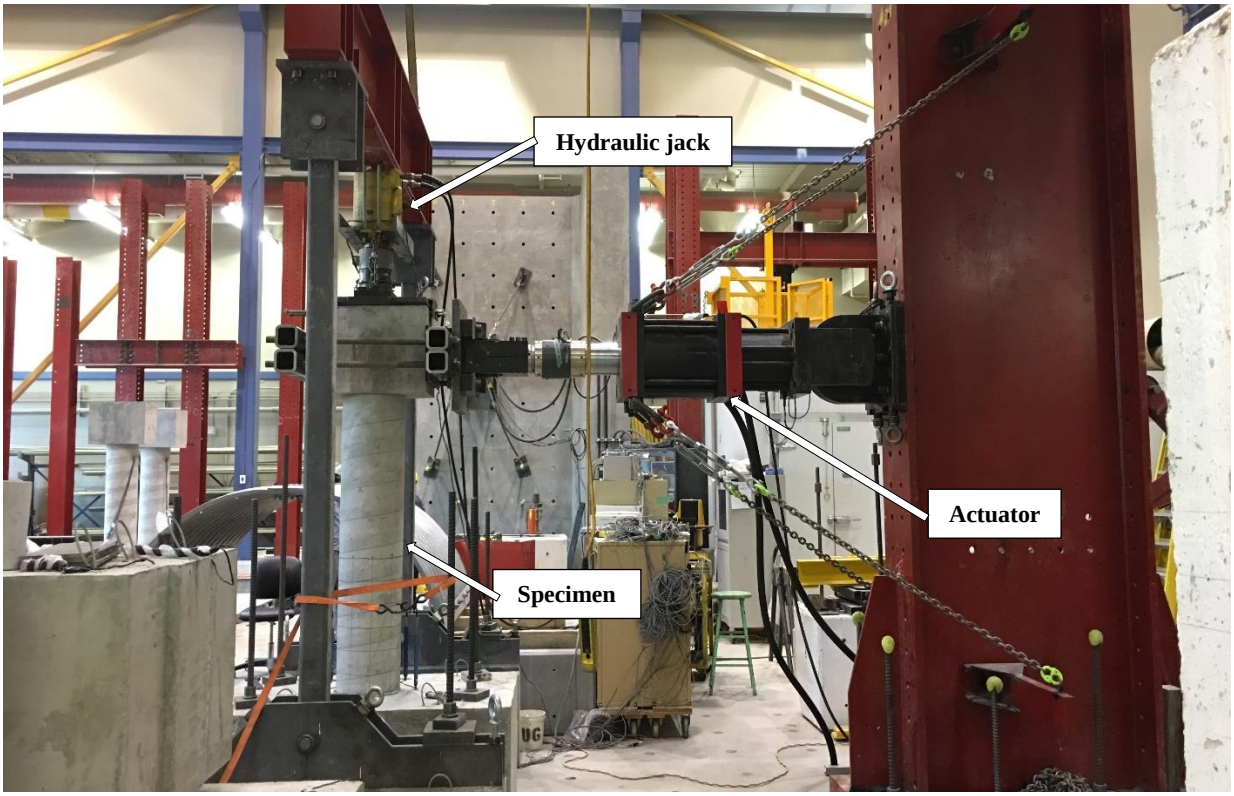

Figure 3.11: Actual test setup

3.7.2. Sprayed-GFRP samples

Sprayed-GFRP samples were pulled off each column specimen after testing to determine the actual fibre content in the composite. Samples were collected from the plastic hinge region. First the density of collected samples were determined by water displacement method. Data for fibre density and resin density were collected from material safety data sheet. Using Equation 3.1, the fibre content in actual samples were determined and results are presented in Table 3.6.

$$R_f = \frac{\frac{\rho_x}{\rho_c} - 1}{\frac{\rho_x}{\rho_f} - 1} \times 100 \qquad \text{Equation 3.1}$$

where,

R_f : Fibre concentration;

ρ_x : Matrix density;

ρ_c : Composite density;

ρ_f : Fibre density.

Table 3.6: Fibre content from density analysis

Specimen	Fibre density (g/cm^3)	Matrix density (g/cm^3)	Composite density (g/cm^3)	Fibre content (%)
I1-3	2.6	1.051	1.305	32.7
D1-3			1.268	28.6
PD1-3			1.337	35.9
I2-6			1.268	28.7
D2-6			1.346	36.8
PD2-6			1.328	35.1

Moreover, similar samples of 2-gram weight were used to determine fibre content following "Burn off" method according to ASTM D2584 (Fig. 3.12). Apparatus used in this test were 35-ml crucibles, digital scale (Fig. 3.12b) and electric furnace (Fig. 3.12d). First the empty weight of crucible was determined using digital scale. Then the sample was put in the crucible and the combined weight was recorded (Fig. 3.12a). Difference of these two weights is the weight of composite sample (w_c). Then the crucible with sample in it was put in the electric furnace and the temperature was set for 550ºC. The sample was kept at 550ºC for 1 hour and then it was left to cool down to room temperature. At this point all the resin was burnt off from the sample and only fibre was left inside the crucible (Fig. 3.12c). Then weight of fibres along with crucible was recorded. By deducting crucible weight from this weight, weight of fibre (w_f) in collected sample

was determined. Then equation 3.2 was used to determine fibre content "R_f". Table 3.7 shows the results obtained from this test. Here "AS" and "OS" indicates that the sample was collected from actuator side and opposite side considering the orientation of the specimen while testing.

$$R_f = \frac{w_f}{w_c} \times 100 \qquad \text{Equation 3.2}$$

Table 3.7: Fibre content from Burn-off test

Sample	Crucible weight (gm)	Crucible + Sample weight (gm)	Crucible + fibre weight (gm)	Fibre content (%)
PD1-3 (AS)	21.28	23.19	21.85	29.7
PD1-3 (OS)	20.28	22.38	20.84	26.7
D1-3 (AS)	20.35	22.33	20.89	27.6
D1-3 (OS)	20.92	22.17	21.29	29.4
I1-3 (AS)	21.09	23.09	21.64	27.36
I1-3 (OS)	20.37	22.14	20.83	26.07
PD2-6 (AS)	20.37	22.42	20.89	25.6
PD2-6 (OS)	21.09	23.43	21.77	28.8
D2-6 (AS)	21.1	23.32	21.75	29.3
D2-6 (OS)	20.37	23.01	21.17	30.4
I2-6 (AS)	21.1	23.64	21.79	27.1
I2-6 (OS)	20.37	22.91	21.1	28.6

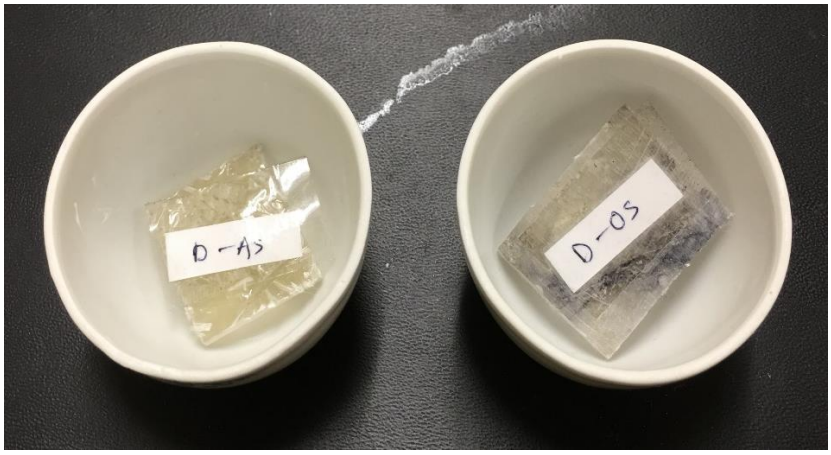

(a) Sprayed-GFRP samples

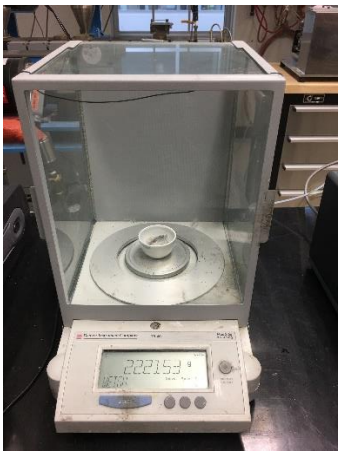

(b) Digital scale

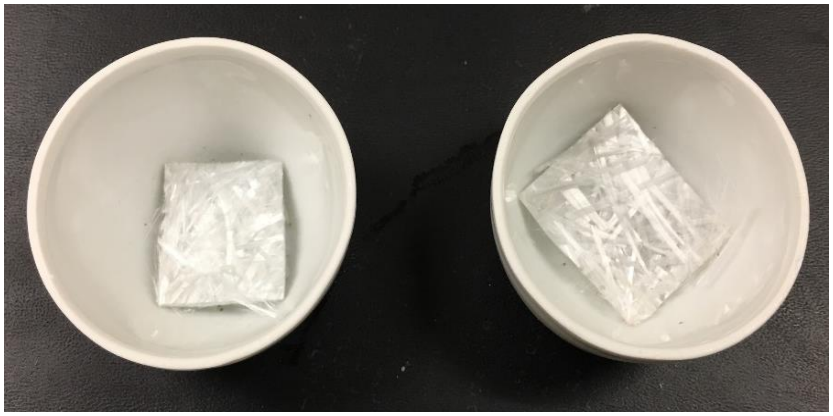

(c) GFRP fibres

(d) Electric furnace

Figure 3.12: Burn-off test to determine fibre content

3.7.3. Strengthened cylinders

Three cylinders of 100-mm diameter and 200-mm height were strengthened using sprayed-GFRP composite (Fig. 3.13a). While spraying the targeted thickness was 6-mm. After spraying, the cylinders were left for curing for one week. Some portion from top and bottom of the strengthened cylinders were cut off to get specimen with effective sprayed-GFRP confinement. These cylinders along with other three control concrete cylinders (cast on the same day and with same batch of

concrete) were tested under uni-axial compression until failure (Fig. 3.13b). ASTM C39/C39M method was followed in this test (Fig. 3.13c). Results obtained for the strengthened cylinders were multiplied by correction factors based on their aspect ratio (height/diameter) following ASTM C42. Data from this test was used to calculate the ultimate tensile strength of sprayed-GFRP composites as shown in Table 3.8. The following steps were followed to calculate the ultimate strength of sprayed-GFRP (ISIS 2008):

- First confined concrete strength (f'_{cc}) was determined from following equation, cylinder axial capacity,

$$P = k_e \phi_c \alpha_1 f'_{cc} A_g \qquad \text{Equation 3.3}$$

Where, k_e = reduction factor = 1; ϕ_c = 1; α_1= 0.85 - 0.0015 f'_c; A_g= cross sectional area;

- For known confined concrete strength, confining pressure (f_{lfrp}) was calculated from equation 3.4,

$$f'_{cc} = f'_c + 2f_{lfrp} \qquad \text{Equation 3.4}$$

Here, f'_c= unconfined concrete compressive strength = 43.52 MPa.

- Now ultimate strength f_{ufrp} was determined using equation 3.5,

$$f_{lfrp} = \frac{2t\phi f_{ufrp}}{D} \qquad \text{Equation 3.5}$$

Where, t = spray thickness; ϕ = reduction factor = 1; D = diameter of cylinder = 100 mm.

Table 3.8: Ultimate strength of sprayed-GFRP composites from cylinder tests

Sample	t (mm)	Axial Capacity (N)	f'_{cc} (MPa)	f_{lfrp} (MPa)	f_{ufrp} (MPa)	Avg (MPa)
1	6	678894.2	110.153	33.31652	277.6377	
2	6	616703.7	100.0624	28.2712	235.5934	235.7882
3	6	555377.8	90.11206	23.29603	194.1336	

(a) Strengthened cylinders

(b) Cylinders after test

(c) Testing of strengthened cylinders

Figure 3.13: Compressive strength test of strengthened cylinders

CHAPTER 4 – RESULTS AND DISCUSSION

4.1 General Behaviour

Figures 4.1 to 4.3 show the failure mode of all specimens. Specimen D1-0 and D2-0 showed similar behaviour throughout the test. For D1-0 the first crack appeared at a lateral load of 37 kN at a distance of approximately 330 mm from footing surface whereas for D2-0 the first crack was found roughly 350 mm above the footing surface at 35 kN. With the increasing load both specimens showed several evenly distributed cracks within a distance of 700 mm from the footing surface up to service cycle. These crackes mainly followed the position of spiral reinforcement. For both specimens, concrete cover spalling started at 2.5% drift ratio at the hinging region (300 mm from footing surface); at 3.5% drift ratio, the longitudinal reinforcement was exposed due to the spallinlg of concrete cover and at 4.5% drift ratio, core concrete crushed at the footing-column interface and both specimens failed (Fig. 4.1a and Fig. 4.1c). No bar slippage was observed during the failure. Collected data also imply proper stress transfer between column longitudinal bar and starter bars. After patching with cement mortar and rehabilitating specimen D1-0 with 3-mm and specimen D2-0 with 6-mm thick sprayed-GFRP composite, both specimens were tested under same loading scheme. Rehabilitated specimen D1-3 failed suddenly by rupture of sprayed-GFRP at the first service cycle while pushing (Fig. 4.1b). The fracture occurred vertically at hinging region with a length around 300-mm. No concrete crushing was visible during the failure. Confiment on pulling side failed in a similar manner but at 6% drift ratio. At 8% drift rario, crushing of repaired concrete was observed along with widening of fracture of the sprayed-GFRP confinement. Specimen D2-6 showed the first crack at 4.5% drift ratio at footing-column interface. The crack horizontally propagated at higher drift cycles on both pulling and pushing side. At the last cycle of 8% drift ratio, the specimen failed without any large crack and abrupt rupture in the

confinement. Failure of the specimens lateral load carrying capacity mainly occurred due to flexural comporession failure of the sprayed-GFRP layer at footing-column interface (Fig. 4.1d).

(a)

(b)

(c)

(d)

Figure 4.1: Failure mode of specimen (a) D1-0 (b) D1-3 (c) D2-0 (d) D2-6

Specimen PD1-0 showed first crack at 35 kN at a distance approximately 180 mm from footing surface. But for specimen PD2-0 the first crack appeared at 24 kN nearly at a height of 250-mm on column surface. However, with the continuation of the test both specimen showed almost similar generation and propagation of cracks with in a distance of 700 mm from the footing surface. Both PD1-0 and PD2-0 were tetsed up to 2.5% drift ratio and both specimen showed small degree of concrete spalling in the plastic hinge region. After retrofitting, specimen PD1-3 was tested up to failure. The first visible crack on sprayed confinement was observed at 4.5% but the specimen ultimately failed at 8% drift ratio (Fig. 4.2 a). Fibre pullout and fibre rupture was observed along the cracked confinement. Specimen PD2-6 also showed the first crack at 4.5% drift ratio. However, the crack was horizontal and it originated at footing-column interface. Specimen failed at the last cycle of 8% drift ratio (Fig. 4.2b). Failure pattern was almost similar to specimen D2-6 i.e., no large crack or rupture of sprayed-GFRP confinement was observed except a horizontal crack along the base of the column.

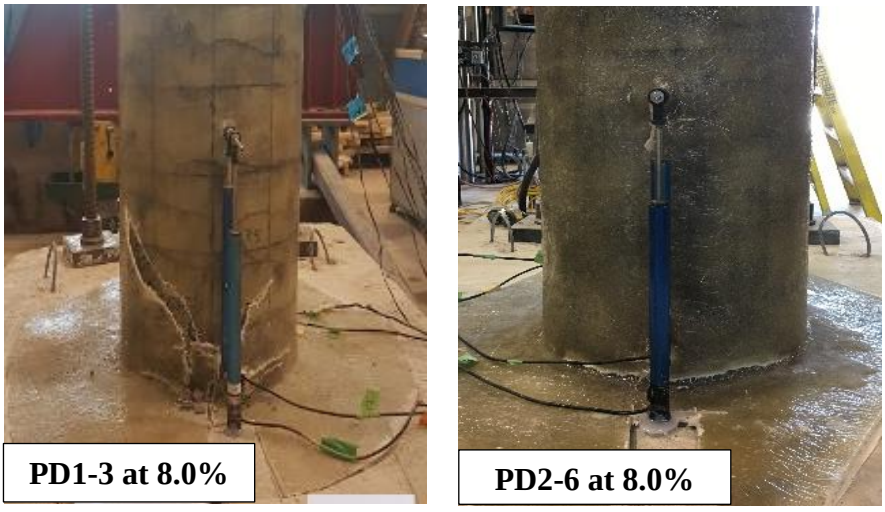

(a) (b)

Figure 4.2: Failure mode of specimen (a) PD1-3 (b) PD2-6

For specimen I1-3, the first visible crack on sprayed-GFRP coating was observed near the footing surface at 4.5% drift. It initiated from the location of threaded bars which were embeded in column surface for rotation measurement. Speciemn failed at 6% drift by simultaneous rupture of sprayed-GFRP coating and concrete crushing (Fig. 4.3a). The fracture occurred vertically and it propagated around 200 mm from the bottom of the column. Little amount of fibre rupture and fibre pullout was observed along the fractured coat. Internal reinforcement was exposed due to concrete crushing. Specimen I2-6 showed the first horizontal crack at 6% drift ratio at footing-column interface. However, it mainly failed by simultaneous fibre rupture and pullout in the confinement at 8% drift ratio (last cyale) (Fig. 4.3b). The rupture pattern was almost similar to specimen I1-3 but it was narrower and shorter (around 150-mm). No concrete crushing was visible except spalling of cover concrete was observed when a portion of confinement was removed to collect sprayed-GFRP samples.

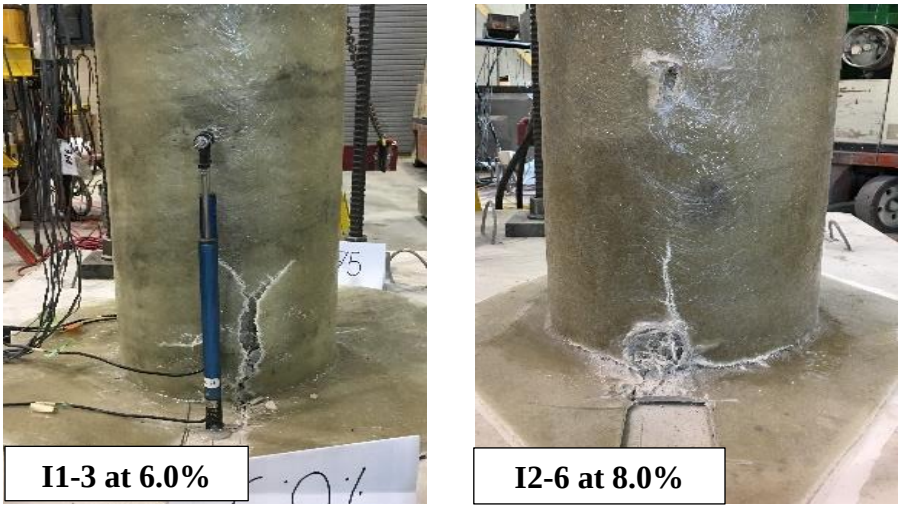

(a) (b)

Figure 4.3: Failure mode of specimen (a) I1-3 (b) I2-6

4.2 Hysteretic Response

All specimens were tested in the same orientation (same pushing and pulling directions) before and after rehabilitation. As depicted in Fig. 4.4, Fig. 4.5a and Fig. 4.5c, specimen D1-0 and D2-0 showed similar lateral load-drift response until failure. The lateral load capacity was nearly constant from 1.5% drift ratio to 3.5% drift ratio. For specimen D1-0, maximum lateral load of +77.5 kN (pushing) and -85.4 kN (pulling) was observed at 3.5% drift ratio. In case of specimen D2-0, the recorded maximum lateral load was +81.9 kN (pushing) and -84.6 kN (pulling) at 2% drift ratio. For both specimens, the lateral load capacity decreased by 25% at the last cycle of 4.5% drift ratio and the column failed by concrete crushing while pushing. Both sides were repaired but more concrete crushing was observed in pushing. The sprayed-GFRP system of 3-mm thickness was unable to restore lateral load capacity as depicted in Fig. 4.5b. In case of specimen D1-3, the strengthening system ruptured at +43.2 kN while pushing which is 44.3% lower than column actual capacity. However, on pulling side the lateral load resistance increased up to -77.2 kN (at 6% drift ratio) which is 8.5% less than that of specimen D1-0. Sprayed-GFRP of 6-mm thickness (D2-6) was not only able to restore the original capacity of the column (pushing side) but it also increased lateral load capacity by 12.3% (pulling side) (Fig. 4.5d). While pushing, the lateral load resistance gradually increased up to +66.2 kN at 3.5% drift ratio and in pulling side it gradually increased up to -95.1 kN at 6% drift ratio. At 8% drift ratio, specimen failed in flexure when the lateral load capacity dropped by 34%.

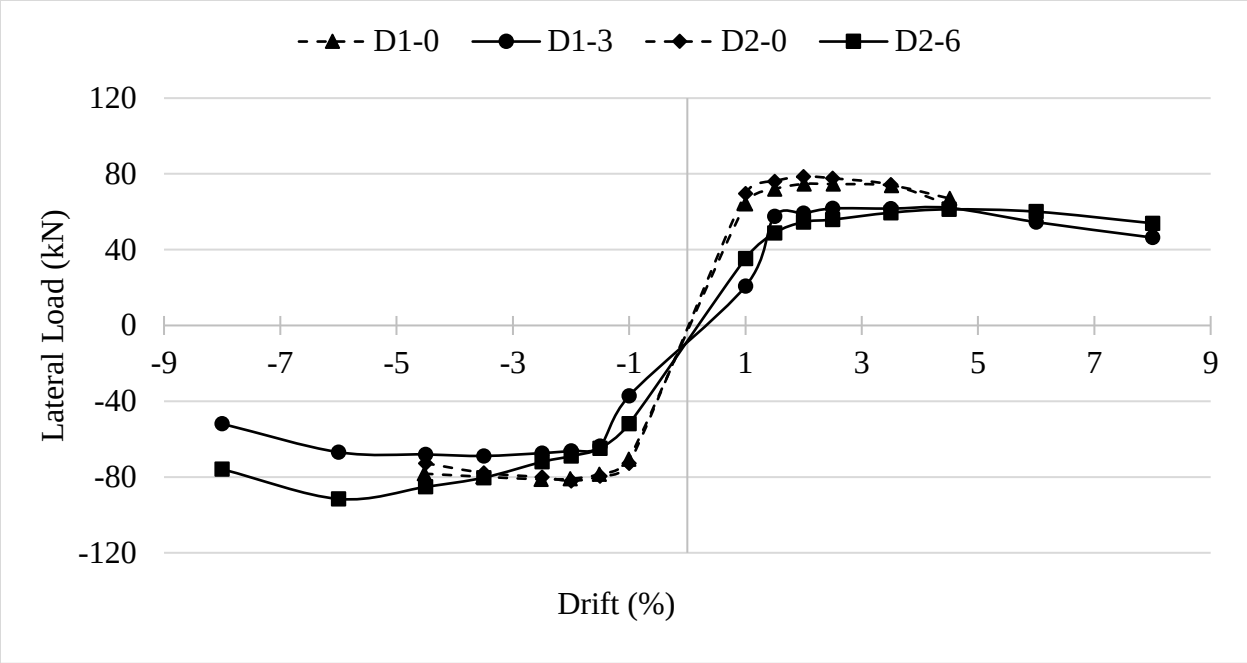

Figure 4.4: Lateral load-drift envelop of specimen D1-0, D1-3, D2-0 and D2-6

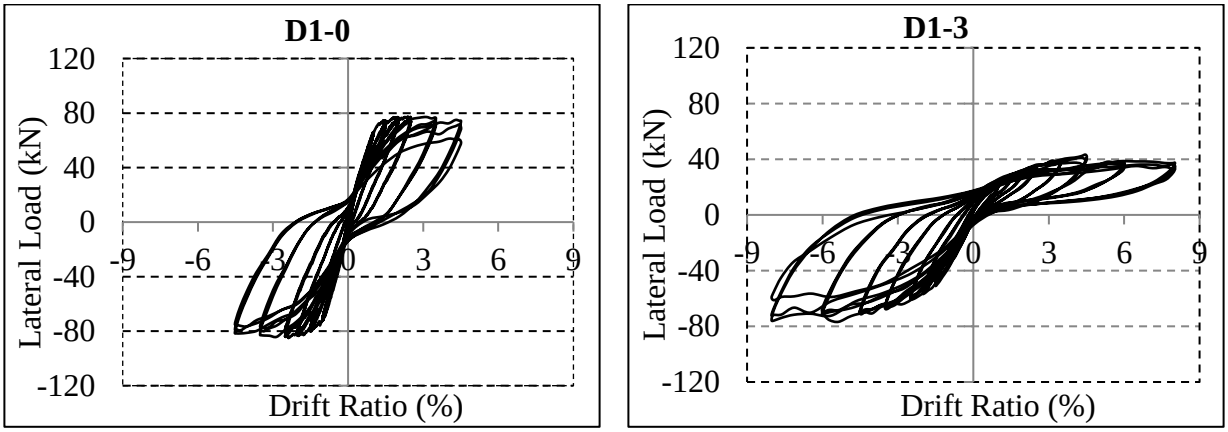

(a) (b)

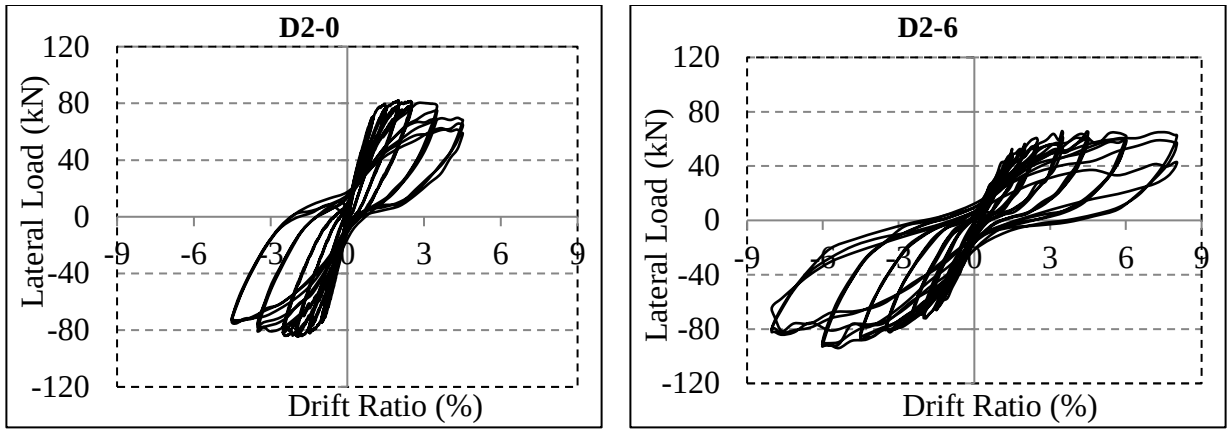

(c) (d)

Figure 4.5: Lateral load vs drift ratio response (a) D1-0 (b) D1-3 (c) D2-0 (d) D2-6

Both specimens PD1-0 and PD2-0 showed maximum lateral load at 2% drift ratio. For specimen PD1-0 maximum lateral load was recorded as +87.1 kN and -77.2 kN (Fig. 4.7a) whereas for specimen PD2-0 maximum lateral load was found +87.8 kN and -91.4 kN (Fig. 4.7c). Patching was carried out on both sides to regain original shape. After rehabilitation with 3-mm sprayed-GFRP i.e., for specimen PD1-3 the maximum lateral load resistance decreased by 8.7% while pushing (+79.5 kN at 4.5% drift ratio) but increased by 16.5% while pulling (-89.97 kN at 3.5% drift ratio) (Fig. 4.7b). However, sprayed-GFRP confinement of 6-mm (specimen PD2-6) increased maximum lateral load resistance in both direction; in pushing 7.6% (+94.6 kN at 6% drift ratio) and in pulling 24.3% (-113.6 kN at 4.5% drift ratio) (Fig. 4.7d). Specimen PD1-3 showed gradual increase in lateral load resistance up to 4.5% drift ratio (Fig. 4.6). After that, lateral load resistance was almost constant until failure. At the last cycle of 8% drift ratio lateral load capacity dropped by 25% in pulling direction. In case of specimen PD2-6, lateral load resistance gradually increased up to 4.5% drift ratio. At the last cycle of 8% drift ratio during pulling, lateral

load resistance dropped by 25% although there was no rupture or large crack on the confinement. Only a horizontal crack at footing column interface was visible at the end of the test.

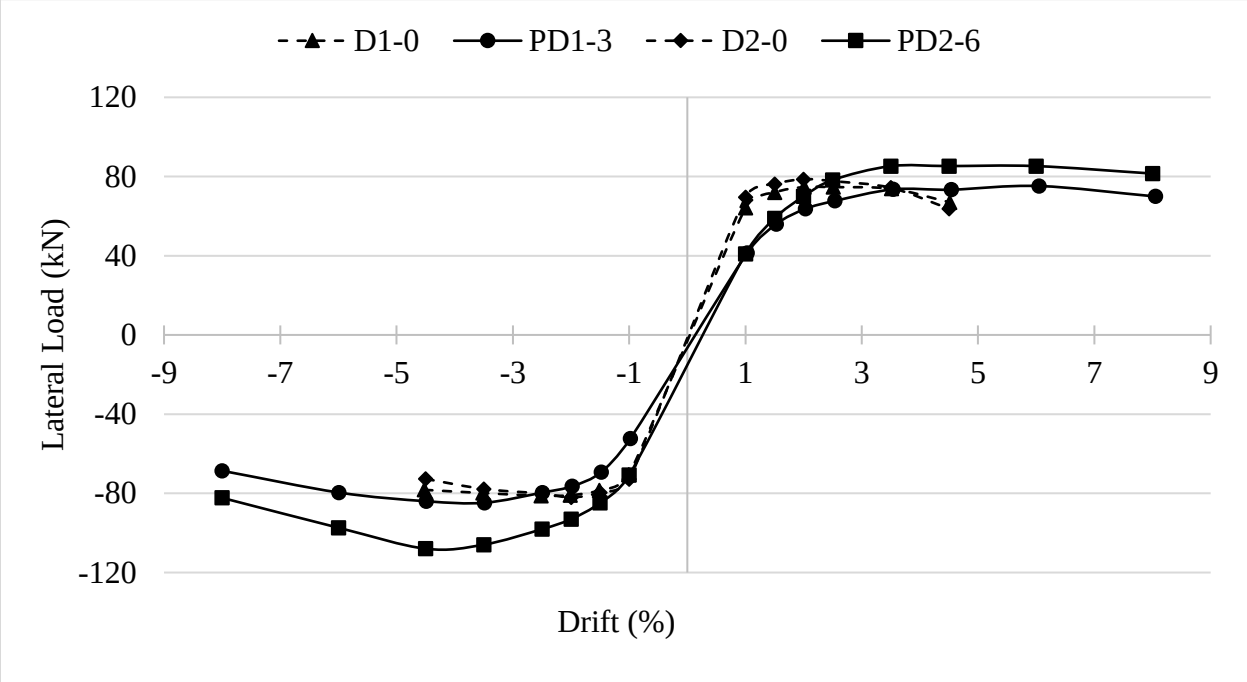

Figure 4.6: Lateral load-drift envelop of specimen D1-0, PD1-3, D2-0 and PD2-6

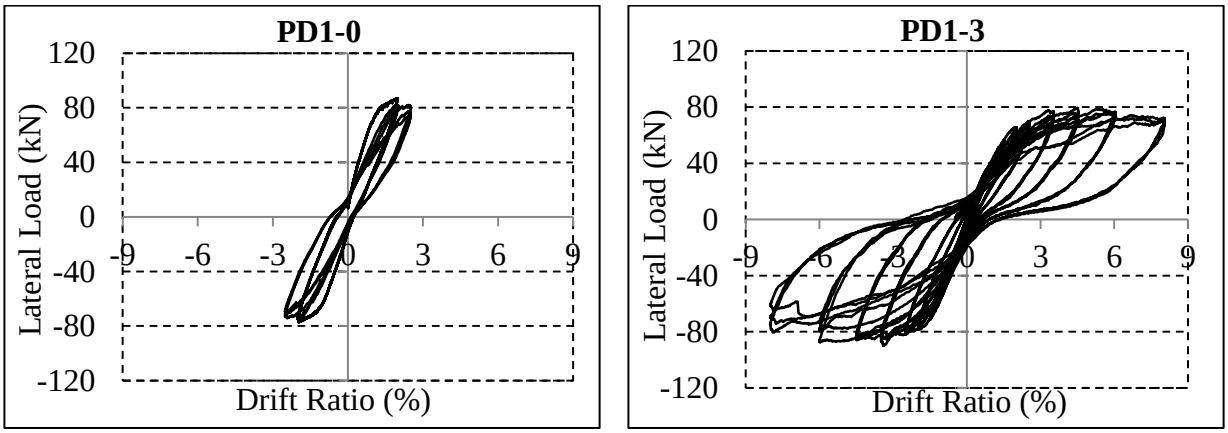

(a) (b)

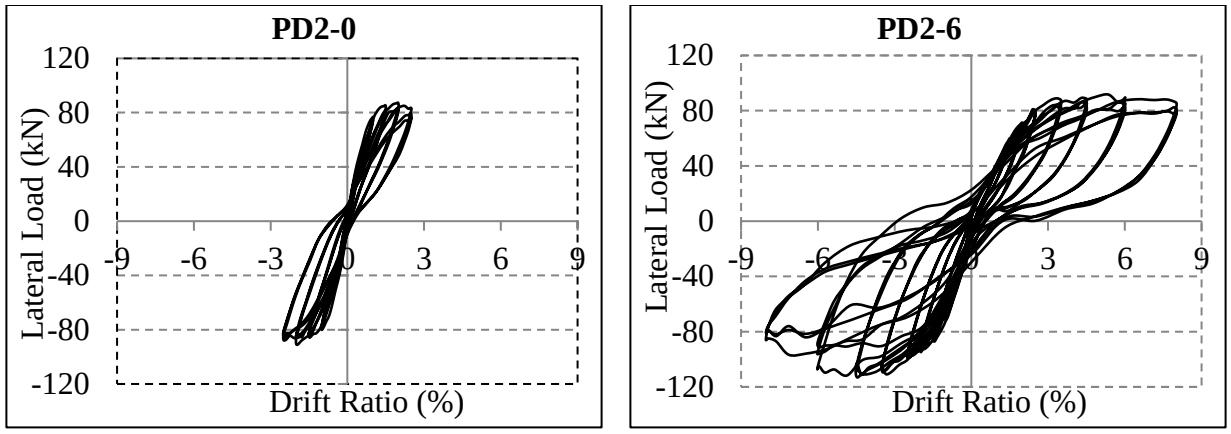

(c) (d)

Figure 4.7: Lateral load vs drift ratio response (a) PD1-0 (b) PD1-3 (c) PD2-0 (d) PD2-6

Specimen I1-3 showed similar behaviour to specimen D1-0 maintaining almost constant lateral load capacity up to last drift cycle starting from 1.5% drift ratio (Fig. 4.8). But it sustained the lateral load capacity till the second cycle of 6% drift ratio. At last cycle while pushing the lateral load resistance decreased by 26% as the sprayed-GFRP confinement ruptured. Maximum lateral load of +82.96 kN (pushing) and -91.8 kN (pulling) was recorded at 3.5% drift ratio (Fig. 4.9a). On average the sprayed-GFRP strengthening system increased the lateral load carrying capacity by 7.2% compared to the original column. Specimen I2-6 showed higher increase in lateral load capacity compared to specimen D2-0 (Fig. 4.8). While pushing maximum lateral load was recorded as +100.96 kN (at 4.5% drift ratio) and in pulling it was found -110.5 kN (at 6% drift ratio) (Fig. 4.9b). So, lateral load resistance increased by 23.5% (pushing) and 30.95% (pulling). Gradual increase in lateral load capacity was observed up to 6% drift ratio. At the last cycle of 8% drift ratio, specimen failed by confinement rupture and lateral load resistance dropped by 36% while pushing.

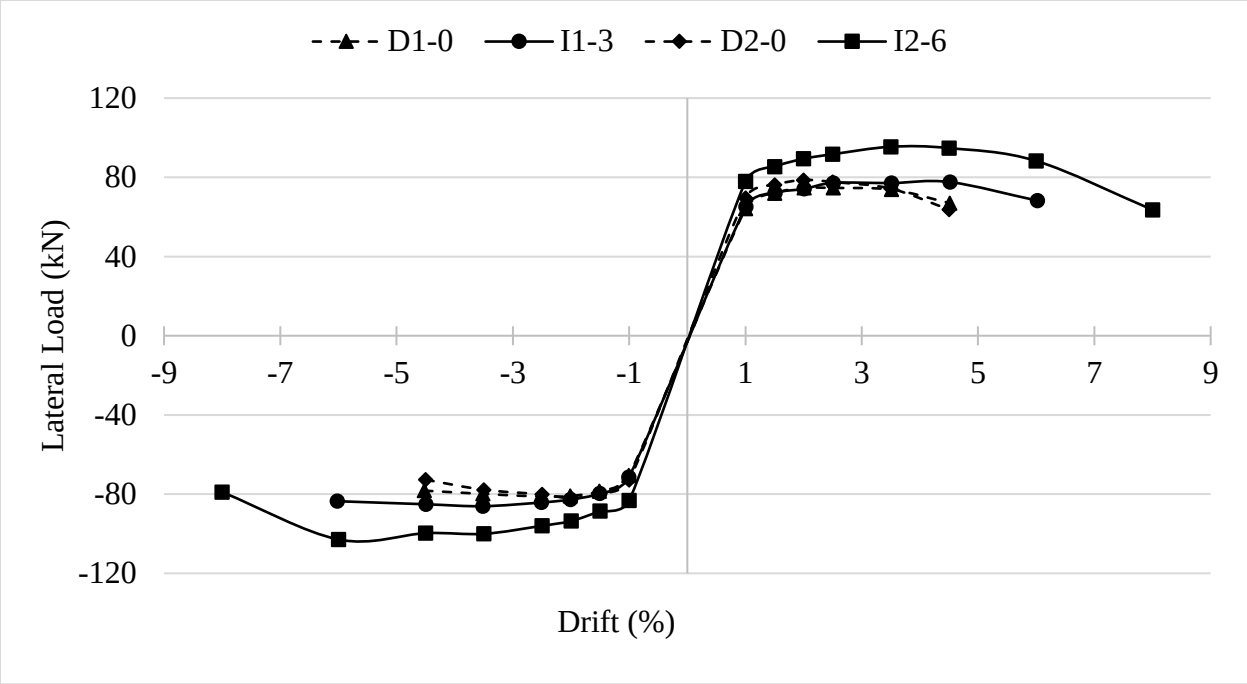

Figure 4.8: Lateral load-drift envelop of specimen D1-0, I1-3, D2-0 and I2-6

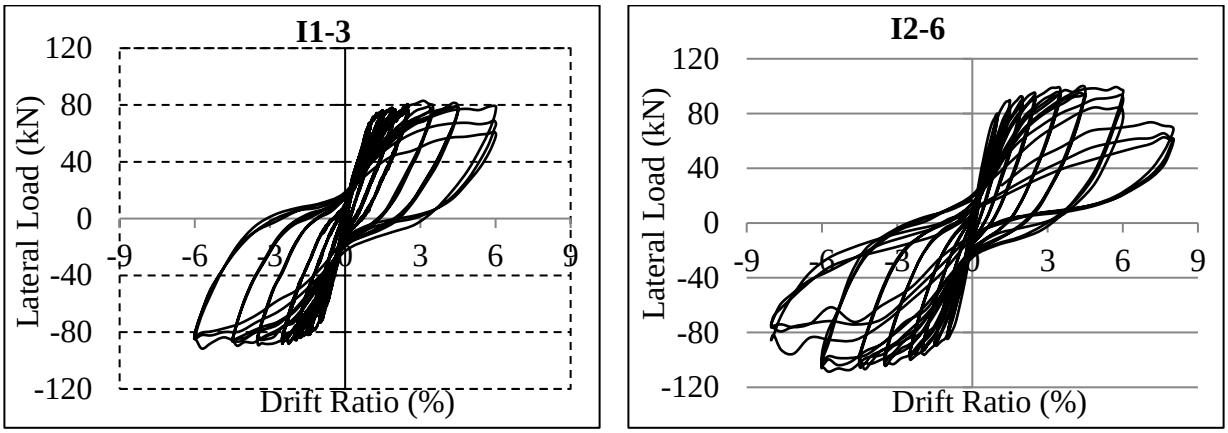

(a) (b)

Figure 4.9: Lateral load vs drift ratio response (a) I1-3 (b) I2-6

4.3 Cumulative Energy Dissipation

Figure 4.10 depicts the cumulative energy dissipation of the specimens in Phase-1 with corresponding drift ratio. Column strengthened with 3-mm thick sprayed-GFRP (I1-3) showed

11.3% higher cumulative energy dissipation at 4.5% drift ratio and overall it dissipated 77.9% higher energy before failure compared to specimen D1-0. Yielding of longitudinal steel accompanied by additional confinement provided by sprayed-GFRP might be responsible for this behavior. The 3-mm thick sprayed GFRP system (D1-3) was not able to partially or fully restore the original capacity of fully damaged column (D1-0). The confinement failed at first service cycle. Speicmen rehabilitated with 3-mm sprayed-GFRP after being partially damaged (PD1-3) showed considerably higher cumulative energy dissipation than all other specimens in series-I although at 4.5% drift ratio it was 12.3% lower than specimen D1-0 and 21.2% lower than specimen I1-3. Again at 6% drift ratio, specimen PD1-3 showed 20% lower energy dissipation than specimen I1-3. However, the calculated cumulative energy dissipated by PD1-3 was found 116% and 21.4% higher than specimen D1-0 and I1-3, respectively as it went up to 8% drift ratio. This behavior might be the result of improper stress transfer by repaired concrete on column surface up to 4.5% drift ratio. After that the sprayed-GFRP confinement became active due to bulging of concrete and started contributing in increasing energy dissipation capacity.

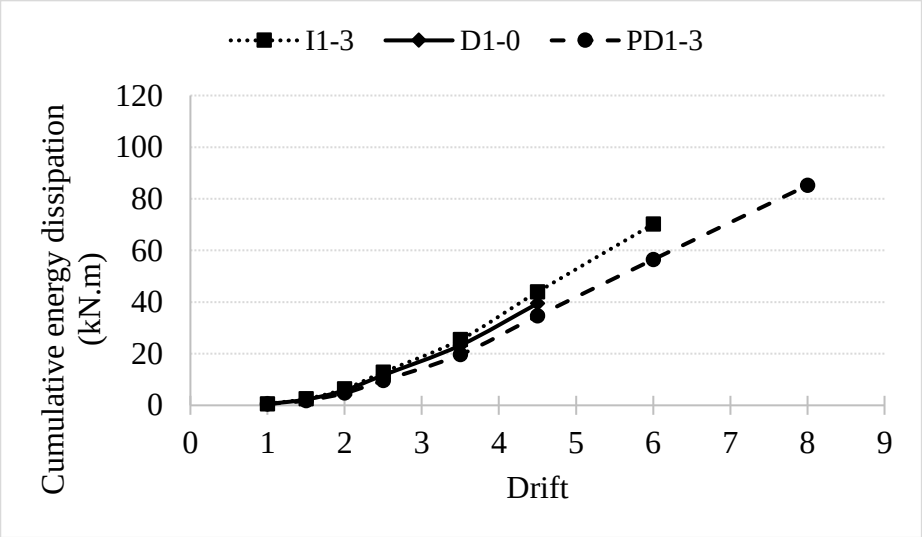

Figure 4.10: Cumulative energy dissipation of the specimens in Phase-1

Figure 4.11 shows the cumulative energy dissipation response of specimens in Phase-2. Similar to specimens in Phase-1, specimen I2-6 showed higher energy dissipation than the control specimen (D2-0) from the initial drift ratios. At 4.5% drift ratio it showed 28% and overall 175.3% higher energy dissipation than specimen D2-0. 6-mm thick sprayed-GFRP was found adequate to restore original capacity of fully damaged column (D2-0). Specimen PD2-6 showed similar energy dissipation to specimen D2-0 up to 4.5% drift ratio (failure of D2-0). However, PD2-6 failed at 8% drift ratio, thus dissipated 155% higher energy than specimen D2-0 at failure. For specimen D2-6, energy dissipation was found to be 20.5% lower than specimen D2-0 at 4.5% drift ratio. Similarly, D2-6 it went up to 8% drift ratio and cumulatively dissipated 102% higher energy than specimen D2-0 at failure. Again, this behaviour indicates improper stress transfer by repaired column surface up to 4.5% drift ratio. The GFRP confinement came into action when the cover concrete started to bulge and contributed in energy dissipation.

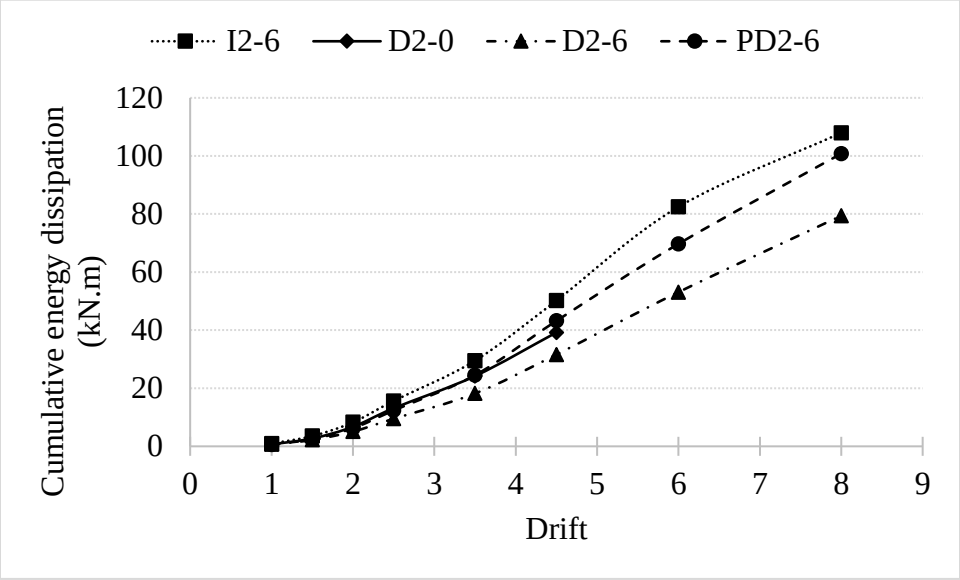

Figure 4.11: Cumulative energy dissipation of the specimens in Phase-2

4.4 Column Rotation Components

The total rotation of column due to seismic load consist of three main components; rotation due to main crack, rotation due to plastic hinge and rotation due to other components. The main crack develops at footing column interface also includes strain penetration (strain of column longitudinal bar that penetrates inside the footing) inside the joint. The plastic hinge was assumed to be formed with in a distance 350-mm from the footing surface. Cracks which were formed outside the plastic hinge region and column curvature was included in other components. One set of LVDT's recorded the column rotation with respect to footing surface. The total rotation of column was obtained from actuator drift data. Difference between these two data provided the rotation due to other components. Another set of LVDT's was used to measure the rotation of plastic hinge. Contribution of main crack in total rotation was calculated by taking the difference of the data gathered from two sets of LVDTs.

Figure 4.12 shows the rotational components of all specimens. For specimen D1-0, contribution of main crack (63.35%) was found higher than plastic hinge (21.46%) and other components (15.19%) as most of the concrete spalling was observed at footing column interface (Fig. 4.12a). After rehabilitation (specimen D1-3) the contribution of other components (5.8%) further decreased due to increased confinement in upper portion of column while the lower portion still experiencing the maximum moment (Fig. 4.12b). There were slight increase in plastic hinge formation at initial drifts due to sprayed-GFRP confinement but later it started decreasing as the confinement got ruptured. The rotational components for specimen D2-0 were found similar to the specimen D1-0 (Fig. 4.12c). However, after rehabilitation (specimen D2-6) the contribution of main crack was found slightly reduced (by 11.6%) indicating comparatively lower damage concentration at footing column interface (Fig. 4.12d). The contribution of plastic hinge formation

increased by 94% compared to specimen D2-0. Again, the proportion of rotation components for specimen PD1-0 (Fig. 4.12e) and PD2-0 (Fig. 4.12g) was recorded quite similar to specimen D1-0. After rehabilitation specimen PD1-3 showed increase in plastic hinge formation (by 55.5%) whereas the contribution of main crack got decreased (by 20%) (Fig. 4.12f). This resulted from increased confinement leading to reduced damage at footing-column interface. Similarly, the percentage of main crack was recorded decreased (by 33%) in specimen PD2-6 but the contribution of other components got increased (by 114%) (Fig. 4.12h). Because further increase in confinement distributed the damage over the length of the column. The rotational components for strengthened specimens I1-3 (Fig. 4.12i) and I2-6 (Fig. 4.12j) were found almost identical to control specimens D1-0 and D2-0, respectively. This behavior indicates that the confinement was moderately inactive at lower drift ratios. Although there in slight increase in plastic hinge formation for specimen I2-6 whereas the portion for main crack got decreased.

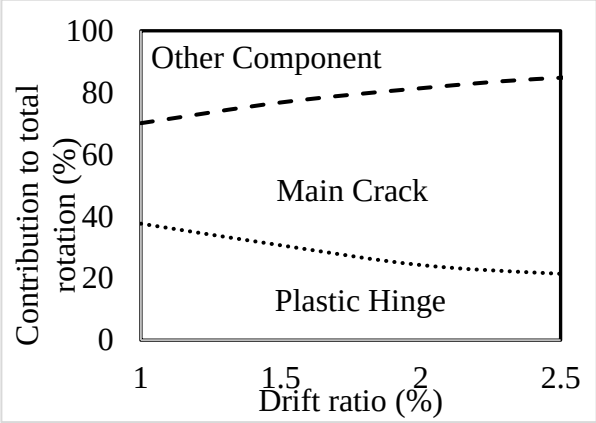

(a) D1-0

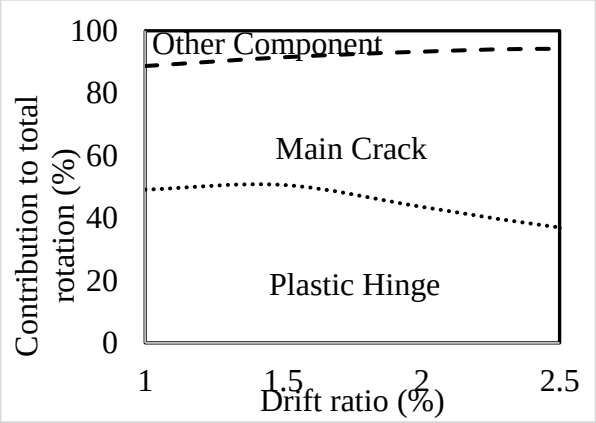

(b) D1-3

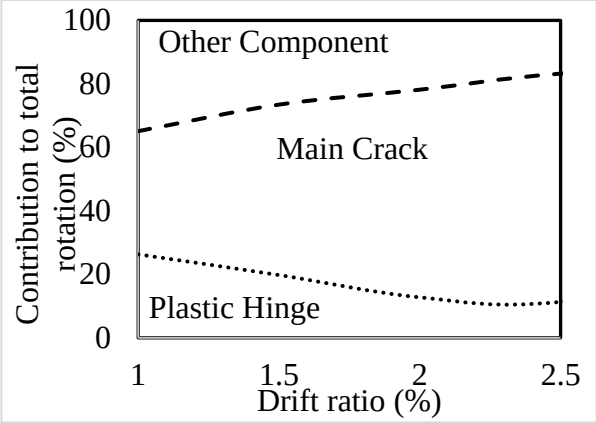

(c) D2-0

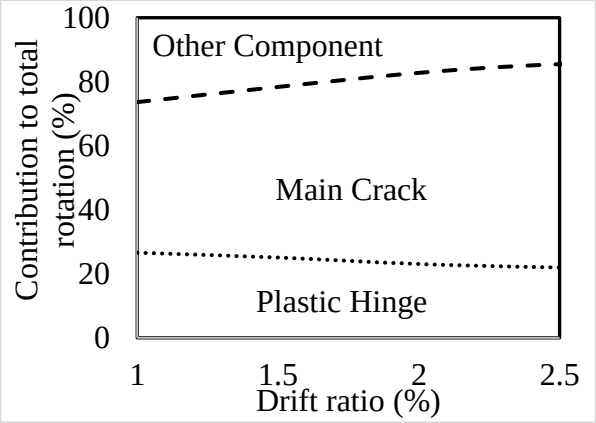

(d) D2-6

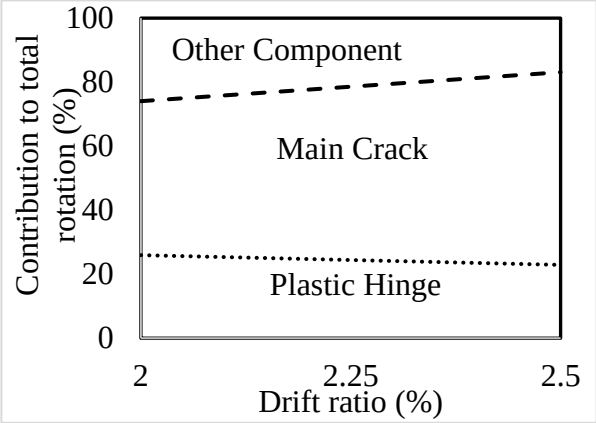

(e) PD1-0

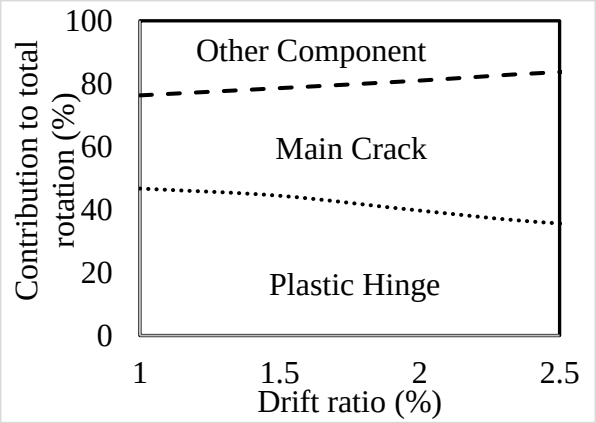

(f) PD1-3

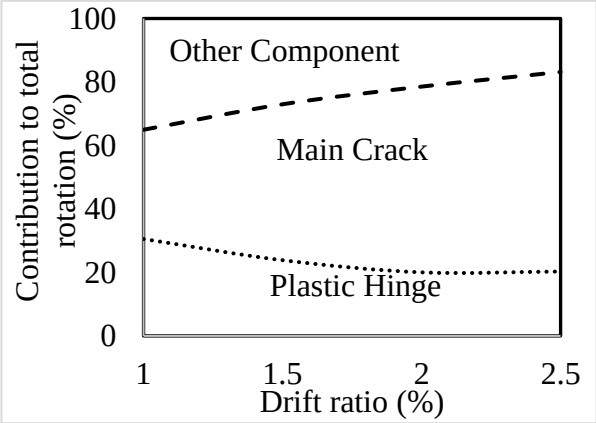

(g) PD2-0

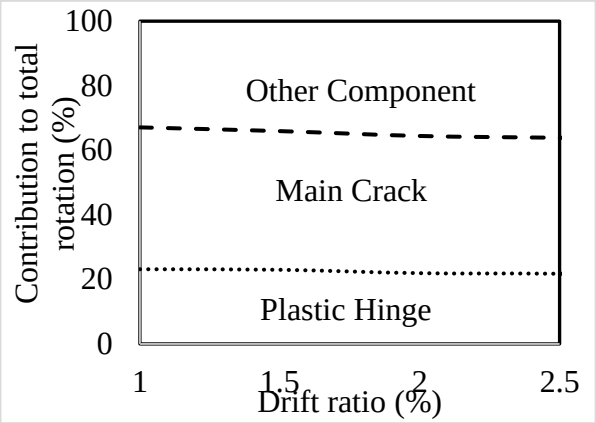

(h) PD2-6

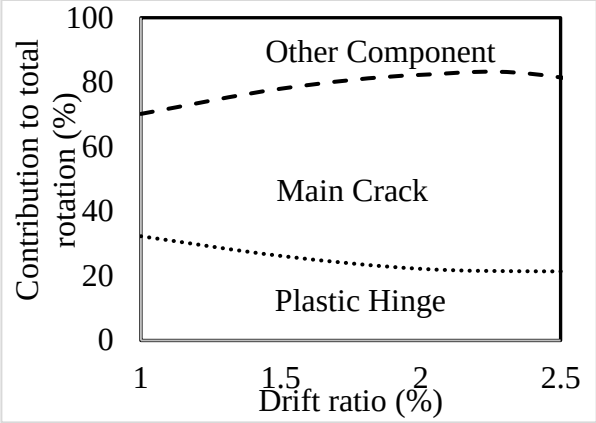

(i) I1-3

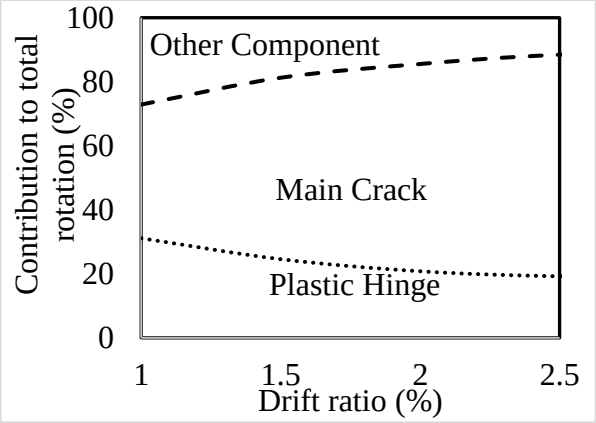

(j) I2-6

Figure 4.12: Column rotation components

CHAPTER 5 – CONCLUSIONS AND FUTURE WORK

5.1 Summary

Recent upgrade in seismic design standards and the alarming increase in earthquake hazard level have created some doubt on the seismic performance of existing structures. The FRP sheets wrapping technique has already been established as a sustainable repair and strengthening method for column rehabilitation due to superior characteristics of FRP materials (ACI 440.2R-17). However, this technique is relatively expensive, sensitive to rough concrete surface (require prior surface treatment) and its application is complicated on irregular structures (Karbhari 2007). The proposed retrofitting technique; sprayed-FRP composites system, has offered advantages compared to conventional FRP jackets, such as strong bond capacity, ease of construction and installation, and better cost effectiveness (Boyd 2000; Banthia and Boyd 2000). Sprayed-FRP confinement was reported to increase shear strength, ductility and energy absorption capacity of square columns (Lee et al. 2016; Peng et al. 2014). However, no research data is available on seismic behaviour of RC circular columns retrofitted with sprayed-FRP composites.

The seismic performance of steel-RC circular columns rehabilitated with sprayed-GFRP composites is investigated in this research program. Six large-scale RC circular columns were constructed and tested under simulated seismic loading. All column specimens have 305-mm diameter and 1,725-mm cantilever height (1,525-mm shear span). The specimen represents a portion of a column between the foundation and point of inflection in a building or a bridge. Two specimens were tested up to 2.5% drift ratio (design drift limit according to National Building Code of Canada (NBC 2015)) and other two specimens were tested up to failure before the application of sprayed-GFRP to serve as references. These four specimens were rehabilitated and then retested to failure. Two specimens were first sprayed with FRP composites, then tested up to

failure. It should be mentioned that maintaining a uniform thickness of sprayed-GFRP all around the column was a challenge as it depends on operators experience as well as many other factors (operation temperature, gun calibration. etc.). However, minimum targeted thickness was ensured while spraying at plastic hinge location.

The primary objective of this research was to evaluate the seismic response of deficient (in lap splice length) reinforced concrete circular columns retrofitted with sprayed-GFRP composites technique. Parameters included in this study were degree of damage and thickness of sprayed-GFRP composite.

5.2 Conclusions

Based on the experimental results, the following conclusions can be drawn:

- Increasing the sprayed-GFRP composites thickness from 3-mm to 6-mm significantly changed the failure pattern of the GFRP coat. At 3-mm thickness, sprayed-GFRP confinement failed abruptly, the fracture occurred vertically in the plastic hinge region and it was apparently wide. For 6-mm sprayed-GFRP, failure was gradual with a horizontal crack at footing-column interface and the crack width was significantly small.
- The GFRP-sprayed coat did not have a significant effect on the stiffness of the tested specimens. At initial drift ratios, rehabilitated fully-damaged and partially-damaged specimens showed less stiff response compared to original column. However, for strengthened intact specimen, stiffness at initial drift ratio was found similar to the original column.
- After rehabilitation, significant increase in energy dissipation capacity was observed for all specimens except for fully-damaged column rehabilitated with 3-mm thickness. Comparatively higher cumulative energy dissipation capacity was recorded when the

sprayed-GFRP thickness doubled. The 6-mm thickness sprayed-GFRP system showed approximately 153%, 42% and 98% higher cumulative energy dissipation than the 3-mm thickness counterpart for fully-damaged, partially-damaged and intact columns, respectively.

- For the 3-mm sprayed-GFRP coat, rehabilitated partially-damaged column (Specimen PD1-3) showed 21% higher cumulative energy dissipation than the strengthened intact column (Specimen I1-3) as the former went up to 8% drift ratio whereas the latter failed at 6% drift ratio only. Rehabilitated specimens with 6-mm sprayed-GFRP from fully-damaged (Specimen D2-6) and partially-damaged (Specimen PD2-6) condition showed similar cumulative energy dissipation which was approximately 16% lower compared to the strengthened intact (Specimen I2-6) column.
- Sprayed-GFRP composites can be used as a practical strengthening system for RC circular column in seismic regions. Although the observed increase in lateral load capacity for 3-mm thickness was only 7.2%, increasing the thickness to 6-mm increased the lateral load capacity by 27.2%. Also 3- and 6-mm thick sprayed-GFRP increased the drift capacity by 33.3% and 77.8%, respectively.
- Sprayed-GFRP system of adequate thickness (6 mm) can be used to rehabilitate fully-damaged columns after an earthquake event. Sprayed-GFRP of 3-mm thickness was found inadequate to restore the strength of seismically damaged RC columns. However, 6-mm thick sprayed-GFRP not only restored the full original capacity of the column but also increased the lateral load capacity by approximately 12%. Moreover, it increased the drift capacity by approximately 78%.

- Sprayed-GFRP composite system of 3- and 6-mm thickness increased the displacement capacity of partially-damaged RC circular column by 77.8% while maintaining almost same or higher lateral load carrying capacity. This new technique can be used to restore lateral load capacity and energy absorption capacity of partially-damaged columns of buildings and bridges in seismic region.

5.3 Future Work

The following are suggestions for further studies on seismic behaviour of deficient RC circular columns rehabilitated with sprayed-GFRP:

1. Study the effect of axial load on seismic behaviour of RC circular columns rehabilitated with sprayed-GFRP.
2. Analyze the behaviour of circular column deficient in spiral pitch and rehabilitated with sprayed-GFRP composites under seismic load.
3. Establish the optimum fibre length, fibre volume and fibre-resin mix ratio for circular columns rehabilitation in seismic region.
4. Use carbon and basalt fibre or combination of fibres to evaluate the effect of fibre type on behaviour of rehabilitated circular columns under seismic load.
5. Analyze the influence of different parameter related to application process such as, but not limited to:
    a) Gun speed.
    b) Height of the chopper and spray gun above the substrate.
    c) Offset distance and spray-fan pattern
6. Research on hybrid system; combination of FRP sheets and sprayed-FRP to optimize the performance of rehabilitated circular column by utilizing advantages from both technique.
7. Examine the feasibility of applying sprayed-FRP composites without any prior repair work or surface patching in circular columns rehabilitation.
8. Investigate the long-term behaviour of sprayed-GFRP composites used in circular columns rehabilitation under different environmental condition.

REFERENCES

ACI Committee 318. (2014). "Building code requirements for structural concrete (ACI 318-14) and commentary (318R-05)." *American Concrete Institute,* Farmington Hills, MI.

ACI Committee 374. (2005). "Acceptance criteria for moment frames based on structural testing and commentary." ACI 374.1-05, *American Concrete Institute,* Farmington Hills, MI.

ACI Committee 440. (2008) "Guide for the design and construction of externally bonded FRP systems for strengthening concrete structures." ACI 440.2R, *American Concrete Institute,* Farmington Hills, MI.

ACI Committee 440. (2017) "Guide for the design and construction of externally bonded FRP systems for strengthening concrete structures." ACI 440.2R, *American Concrete Institute,* Farmington Hills, MI.

ACI Committee 446. (2001). "Standard test method for determining fracture properties of concrete." ACI 446, *American Concrete Institute,* Farmington Hills, MI.

American Composites Manufactures Association (ACMA). (2004). "Composites open molding resin and gel coat application." *Controlled Spraying Handbook,* ACMA, Arlington, VA, 1-27.

Ali, M. and El-Salakawy, E. (2016). "Seismic performance of GFRP-reinforced concrete rectangular columns." *Journal of Composites for Concrete Construction,* 20(3): 04015074.

ASTM C1018. (1997). "Standard test method for flexural toughness and first-crack strength of fiber-reinforced concrete (using beam with third-point loading)." (Withdrawn 2006), *ASTM International*, West Conshohocken, PA.

ASTM C39/C39M. (2018). "Standard test method for compressive strength of cylindrical concrete specimens." *ASTM International*, West Conshohocken, PA.

ASTM C42/C42M. (2018). "Standard test method for obtaining and testing drilled cores and sawed beams of concrete." *ASTM International*, West Conshohocken, PA.

ASTM C78/C78M. (2018). "Standard test method for flexural strength of concrete (using simple beam with third-point loading)." *ASTM International*, West Conshohocken, PA.

ASTM D2584. (2011). "Standard test method for ignition loss of cured reinforced resins." *ASTM International*, West Conshohocken, PA.

Banthia, N. and Boyd, A. J. (2000). "Sprayed fibre-reinforced polymers for repairs." *Canadian Journal of Civil Engineering*, 27(5): 907-915.

Banthia, N., Nandakumar, N. and Boyd, A. (2002). "Sprayed fibre-reinforced polymers: from laboratory to a real bridge." *Concrete International*, 24(11): 47-52.

Bousias, S., Spathis, A. and Fardis, M. N. (2007). "Seismic retrofitting of columns with lap spliced smooth bars through FRP or concrete jackets." *Journal of Earthquake Engineering*, 11(5): 653–674.

Boyd, A. J. (2000). "Rehabilitation of reinforced concrete beams with sprayed glass fibre reinforced polymers." *PhD Thesis*, University of British Columbia, BC, Canada.

California Department of Transportation (1999). "Seismic design criteria: version 1.0." *Caltrans 1999*, Caltrans, Sacramento, Calif.

Canadian Standards Association (CSA). (2012). "Design and construction of building structures with fibre-reinforced polymers." CSA/S806-12, *Canadian Standards Association*, Toronto, Ontario, Canada.

Canadian Standards Association (CSA). (2014a). "Design of concrete structures." CSA/A23.3-14, *Canadian Standards Association*, Toronto, Ontario, Canada.

Canadian Standards Association (CSA). (2014b). “Concrete materials and methods of concrete construction / test methods and standard practices for concrete.” CSA/A23.2-14, *Canadian Standards Association*, Toronto, Ontario, Canada.

Canadian Standards Association (CSA). (2014c). “Canadian highway bridge design code.” CSA/S6-14, *Canadian Standards Association*, Toronto, Ontario, Canada.

Canadian Standards Association (CSA). (2016). “Welding of reinforcing bars in reinforced concrete construction.” CSA/W186, *Canadian Standards Association*, Toronto, Ontario, Canada.

Chail, Y. H., Priestley, M. J. N. and Seible, F. (1990). “Seismic retrofit of circular bridge columns for enhanced flexural performance.” *Structural Journal*, 88(5): 572–584.

Chajes, M. J., Thomson, T. A., Januszka, T. F. and Finch, W. W. (1994). “Flexural strengthening of concrete beams using externally bonded composite materials.” *Construction and Building Materials*, 8(3): 191-201.

Choi, J. (2008). “Seismic retrofit of reinforced concrete circular columns using stainless steel wire mesh composite.” *Canadian Journal of Civil Engineering*, 35(2): 140-147.

Choo, C. C. (2005). "Investigation of rectangular concrete columns reinforced or prestressed with fibre reinforced polymer bars or tendons." *Ph.D. Thesis*, University of Kentucky, U.S.A.

Considere, A. (1903). "Experimental researches on reinforced concrete." *McGraw Hill*, New York, U.S.A.

Ehsani, M. R. (1994). “Rehabilitation of the infrastructure with advanced composite materials.” *Repair and Rehabilitation of the Infrastructure of the Americas*, Proceedings of National Science Foundation, Mayaguez, Puerto Rico, 193-205.

Federal Highway Administration (FHWA) (2017) "National bridge inventory ASCII-2016." *Federal Highway Administration*, 1200 New Jersey Avenue, SE, Washington, DC 20590, U.S.A.

Furuta, T., Kanakubo, T., Nemoto, T., Takahashi, K. and Fukuyama, H. (2001). "Sprayed-up FRP strengthening for concrete structures." *Proceeding of International Conference on FRP Composites in Civil Engineering*, 2: 1109-1116.

Goksu, C., Yilmaz, H., Chowdhury, S. R., Orakcal, K. and Ilki, A. (2014). "The effect of lap splice length on the cyclic lateral load behavior of RC members with low-Strength concrete and plain bars." *Advances in Structural Engineering*, 17(5): 639-658.

Gu, D. S., Wu, G., Wu, Z. S. and Wu, Y. F. (2010). "Confinement effectiveness of FRP in retrofitting circular concrete columns under simulated seismic load." *Journal of Composites for Construction*, 14(5): 531-540.

Ha, S. K., Jang, J. G., Park, S. H. and Lee, H. K. (2014). "Advanced spray multiple layup process for quality control of sprayed FRP composites used to retrofit concrete structures." *Journal of Construction Engineering and Management*, 141(1): 04014060.

Harajli, M. H. (2006). "Axial stress-strain relationship for FRP confined circular and rectangular concrete column." *Cement and Concrete* Composites, 28: 938-948.

Harries, K. A. and Young, S. C. (2003). "Sprayed-fibre-reinforced composite materials for infrastructure rehabilitation." *Concrete International*, 25(1): 47-51.

Haroun, M. A. and Elsanadedy, M. H. (2005). "Fibre-reinforced plastic jackets for ductility enhancement of reinforced concrete bridge columns with poor lap-splice detailing." *Journal of Bridge Engineering*, 10(6): 749-757.

Hasegawa, T., Harimoto, S., Watanabe, E. and Suguira, K. (1992). "The effective cross section for strength and ductility." *In proceeding of Tenth World Conference on Earthquake Engineering,* Balkema, Rotterdam, 3059-3064.

Hassan, W. M., Hodhod, O. A., Hilal, M. S. and Bahnasaway, H. H. (2017). "Behavior of eccentrically loaded high strength concrete columns jacketed with FRP laminates." *Construction and Building Materials,* 138: 508–527.

Ibrahim, A. M. A., Wu, Z., Fahmy, M. F. M. and Kamal, D. (2016). "Experimental study on cyclic response of concrete bridge column reinforced by steel and basalt FRP reinforcement." *Journal of Composite Construction,* 20 (3), 04015062-3.

ISIS Canada Research Network. (2008). "FRP rehabilitation of reinforced concrete structures." Design manual 4, Version 2, *ISIS Canada Corporation,* University of Manitoba, Canada.

Karbhari, V. M. (2007). "Durability of composites for civil structural applications." *Woodhead Publishing Materials,* U.S.A.

Lee, H. K. and Hausmann L. R. (2004). "Structural repair and strengthening of damaged RC beams with sprayed FRP." *Composite Structure,* 63(2): 201-209.

Lee, H. K., Hausmann R. L. and Seaman, W. C. (2008). "Effectiveness of retrofitting damaged concrete beams with sprayed fibre-reinforced polymer coating." *Journal of Reinforced Plastics and Composites,* 27(12): 1269-1286.

Lee, K. S. (2012). "Experimental study on sprayed FRP system for strengthening reinforced concrete beam." *Journal of Advanced Concrete Technology,* 10(6): 219-230.

Lee, K. S., Lee, B. Y. and Seo, S. Y. (2016). "A seismic strengthening technique for reinforced concrete columns using sprayed FRP." *Polymers,* 8(4): 107-128.

Lin, M., Chen, P., Tsai, K., Yu, Y. and Lui, J. (2010). "Seismic steel jacketing of rectangular RC bridge columns for the mitigation of lap-splice failures." *Earthquake Engineering and Structural Dynamics*, 39(15): 1687–1710.

Lukose, K., Gergely, P. and White, R. N. (1982). "Behavior of reinforced concrete lapped splices for inelastic cyclic loading." *ACI Journal Proceeding*, 79(5): 335-365.

Mander, J. B., Priestley, M. J. N. and Park, R. (1988). "Theoretical stress-strain model for confined concrete." *Journal of Structural Engineering*, 114(8): 1804–1826.

Melek, M. and Wallace, J. W. (2004). "Cyclic behavior of columns with short lap splices." *ACI Structural Journal*, 101(6): 802-811.

National Research Council (NRC). (2015). "National building code of Canada." NBC 2015, *National Research Council*, Ontario, Canada.

Naqvi, S. K. R. (2016). "Lap splice in glass fibre reinforced polymer – reinforced concrete rectangular columns subjected to cyclic-reversed loads." *M. Sc. thesis*, University of Manitoba, Canada.

Naqvi, S. and El-Salakawy, E. 2016. "Lap splice in GFRP-RC rectangular columns subjected to cyclic-reversed loads." *Journal of Composite Construction*, ASCE, **21**(4), 04016117(1-2).

CPD Construction Products. (2017). CPD non-shrinking grout (pre-mix). *Safety Data Sheet*, Ontario, Canada.

Owens Corning Composite Materials. (2015). Continuous filament glass fibre: roving and dry chopped strands. *Safe Use Instruction Sheet*, Toledo, Ohio.

Pam, H. J. and Ho, J. C. M. (2010). "Effects of steel lap splice locations on strength and ductility of reinforced concrete columns." *Advances in Structural Engineering*, 13 (1).

Paulay, T., Zanza, T. M. and Scarpas, A. (1981). “Lapped splices in bridge piers and in columns of earthquake resisting reinforced concrete frames”. *Research report*, Department of Civil Engineering, University of Canterbury, New Zealand, 81(6): 1-117.

Peng, Y., Gu, Q., Gao, R. and Bitewlgn, G. (2014). “Experimental research on seismic behavior of seismically damaged RC frame column strengthened with sprayed hybrid BF/CFRP.” *Applied Mechanics and Materials*, 501-504, 1592-1599.

Polynt Composites Canada Inc. 2017. 41X Epoxy vinyl ester resin (EPOVIA© KRF-1001 MV). *Safety Data Sheet*, Quebec, Canada.

Rabbat, B., Daniel, J., Weinmann, T. and Hanson, N. (1986). “Seismic behavior of lightweight and normal weight concrete columns.” *ACI Structural Journal,* 83(9): 69-79.

Raval, R. and Dave, U. (2013). “Behavior of GFRP wrapped RC columns of different shapes.” *Procedia Engineering*, 51: 240-249.

Rodriguez, M. and Park, R. (l994). “Seismic load tests on reinforced concrete columns strengthened by jacketing.” *ACI Structural Journal*, 91(2): 150-159.

Sheikh, S. A. and Uzumeri, S. M. (1982). "Analytical model for concrete confinement in tied columns." *Journal of the Structural Division,* 108(12): 2703–2722.

Sheikh, S. A. and Yau, G. (2002). “Seismic behavior of concrete columns confined with steel and fibre-reinforced polymers.” *ACI Structural Journal*, 99(1): 72-80.

Tavassoli, A. (2013). "Behaviour of GFRP-reinforced concrete columns under combined axial load and flexure." *M.Sc. Thesis*, University of Toronto, Canada.

United Initiators, Inc. 2017. NOROX MEKP-925H. *Material Safety Data Sheet*, Helena, USA.

Xiao, Y. and Ma, R. (1997). “Seismic retrofit of RC circular columns using prefabricated composite jacketing.” *Journal of Structural Engineering,* 123(10): 1357-1364.

APPENDIX A: DESIGN OF SPECIMEN D1-0

A.1 Design for Flexure

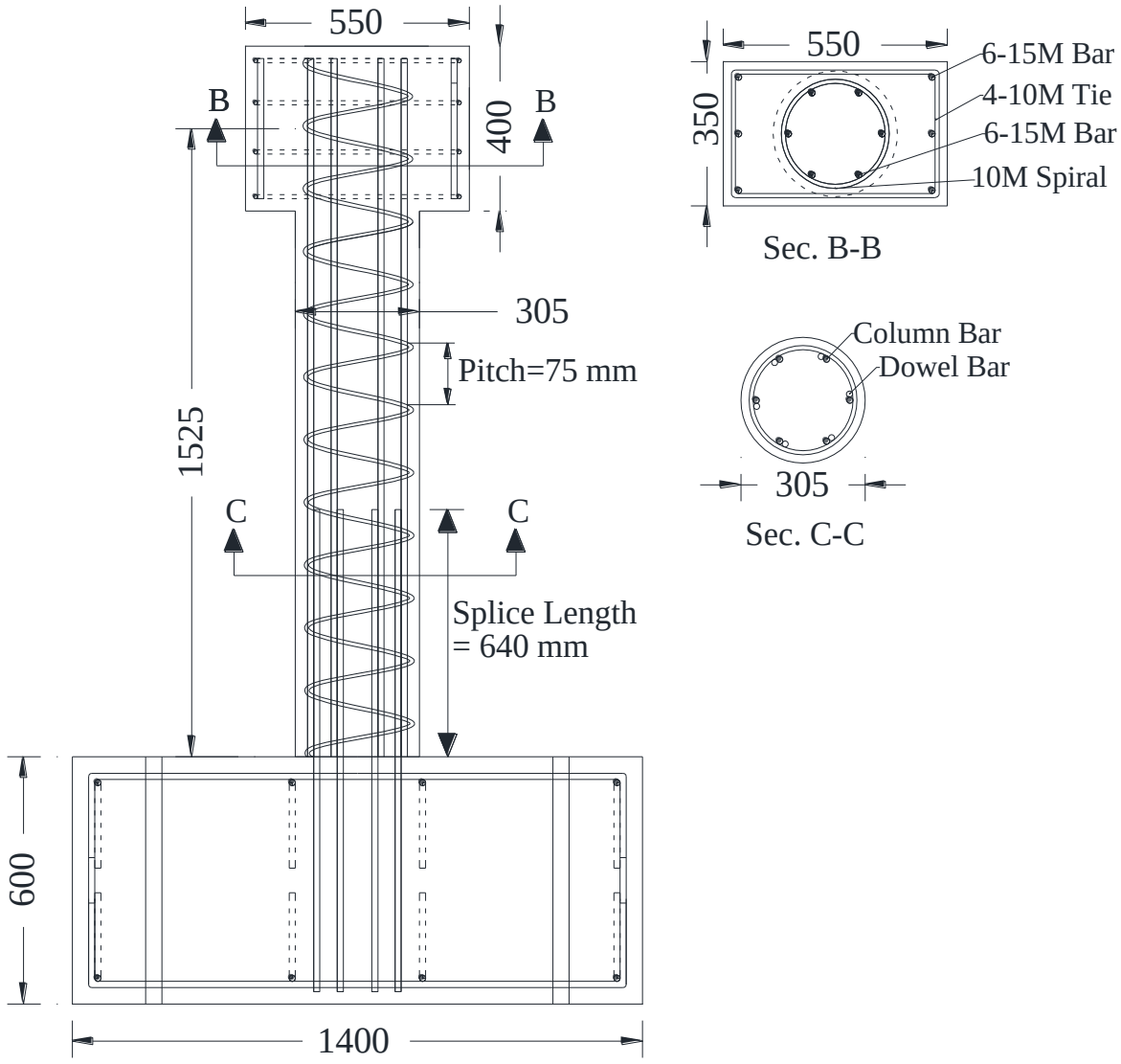

Figure A.1: Specimen D1-0 reinforcement details

A.1.1 Material and cross-sectional properties

- Concrete properties

f_c' = 35 MPa; ϕ_c = 1; $E_c = 4500\sqrt{f_c'}$ = 26622 MPa;

α_1= 0.85 - 0.0015 f_c' = 0.797; β_1 = 0.97 - 0.0025 = 0.883; ε_{cu}= 0.0035;

- Longitudinal reinforcement: Steel bars

f_y = 400 MPa; ϕ_s = 1; E_s = 200 GPa; A_b = 200 mm^2; ε_y = 0.002;

- Cross section properties

A_{st} = 6 × 200 = 1200 mm^2; ρ_s = 1.64%; d = 305 mm; R = 152.5 mm;

$A_g = \pi R^2$ = 3.1416 × 152.2^2 = 73061.84 mm^2

A.1.2 Calculations required to develop interaction diagram

- Point 1: Pure axial load

$P_1 = \alpha_1 \phi_c f_c' \left(A_g - A_{st}\right) + \phi_s f_y A_{st}$ Clause (10.10.4)

$P_1 = (0.797 \times 1 \times 35 \times (73061.84 - 1200) + 1 \times 400 \times 1200) \times 10^{-3}$ = 2485.84 kN

Point 1: M_1 = 0.0 kN.m; P_1 = 2485.84 kN

- Balance point

ε_{cu}= 0.0035

$\varepsilon_{s4} = \varepsilon_y = 0.002$

$f_{s4} = f_y$ = 400 MPa

$c_b = \left(\frac{\varepsilon_{cu}}{\varepsilon_{cu} + \varepsilon_{s4}}\right) d_4 = \frac{0.0035}{0.0035+0.002} \times 262.5 = 167.05$ mm

$a_b = \beta_1 c_b$ = 0.883 ×167.05 = 147.4 mm

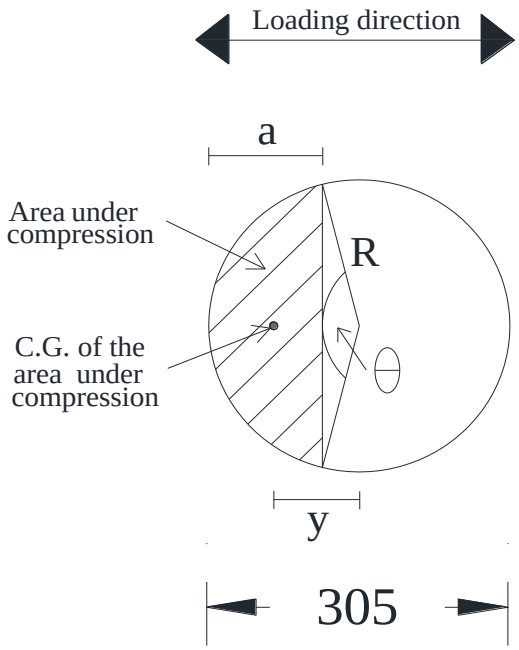

Figure A.2: Cross section properties

Concrete area under compression,

$$A_{compb} = R^2\left(\cos^{-1}\left(\frac{R-a}{R}\right)\right) - (R-a)\sqrt{2Ra-a^2}$$

$$= 152.5^2\left(\cos^{-1}\left(\frac{152.5-147.4}{152.5}\right)\right) - (152.5-147.4)\sqrt{2\times 152.5\times 147.4 - 147.4^2}$$

$= 34980.99$ mm^2

Distance of the C.G. of A_{compb} from the center of cross section of the column,

$$y = \frac{4Rsin^3\frac{\theta}{2}}{3(\theta-\sin\theta)}$$

Where,

$\theta = 2\cos^{-1}\left(1-\frac{a}{R}\right) = 2\cos^{-1}\left(1-\frac{147.4}{152.5}\right) = 176.2° = 3.07$ rad

$y_b = \frac{4\times 152.5\times sin^3\frac{176.2}{2}}{3(3.07-\sin 176.2)} = 67.5$ mm

$C_{cb} = \alpha_1\phi_c f_c' A_{compb} = 0.797\times 1\times 35\times 34980.99 = 976.4$ kN

$\varepsilon_{s1} = \varepsilon_{cu}\left(1 - \frac{d_1}{c_b}\right) = 0.0035 \times \left(1 - \frac{42.5}{167.05}\right) = 0.0026 > \varepsilon_y = 0.002$

$f_{s1} = f_y = 400$ MPa

$F_{s1} = \phi_s A_{s1}(f_{s1} - \alpha_1 \phi_c f_c') = 1 \times 200 \times (400 - (0.797 \times 1 \times 35)) = 74.4$ kN

$\varepsilon_{s2} = \varepsilon_{cu}\left(1 - \frac{d_2}{c_b}\right) = 0.0035 \times \left(1 - \frac{97.5}{167.05}\right) = 0.0015 < \varepsilon_y = 0.002$

$f_{s2} = E_s \varepsilon_{s2} = 200000 \times 0.0015 = 291.4$ MPa

$F_{s2} = \phi_s A_{s2}(f_{s2} - \alpha_1 \phi_c f_c') = 1 \times 400 \times (291.4 - (0.797 \times 1 \times 35)) = 105.4$ kN

$\varepsilon_{s3} = \varepsilon_{cu}\left(1 - \frac{d_3}{c_b}\right) = 0.0035 \times \left(1 - \frac{207.5}{167.05}\right) = -0.0008 < \varepsilon_y = 0.002$

$f_{s3} = E_s \varepsilon_{s3} = 200000 \times (-0.0008) = -169.5$ MPa

$F_{s3} = \phi_s A_{s3} f_{s3} = 1 \times 400 \times (-169.5) = -67.8$ kN $= 67.8$ kN (Tension)

$\varepsilon_{s4} = \varepsilon_{cu}\left(1 - \frac{d_4}{c_b}\right) = 0.0035 \times \left(1 - \frac{262.5}{167.05}\right) = -0.002 \geq \varepsilon_y = 0.002$

$f_{s4} = f_y = -400$ MPa

$F_{s4} = \phi_s A_{s4} f_{s4} = 1 \times 200 \times (-400) = -80.0$ kN $= 80.0$ kN (Tension)

$P_b = C_{cb} + F_{s1} + F_{s2} + F_{s3} + F_{s4} = 976.4 + 74.4 + 105.4 - 67.8 - 80 = 1008.4$ kN

$M_b = C_{cb} \times y_b + F_{s1}(R - d_1) + F_{s2}(R - d_2) + F_{s3}(R - d_3) + F_{s4}(R - d_4)$

$= 976.4 \times 67.5 + 74.4\,(152.5 - 42.5) + 105.4\,(152.5 - 97.5) + (-67.8)\,(152.5 - 207.5) + (-80)$

$(152.5 - 262.5) = 92.4$ kN.m

$e_b = \frac{M_b}{P_b} = \frac{92.4}{1008.4} = 91.6$ mm

Balance point: $M_b = 92.4$ kN.m; $P_b = 1008.4$ kN

- Point 2: $c_2 = 305$ mm

$a_2 = \beta_1 c_2 = 0.883 \times 305 = 269.2$ mm

$A_{comp2} = R^2\left(\cos^{-1}\left(\frac{R-a}{R}\right)\right) - (R-a)\sqrt{2Ra - a^2}$

$= 152.5^2 \left(\cos^{-1}\left(\frac{152.5-269.2}{152.5}\right)\right) - (152.5 - 269.2)\sqrt{2 \times 152.5 \times 269.2 - 269.2^2}$

$= 68245.95$ mm^2

Distance of the C.G. of A_{comp2} from the center of cross section of the column,

$$y = \frac{4Rsin^3\frac{\theta}{2}}{3(\theta - \sin\theta)}$$

Where,

$\theta = 2\cos^{-1}\left(1 - \frac{a}{R}\right) = 2\cos^{-1}\left(1 - \frac{269.2}{152.5}\right) = 279.9° = 4.88$ rad

$y_2 = \frac{4\times152.5\times sin^3\frac{279.9}{2}}{3(4.88-\sin 279.9)} = 9.25$ mm

$C_{c2} = \alpha_1\phi_c f_c' A_{comp2} = 0.797 \times 1 \times 35 \times 68245.95 = 1904.9$ kN

$\varepsilon_{s1} = \varepsilon_{cu}\left(1 - \frac{d_1}{c_2}\right) = 0.0035\times\left(1 - \frac{42.5}{305}\right) = 0.003 > \varepsilon_y = 0.002$

$f_{s1} = f_y = 400$ MPa

$F_{s1} = \phi_s A_{s1}(f_{s1} - \alpha_1\phi_c f_c') = 1 \times 200 \times (400 - (0.797 \times 1 \times 35)) = 74.4$ kN

$\varepsilon_{s2} = \varepsilon_{cu}\left(1 - \frac{d_2}{c_2}\right) = 0.0035\times\left(1 - \frac{97.5}{305}\right) = 0.0024 > \varepsilon_y = 0.002$

$f_{s2} = f_y = 400$ MPa

$F_{s2} = \phi_s A_{s2}(f_{s2} - \alpha_1\phi_c f_c') = 1 \times 400 \times (400 - (0.797 \times 1 \times 35)) = 148.8$ kN

$\varepsilon_{s3} = \varepsilon_{cu}\left(1 - \frac{d_3}{c_2}\right) = 0.0035\times\left(1 - \frac{207.5}{305}\right) = 0.0011 < \varepsilon_y = 0.002$

$f_{s3} = E_s\varepsilon_{s3} = 200000 \times (0.0011) = 223.8$ MPa

$F_{s3} = \phi_s A_{s3}(f_{s3} - \alpha_1\phi_c f_c') = 1 \times 400 \times (223.8 - (0.797 \times 1 \times 35)) = 78.3$ kN

$\varepsilon_{s4} = \varepsilon_{cu}\left(1 - \frac{d_4}{c_2}\right) = 0.0035\times\left(1 - \frac{262.5}{305}\right) = 0.0005 < \varepsilon_y = 0.002$

$f_{s4} = E_s\varepsilon_{s4} = 200000 \times (0.0005) = 97.5$ MPa

$F_{s4} = \phi_s A_{s4}(f_{s4} - \alpha_1\phi_c f_c') = 1 \times 200 \times (97.5 - (0.797 \times 1 \times 35)) = 13.9$ kN

$P_2 = C_{c2} + F_{s1} + F_{s2} + F_{s3} + F_{s4}$ = 1904.9 + 74.4 + 148.8 + 78.3 + 13.9 = 2220.4 kN

$M_2 = C_{c2} \times y_2 + F_{s1}(R - d_1) + F_{s2}(R - d_2) + F_{s3}(R - d_3) + F_{s4}(R - d_4)$

= 1904.9 × 9.25 + 74.4 (152.5 – 42.5) + 148.8 (152.5 − 97.5) + 78.3 (152.5 – 207.5) + 13.9 (152.5 – 262.5) = 28.2 kN.m

$e_2 = \frac{M_2}{P_2} = \frac{28.2}{2220.4} = 12.7$ mm

Point 2: $M_2 = 28.2$ kN.m; $P_2 = 2220.4$ kN

- Point 3: $c_3 = 240$ mm

$a_3 = \beta_1 c_3 = 0.883 \times 240 = 211.8$ mm

$A_{comp3} = R^2\left(\cos^{-1}\left(\frac{R-a}{R}\right)\right) - (R-a)\sqrt{2Ra - a^2}$

$= 152.5^2\left(\cos^{-1}\left(\frac{152.5-211.8}{152.5}\right)\right) - (152.5 - 211.8)\sqrt{2 \times 152.5 \times 211.8 - 211.8^2}$

= 54150.59 mm^2

Distance of the C.G. of A_{comp3} from the center of cross section of the column,

$$y = \frac{4R\sin^3\frac{\theta}{2}}{3(\theta - \sin\theta)}$$

Where,

$\theta = 2\cos^{-1}\left(1 - \frac{a}{R}\right) = 2\cos^{-1}\left(1 - \frac{211.8}{152.5}\right) = 225.7° = 3.94$ rad

$y_3 = \frac{4\times152.5\times\sin^3\frac{225.7}{2}}{3(3.94-\sin 225.7)} = 34.14$ mm

$C_{c3} = \alpha_1\phi_c f_c' A_{comp3} = 0.797 \times 1 \times 35 \times 54150.59 = 1511.5$ kN

$\varepsilon_{s1} = \varepsilon_{cu}\left(1 - \frac{d_1}{c_3}\right) = 0.0035 \times \left(1 - \frac{42.5}{240}\right) = 0.0029 > \varepsilon_y = 0.002$

$f_{s1} = f_y = 400$ MPa

$F_{s1} = \phi_s A_{s1}(f_{s1} - \alpha_1\phi_c f_c') = 1 \times 200 \times (400 - (0.797 \times 1 \times 35)) = 74.4$ kN

$\varepsilon_{s2} = \varepsilon_{cu}\left(1 - \frac{d_2}{c_3}\right) = 0.0035 \times \left(1 - \frac{97.5}{240}\right) = 0.002 \geq \varepsilon_y = 0.002$

$f_{s2} = f_y = 400$ MPa

$F_{s2} = \phi_s A_{s2}(f_{s2} - \alpha_1 \phi_c f_c') = 1 \times 400 \times (400 - (0.797 \times 1 \times 35)) = 148.8$ kN

$\varepsilon_{s3} = \varepsilon_{cu}\left(1 - \frac{d_3}{c_3}\right) = 0.0035 \times \left(1 - \frac{207.5}{240}\right) = 0.0005 < \varepsilon_y = 0.002$

$f_{s3} = E_s \varepsilon_{s3} = 200000 \times 0.0005 = 94.8$ MPa

$F_{s3} = \phi_s A_{s3}(f_{s3} - \alpha_1 \phi_c f_c') = 1 \times 400 \times (94.8 - (0.797 \times 1 \times 35)) = 26.8$ kN

$\varepsilon_{s4} = \varepsilon_{cu}\left(1 - \frac{d_4}{c_3}\right) = 0.0035 \times \left(1 - \frac{262.5}{240}\right) = -0.0003 < \varepsilon_y = 0.002$

$f_{s4} = E_s \varepsilon_{s4} = 200000 \times (-0.0003) = -65.6$ MPa

$F_{s4} = \phi_s A_{s4} f_{s4} = 1 \times 200 \times (-65.6) = -13.1$ kN

$P_3 = C_{c3} + F_{s1} + F_{s2} + F_{s3} + F_{s4} = 1511.5 + 74.4 + 148.8 + 26.8 - 13.1 = 1748.3$ kN

$M_3 = C_{c3} \times y_3 + F_{s1}(R - d_1) + F_{s2}(R - d_2) + F_{s3}(R - d_3) + F_{s4}(R - d_4)$

$= 1511.5 \times 34.14 + 74.4\,(152.5 - 42.5) + 148.8\,(152.5 - 97.5) + 26.8\,(152.5 - 207.5) +$

$(-13.1)\,(152.5 - 262.5) = 67.9$ kN.m

$e_3 = \frac{M_3}{P_3} = \frac{67.9}{1748.3} = 38.8$ mm

Point 3: $M_3 = 67.9$ kN.m; $P_3 = 1748.3$ kN

- Point 4: $c_4 = 200$ mm

$a_4 = \beta_1 c_4 = 0.883 \times 200 = 176.5$ mm

$A_{comp4} = R^2\left(\cos^{-1}\left(\frac{R-a}{R}\right)\right) - (R-a)\sqrt{2Ra - a^2}$

$= 152.5^2\left(\cos^{-1}\left(\frac{152.5-176.5}{152.5}\right)\right) - (152.5 - 176.5)\sqrt{2 \times 152.5 \times 176.5 - 176.5^2}$

$= 43820.50$ mm^2

Distance of the C.G. of A_{comp4} from the center of cross section of the column,

$$y = \frac{4sin^3\frac{\theta}{2}}{3(\theta - \sin\theta)}$$

Where,

$\theta = 2\cos^{-1}\left(1 - \frac{a}{R}\right) = 2\cos^{-1}\left(1 - \frac{176.5}{152.5}\right) = 198.2° = 3.46$ rad

$y_4 = \frac{4\times152.5\times sin^3\frac{198.2}{2}}{3(3.46-\sin 198.2)} = 51.96$ mm

$C_{c4} = \alpha_1\phi_c f_c' A_{comp4} = 0.797 \times 1 \times 35 \times 43820.50 = 1223.1$ kN

$\varepsilon_{s1} = \varepsilon_{cu}\left(1 - \frac{d_1}{c_4}\right) = 0.0035\times\left(1 - \frac{42.5}{200}\right) = 0.0028 > \varepsilon_y = 0.002$

$f_{s1} = f_y = 400$ MPa

$F_{s1} = \phi_s A_{s1}(f_{s1} - \alpha_1\phi_c f_c') = 1 \times 200 \times (400 - (0.797 \times 1 \times 35)) = 74.4$ kN

$\varepsilon_{s2} = \varepsilon_{cu}\left(1 - \frac{d_2}{c_4}\right) = 0.0035\times\left(1 - \frac{97.5}{200}\right) = 0.0018 < \varepsilon_y = 0.002$

$f_{s2} = E_s\varepsilon_{s2} = 200000 \times 0.0018 = 358.8$ MPa

$F_{s2} = \phi_s A_{s2}(f_{s2} - \alpha_1\phi_c f_c') = 1 \times 400 \times (358.8 - (0.797 \times 1 \times 35)) = 132.3$ kN

$\varepsilon_{s3} = \varepsilon_{cu}\left(1 - \frac{d_3}{c_4}\right) = 0.0035\times\left(1 - \frac{207.5}{200}\right) = -0.00013 < \varepsilon_y = 0.002$

$f_{s3} = E_s\varepsilon_{s3} = 200000 \times (-0.00013) = -26.3$ MPa

$F_{s3} = \phi_s A_{s3} f_{s3} = 1 \times 400 \times (-26.3) = -10.5$ kN

$\varepsilon_{s4} = \varepsilon_{cu}\left(1 - \frac{d_4}{c_4}\right) = 0.0035\times\left(1 - \frac{262.5}{200}\right) = -0.0011 < \varepsilon_y = 0.002$

$f_{s4} = E_s\varepsilon_{s4} = 200000 \times (-0.0011) = -218.8$ MPa

$F_{s4} = \phi_s A_{s4} f_{s4} = 1 \times 200 \times (-218.8) = -43.8$ kN

$P_4 = C_{c4} + F_{s1} + F_{s2} + F_{s3} + F_{s4} = 1223.1 + 74.4 + 132.3 - 10.5 - 43.8 = 1375.6$ kN

$M_4 = C_{c4} \times y_4 + F_{s1}(R - d_1) + F_{s2}(R - d_2) + F_{s3}(R - d_3) + F_{s4}(R - d_4)$

= 1223.1 × 51.96 + 74.4 (152.5 – 42.5) + 132.3 (152.5 − 97.5) + (– 10.5) (152.5 – 207.5) +

(– 43.8) (152.5 – 262.5) = 84.4 kN.m

$e_4 = \frac{M_4}{P_4} = \frac{84.4}{1375.6} = 61.4$ mm

Point 4: $M_4 = 84.4$ kN.m; $P_4 = 1375.6$ kN

- Point 5: $c_5 = 160$ mm

$a_5 = \beta_1 c_5 = 0.883 \times 160 = 141.2$ mm

$$A_{comp5} = R^2\left(\cos^{-1}\left(\frac{R-a}{R}\right)\right) - (R-a)\sqrt{2Ra-a^2}$$

$$= 152.5^2\left(\cos^{-1}\left(\frac{152.5-141.2}{152.5}\right)\right) - (152.5-141.2)\sqrt{2\times 152.5\times 141.2 - 141.2^2}$$

= 33087.49 mm^2

Distance of the C.G. of A_{comp5} from the center of cross section of the column,

$$y = \frac{4R\sin^3\frac{\theta}{2}}{3(\theta - \sin\theta)}$$

Where,

$\theta = 2\cos^{-1}\left(1 - \frac{a}{R}\right) = 2\cos^{-1}\left(1 - \frac{141.2}{152.5}\right) = 171.3° = 2.99$ rad

$y_5 = \frac{4\times 152.5\times \sin^3\frac{171.3}{2}}{3(2.99-\sin 171.3)} = 70.87$ mm

$C_{c5} = \alpha_1\phi_c f_c' A_{comp5} = 0.797 \times 1 \times 35 \times 33087.49 = 923.6$ kN

$\varepsilon_{s1} = \varepsilon_{cu}\left(1 - \frac{d_1}{c_5}\right) = 0.0035\times\left(1 - \frac{42.5}{160}\right) = 0.0026 > \varepsilon_y = 0.002$

$f_{s1} = f_y = 400$ MPa

$F_{s1} = \phi_s A_{s1}(f_{s1} - \alpha_1\phi_c f_c') = 1 \times 200 \times (400 - (0.797 \times 1 \times 35)) = 74.4$ kN

$\varepsilon_{s2} = \varepsilon_{cu}\left(1 - \frac{d_2}{c_5}\right) = 0.0035\times\left(1 - \frac{97.5}{160}\right) = 0.0014 < \varepsilon_y = 0.002$

$f_{s2} = E_s\varepsilon_{s2} = 200000 \times (0.0014) = 273.4$ MPa

$F_{s2} = \phi_s A_{s2}(f_{s2} - \alpha_1 \phi_c f_c') = 1 \times 400 \times (273.4 - (0.797 \times 1 \times 35)) = 98.2$ kN

$\varepsilon_{s3} = \varepsilon_{cu}\left(1 - \frac{d_3}{c_5}\right) = 0.0035 \times \left(1 - \frac{207.5}{160}\right) = -0.001 < \varepsilon_y = 0.002$

$f_{s3} = E_s \varepsilon_{s3} = 200000 \times (-0.001) = -207.8$ MPa

$F_{s3} = \phi_s A_{s3} f_{s3} = 1 \times 400 \times (-207.8) = -83.1$ kN

$\varepsilon_{s4} = \varepsilon_{cu}\left(1 - \frac{d_4}{c_5}\right) = 0.0035 \times \left(1 - \frac{262.5}{160}\right) = -0.0022 > \varepsilon_y = 0.002$

$f_{s4} = f_y = -400$ MPa

$F_{s4} = \phi_s A_{s4} f_{s4} = 1 \times 200 \times (-400) = -80.0$ kN

$P_5 = C_{c5} + F_{s1} + F_{s2} + F_{s3} + F_{s4} = 923.6 + 74.4 + 98.2 - 83.1 - 80.0 = 933.0$ kN

$M_5 = C_{c5} \times y_5 + F_{s1}(R - d_1) + F_{s2}(R - d_2) + F_{s3}(R - d_3) + F_{s4}(R - d_4)$

$= 923.6 \times 70.87 + 74.4\,(152.5 - 42.5) + 98.2\,(152.5 - 97.5) + (-83.1)\,(152.5 - 207.5) +$

$(-80)\,(152.5 - 262.5) = 92.4$ kN.m

$e_5 = \frac{M_5}{P_5} = \frac{92.4}{933.0} = 99.0$ mm

Point 5: $M_5 = 92.4$ kN.m; $P_5 = 933.0$ kN

- Point 6: $c_6 = 120$ mm

$a_6 = \beta_1 c_6 = 0.883 \times 120 = 105.9$ mm

$A_{comp6} = R^2\left(\cos^{-1}\left(\frac{R-a}{R}\right)\right) - (R-a)\sqrt{2Ra - a^2}$

$= 152.5^2\left(\cos^{-1}\left(\frac{152.5-105.9}{152.5}\right)\right) - (152.5 - 105.9)\sqrt{2 \times 152.5 \times 105.9 - 105.9^2}$

$= 22542.23$ mm^2

Distance of the C.G. of A_{comp6} from the center of cross section of the column,

$$y = \frac{4R\sin^3\frac{\theta}{2}}{3(\theta - \sin\theta)}$$

Where,

$\theta = 2\cos^{-1}\left(1 - \frac{a}{R}\right) = 2\cos^{-1}\left(1 - \frac{105.9}{152.5}\right) = 144.4° = 2.52$ rad

$y_6 = \frac{4 \times 152.5 \times sin^3\frac{144.4}{2}}{3(2.52 - \sin 144.4)} = 90.54$ mm

$C_{c6} = \alpha_1 \phi_c f_c' A_{comp6} = 0.797 \times 1 \times 35 \times 22542.23 = 629.2$ kN

$\varepsilon_{s1} = \varepsilon_{cu}\left(1 - \frac{d_1}{c_6}\right) = 0.0035 \times \left(1 - \frac{42.5}{120}\right) = 0.0023 > \varepsilon_y = 0.002$

$f_{s1} = f_y = 400$ MPa

$F_{s1} = \phi_s A_{s1}(f_{s1} - \alpha_1 \phi_c f_c') = 1 \times 200 \times (400 - (0.797 \times 1 \times 35)) = 74.4$ kN

$\varepsilon_{s2} = \varepsilon_{cu}\left(1 - \frac{d_2}{c_6}\right) = 0.0035 \times \left(1 - \frac{97.5}{120}\right) = 0.0006 < \varepsilon_y = 0.002$

$f_{s2} = E_s \varepsilon_{s2} = 200000 \times (0.0006) = 131.3$ MPa

$F_{s2} = \phi_s A_{s2}(f_{s2} - \alpha_1 \phi_c f_c') = 1 \times 400 \times (131.3 - (0.797 \times 1 \times 35)) = 41.3$ kN

$\varepsilon_{s3} = \varepsilon_{cu}\left(1 - \frac{d_3}{c_6}\right) = 0.0035 \times \left(1 - \frac{207.5}{120}\right) = -0.0026 > \varepsilon_y = 0.002$

$f_{s3} = f_y = -400$ MPa

$F_{s3} = \phi_s A_{s3} f_{s3} = 1 \times 400 \times (-400) = -160.0$ kN

$\varepsilon_{s4} = \varepsilon_{cu}\left(1 - \frac{d_4}{c_6}\right) = 0.0035 \times \left(1 - \frac{262.5}{120}\right) = -0.004 > \varepsilon_y = 0.002$

$f_{s4} = f_y = -400$ MPa

$F_{s4} = \phi_s A_{s4} f_{s4} = 1 \times 200 \times (-400) = -80.0$ kN

$P_6 = C_{c6} + F_{s1} + F_{s2} + F_{s3} + F_{s4} = 629.2 + 74.4 + 41.3 - 160.0 - 80.0 = 504.9$ kN

$M_6 = C_{c6} \times y_6 + F_{s1}(R - d_1) + F_{s2}(R - d_2) + F_{s3}(R - d_3) + F_{s4}(R - d_4)$

$= 629.2 \times 90.54 + 74.4\,(152.5 - 42.5) + 41.3\,(152.5 - 97.5) + (-160)\,(152.5 - 207.5) + (-80)$

$(152.5 - 262.5) = 85.0$ kN.m

$e_6 = \frac{M_6}{P_6} = \frac{85.0}{504.9} = 168.35$ mm

Point 6: $M_6 = 85.0$ kN.m; $P_6 = 504.9$ kN

- Point 7: $c_7 = 80$ mm

$a_7 = \beta_1 c_7 = 0.883 \times 80 = 70.6$ mm

$$A_{comp7} = R^2\left(\cos^{-1}\left(\frac{R-a}{R}\right)\right) - (R-a)\sqrt{2Ra-a^2}$$

$$= 152.5^2\left(\cos^{-1}\left(\frac{152.5-70.6}{152.5}\right)\right) - (152.5-70.6)\sqrt{2\times 152.5\times 70.6 - 70.6^2}$$

$= 12810.31$ mm^2

Distance of the C.G. of A_{comp7} from the center of cross section of the column,

$$y = \frac{4R\sin^3\frac{\theta}{2}}{3(\theta - \sin\theta)}$$

Where,

$\theta = 2\cos^{-1}\left(1-\frac{a}{R}\right) = 2\cos^{-1}\left(1-\frac{70.6}{152.5}\right) = 115.2° = 2.01$ rad

$y_7 = \frac{4\times 152.5\times \sin^3\frac{115.2}{2}}{3(2.01-\sin 115.2)} = 110.79$ mm

$C_{c7} = \alpha_1\phi_c f_c' A_{comp7} = 0.797 \times 1 \times 35 \times 12810.31 = 357.6$ kN

$\varepsilon_{s1} = \varepsilon_{cu}\left(1-\frac{d_1}{c_7}\right) = 0.0035\times\left(1-\frac{42.5}{80}\right) = 0.0016 < \varepsilon_y = 0.002$

$f_{s1} = E_s\varepsilon_{s1} = 200000 \times (0.0016) = 328.1$ MPa

$F_{s1} = \phi_s A_{s1}(f_{s1} - \alpha_1\phi_c f_c') = 1 \times 200 \times (328.1 - (0.797 \times 1 \times 35)) = 60$ kN

$\varepsilon_{s2} = \varepsilon_{cu}\left(1-\frac{d_2}{c_7}\right) = 0.0035\times\left(1-\frac{97.5}{80}\right) = -0.0008 < \varepsilon_y = 0.002$

$f_{s2} = E_s\varepsilon_{s2} = 200000 \times (-0.0008) = -153.1$ MPa

$F_{s2} = \phi_s A_{s2} f_{s2} = 1 \times 400 \times (-153.1) = -61.3$ kN

$\varepsilon_{s3} = \varepsilon_{cu}\left(1-\frac{d_3}{c_7}\right) = 0.0035\times\left(1-\frac{207.5}{80}\right) = -0.0056 > \varepsilon_y = 0.002$

$f_{s3} = f_y = -400$ MPa

$F_{s3} = \phi_s A_{s3} f_{s3} = 1 \times 400 \times (-400) = -160.0$ kN

$\varepsilon_{s4} = \varepsilon_{cu}\left(1 - \frac{d_4}{c_7}\right) = 0.0035 \times \left(1 - \frac{262.5}{80}\right) = -0.008 > \varepsilon_y = 0.002$

$f_{s4} = f_y = -400$ MPa

$F_{s4} = \phi_s A_{s4} f_{s4} = 1 \times 200 \times (-400) = -80.0$ kN

$P_7 = C_{c7} + F_{s1} + F_{s2} + F_{s3} + F_{s4} = 357.6 + 60.0 - 61.3 - 160.0 - 80.0 = 116.3$ kN

$M_7 = C_{c7} \times y_7 + F_{s1}(R - d_1) + F_{s2}(R - d_2) + F_{s3}(R - d_3) + F_{s4}(R - d_4)$

$= 357.6 \times 110.79 + 60\ (152.5 - 42.5) + (-61.3)\ (152.5 - 97.5) + (-160)\ (152.5 - 207.5) +$

$(-80)\ (152.5 - 262.5) = 60.4$ kN.m

$e_7 = \frac{M_7}{P_7} = \frac{60.4}{116.3} = 519.3$ mm

Point 7: $M_7 = 60.4$ kN.m; $P_7 = 116.3$ kN

- Point 8: $c_8 = 40$ mm

$a_8 = \beta_1 c_8 = 0.883 \times 40 = 35.3$ mm

$A_{comp8} = R^2\left(\cos^{-1}\left(\frac{R-a}{R}\right)\right) - (R-a)\sqrt{2Ra - a^2}$

$= 152.5^2\left(\cos^{-1}\left(\frac{152.5-35.3}{152.5}\right)\right) - (152.5 - 35.3)\sqrt{2 \times 152.5 \times 35.3 - 35.3^2}$

$= 4710.48$ mm^2

Distance of the C.G. of A_{comp8} from the center of cross section of the column,

$$y = \frac{4R\sin^3\frac{\theta}{2}}{3(\theta - \sin\theta)}$$

Where,

$\theta = 2\cos^{-1}\left(1 - \frac{a}{R}\right) = 2\cos^{-1}\left(1 - \frac{35.3}{152.5}\right) = 79.56° = 1.39$ rad

$y_8 = \frac{4 \times 152.5 \times \sin^3\frac{79.56}{2}}{3(1.39 - \sin 79.56)} = 131.47$ mm

$C_{c8} = \alpha_1 \phi_c f_c' A_{comp8} = 0.797 \times 1 \times 35 \times 4710.48 = 131.5$ kN

$\varepsilon_{s1} = \varepsilon_{cu} \left(1 - \frac{d_1}{c_8}\right) = 0.0035 \times \left(1 - \frac{42.5}{40}\right) = -0.0002 < \varepsilon_y = 0.002$

$f_{s1} = E_s \varepsilon_{s1} = 200000 \times (-0.0002) = -43.8$ MPa

$F_{s1} = \phi_s A_{s1} f_{s1} = 1 \times 200 \times (-43.8) = -8.8$ kN = 8.8 kN (Tension)

$\varepsilon_{s2} = \varepsilon_{cu} \left(1 - \frac{d_2}{c_8}\right) = 0.0035 \times \left(1 - \frac{97.5}{40}\right) = -0.005 > \varepsilon_y = 0.002$

$f_{s2} = f_y = -400$ MPa

$F_{s2} = \phi_s A_{s2} f_{s2} = 1 \times 400 \times (-400) = -160.0$ kN

$\varepsilon_{s3} = \varepsilon_{cu} \left(1 - \frac{d_3}{c_8}\right) = 0.0035 \times \left(1 - \frac{207.5}{40}\right) = -0.015 > \varepsilon_y = 0.002$

$f_{s3} = f_y = -400$ MPa

$F_{s3} = \phi_s A_{s3} f_{s3} = 1 \times 400 \times (-400) = -160.0$ kN

$\varepsilon_{s4} = \varepsilon_{cu} \left(1 - \frac{d_4}{c_8}\right) = 0.0035 \times \left(1 - \frac{262.5}{40}\right) = -0.019 > \varepsilon_y = 0.002$

$f_{s4} = f_y = -400$ MPa

$F_{s4} = \phi_s A_{s4} f_{s4} = 1 \times 200 \times (-400) = -80.0$ kN

$P_8 = C_{c8} + F_{s1} + F_{s2} + F_{s3} + F_{s4} = 131.5 - 8.8 - 160.0 - 160.0 - 80.0 = -277.3$ kN

For interaction diagram, $P_8 = 0.0$ kN

$M_8 = C_{c8} \times y_8 + F_{s1}(R - d_1) + F_{s2}(R - d_2) + F_{s3}(R - d_3) + F_{s4}(R - d_4)$

$= 131.5 \times 131.47 + (-8.8)(152.5 - 42.5) + (-160)(152.5 - 97.5) + (-160)(152.5 - 207.5)$

$+ (-80)(152.5 - 262.5) = 25.1$ kN.m

For interaction diagram, $M_8 = 51.3$ kN (When $P = 0.0$ kN, $M = 51.3$ kN)

$e_8 = \frac{M_8}{P_8} = \frac{51.3}{0.0} = 0.0$ mm

Point 8: $M_8 = 51.3$ kN.m; $P_8 = 0.0$ kN

Assuming, when the internal axial load resistance is equal to external axial load (20% of column axial load capacity), resultant axial load will be zero and at that condition the calculated lateral load will be maximum lateral load capacity.

Applied axial load, P_A = 20% × $(f_c' \left(A_g - A_{st}\right) + f_y A_{st}) \approx$ 500 kN

Assume c = 119.5 mm

$a = \beta_1 \mathrm{c} = 0.883 \times 119.5 = 105.46$ mm

$$A_{comp} = R^2 \left(\cos^{-1}\left(\frac{R-a}{R}\right)\right) - (R-a)\sqrt{2Ra - a^2}$$

$$= 152.5^2 \left(\cos^{-1}\left(\frac{152.5-105.46}{152.5}\right)\right) - (152.5 - 105.46)\sqrt{2 \times 152.5 \times 105.46 - 105.46^2}$$

= 22414.15 mm^2

Distance of the C.G. of A_{comp} from the center of cross section of the column,

$$y = \frac{4R sin^3 \frac{\theta}{2}}{3(\theta - \sin\theta)}$$

Where,

$\theta = 2\cos^{-1}\left(1 - \frac{a}{R}\right) = 2\cos^{-1}\left(1 - \frac{105.46}{152.5}\right)$ = 143.8° = 2.51 rad

$\mathrm{y} = \frac{4 \times 152.5 \times sin^3 \frac{143.8}{2}}{3(2.51 - \sin 143.8)}$ = 90.79 mm

$\mathrm{C}_c = \alpha_1 \phi_c f_c' A_{comp} = 0.797 \times 1 \times 35 \times 22414.15 = 625.6$ kN

$\varepsilon_{s1} = \varepsilon_{cu}\left(1 - \frac{d_1}{\mathrm{c}}\right) = 0.0035 \times \left(1 - \frac{42.5}{119.5}\right) = 0.0023 > \varepsilon_y = 0.002$

$f_{s1} = f_y = 400$ MPa

$F_{s1} = \phi_s A_{s1}(f_{s1} - \alpha_1 \phi_c f_c') = 1 \times 200 \times (400 - (0.797 \times 1 \times 35)) = 74.4$ kN

$\varepsilon_{s2} = \varepsilon_{cu}\left(1 - \frac{d_2}{c}\right) = 0.0035 \times \left(1 - \frac{97.5}{119.5}\right) = 0.0006 < \varepsilon_y = 0.002$

$f_{s2} = E_s\varepsilon_{s2} = 200000 \times (0.0006) = 128.9$ MPa

$F_{s2} = \phi_s A_{s2}(f_{s2} - \alpha_1\phi_c f_c') = 1 \times 400 \times (128.9 - (0.797 \times 1 \times 35)) = 40.4$ kN

$\varepsilon_{s3} = \varepsilon_{cu}\left(1 - \frac{d_3}{c}\right) = 0.0035 \times \left(1 - \frac{207.5}{119.5}\right) = -0.0026 > \varepsilon_y = 0.002$

$f_{s3} = f_y = -400$ MPa

$F_{s3} = \phi_s A_{s3} f_{s3} = 1 \times 400 \times (-400) = -160.0$ kN

$\varepsilon_{s4} = \varepsilon_{cu}\left(1 - \frac{d_4}{c}\right) = 0.0035 \times \left(1 - \frac{262.5}{119.5}\right) = -0.004 > \varepsilon_y = 0.002$

$f_{s4} = f_y = -400$ MPa

$F_{s4} = \phi_s A_{s4} f_{s4} = 1 \times 200 \times (-400) = -80.0$ kN

Check force equilibrium:

$P_A = C_{c8} + F_{s1} + F_{s2} + F_{s3} + F_{s4}$

Or, $500 = 625.6 + 74.4 + 40.4 - 160.0 - 80.0$

Or, 500 kN ≈ 500.4 kN

$M = C_c \times y + F_{s1}(R - d_1) + F_{s2}(R - d_2) + F_{s3}(R - d_3) + F_{s4}(R - d_4)$

$= 625.6 \times 90.79 + 74.4\,(152.5 - 42.5) + 40.4\,(152.5 - 97.5) + (-160)\,(152.5 - 207.5) + (-80)$

$(152.5 - 262.5) = 84.8$ kN.m

Lateral load capacity, P_L = M/1.525 = 84.8/1.525 = 55.6 kN

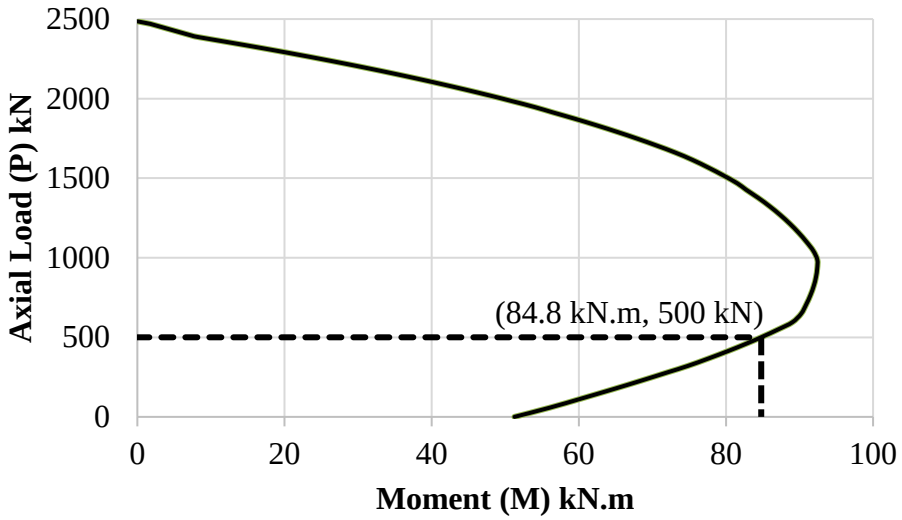

Figure A.3: Column interaction diagram for specimen D1-0

A.2 Design for Shear

A.2.1 Material and cross-Section properties

- Shear reinforcement and characteristics:

f_y = 400 MPa; ϕ_s = 1; E_s = 200 GPa; A_v = 200 mm^2; ε_y = 0.002;

Applied lateral shear force, V_L = 55.6 kN

$V_r = V_c + V_s$

$V_c = \varphi_c \lambda \beta \sqrt{f_c'} b_w d_v$

b_w= 305 mm (Clause 11.2.10.3)

d_e = 225.8 mm $< 0.8h = 0.8 \times 305 = 244$ mm

$d_v \geq 0.9 d_e = 0.9 \times 225.8 = 203.25$ mm

$\geq 0.72h = 0.72 \times 305 = 219.6$ mm (Govern)

From CSA/A23.3-14 Clause 21.3.2.7.2.

$\beta \leq 0.1$ and $\theta_v \geq 45°$

From CSA/A23.3-14 Clause 11.3.6.4.

$$\varepsilon_x = \frac{\left(\frac{M_f}{d_v} + v_f + 0.5N_f\right)}{2E_S A_S}$$

$$\varepsilon_x = \frac{\left(\frac{84.8\times10^6}{219.6} + 55.6\times10^3 - 0.5\times500\times10^3\right)}{2\times200000\times200} = 2.397\times 10^{-3}$$

$$\beta = \frac{0.4}{(1+1500\varepsilon_x)} \times \frac{1300}{(1000+S_{Ze})}$$

Since, $A_v > A_{v,min}$

S_{Ze} = 300 mm (as the section contains at least minimum reinforcement)

$$\beta = \frac{0.4}{(1+1500\times2.397\times10^{-3})} \times \frac{1300}{(1000+300)} = .087 < 0.1$$

$\theta_v = 29 + 7000\varepsilon_x = 29 + 7000 \times 2.397\times 10^{-3} = 45.8° > 45°$

$V_c = 1 \times 1 \times 0.087 \times \sqrt{35} \times 305 \times 219.6 \times 10^{-3} = 34.5$ kN

$V_{rmax} = 0.25\varphi_c f_c' b_w d_v = 0.25 \times 1 \times 35 \times 305 \times 219.6 \times 10^{-3} = 586.06$ kN $> V_r = 55.6$ kN

$V_s = V_r - V_c = 55.6 - 34.5 = 21.1$ kN

From CSA/A23.3-14 Clause 11.3.5.1

$$s = \frac{\varphi_s A_v f_y d_v \cot\theta_v}{V_s} = \frac{1\times200\times400\times219.6\times\cot 45.8}{21100} = 809.7 \text{ mm}$$

From CSA/A23.3-14 Clause 11.2.8.2

$$A_{v,min} = 0.06\sqrt{f_c'}\frac{b_w s}{f_y}$$

or, $200 = 0.06\sqrt{35}\frac{305\times s}{400}$

or, s = 739 mm

When s = 75 mm

$$V_s = \frac{1\times200\times400\times219.6\times\cot 45.8}{75} = 227.8 \text{ kN}$$

$V_r = V_s + V_c = 227.8 + 34.5 = 262.3$ kN $> V_f = 55.6$ kN

From CSA/A23.3-14 Clause 21.4.4.3

Confinement reinforcement in accordance with Clause 21.2.8.2 shall be provided at both ends of the columns over a length equal to the largest of one-sixth of the clear height, the maximum cross sectional dimension, or 450 mm, with the spacing not exceeding the smallest of

- Eight longitudinal bar diameters = 8 × 15 = 120 mm
- 24 tie diameter = 24 × 10 = 240 mm
- One-half of the minimum column dimension = 305/2 = 152.5 mm

From CSA/A23.3-14 Clause 21.2.8.1

Buckling prevention ties shall comply with Clause 7.6.5.5 or 7.6.5.6 and shall be detailed as hoops, seismic crossties or spirals. The tie spacing shall not exceed the smallest of

- Six longitudinal bar diameters = 6 × 15 = 90 mm
- 24 tie diameter = 24 × 10 = 240 mm
- One-half of the minimum column dimension = 305/2 = 152.5 mm

From CSA/A23.3-14 Clause 21.3.4.2

The first hoop shall be located not more than 50 mm from the face of a supporting member. The maximum spacing of the hoops shall not exceed

- *d* / 4 = 305/4 = 76.25 mm
- eight times the diameter of the smallest longitudinal bars = 8 × 15 = 120 mm
- 24 times the diameter of the hoop bars = 24 × 10 = 240 mm
- 300 mm

Select 10M spiral pitch = 75 mm

Check for minimum spiral reinforcement from Clause 10.9.4

The ratio of spiral reinforcement shall be not less than the value given by

$$\rho_s = 0.5\left(\frac{A_g}{A_c} - 1\right)^{1.4}\frac{f_c'}{f_y} = 0.5 \times \left(\frac{73061.7}{55154.6} - 1\right)^{1.4} \times \frac{35}{400} = 0.009$$

$$\rho_{s,prov} = \frac{A_{sp}l_{sp}}{A_c p} = \frac{100 \times 3.1416 \times 265}{\frac{3.1416 \times 265^2}{4} \times 75} = 0.02 > 0.009 \textbf{ OK}$$

APPENDIX B: DESIGN OF SPECIMEN I1-3

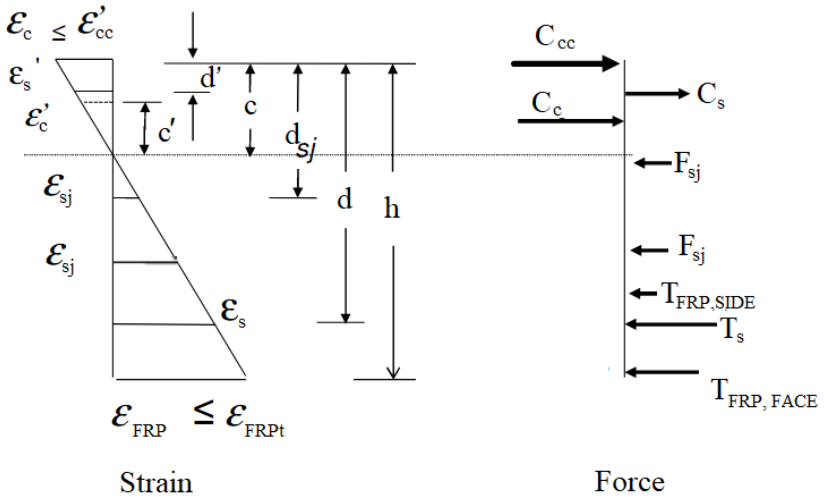

Figure B.1: Strain and forces on rehabilitated section

Assuming, when the internal axial load resistance is equal to external axial load (20% of column axial load capacity), resultant axial load will be zero and at that condition the calculated lateral load will be maximum lateral load capacity.

According to ISIS Design manual 4 (Version 2),

Confined concrete strength, $f'_{cc} = f'_c + 2f_{lfrp}$

$$\boldsymbol{f_{lfrp}} = \frac{\boldsymbol{2t\phi f_{frpu}}}{\boldsymbol{D}}$$

Where,

f_{lfrp} = confinement pressure,

t = thickness = 3 mm,

f_{frpu} = ultimate stress of confinement = 115 MPa (*Lee et al. 2016*),

ϕ = reduction factor = 1,

D = Column diameter = 305 mm.

$f'_{cc} = f'_c + 2f_{lfrp} = 35 + 2 \times \frac{2\times3\times1\times115}{305} = 39.5$ MPa

But here f_{lfrp} = 2.3 MPa < 0.1f_c'=3.5 MPa. So, it did not satisfied the confinement limit condition stated in CSA/S6-06.

From excel sheet the condition for maximum lateral load was satisfied when c= 112.5 mm. so,

Assume, ε_c' = 0.0035

$$\varepsilon_{cc}' = \varepsilon_c' \left(1 + 5\left(\frac{f_{cc}'}{f_c'} - 1\right)\right) = 0.0035\left(1 + 5\left(\frac{39.5}{35} - 1\right)\right) = 0.00575$$

$$c' = \frac{c \times \varepsilon_c'}{\varepsilon_{cc}'} = \frac{112.5 \times 0.0035}{0.00575} = 68.332 \text{ mm}$$

Assumptions,

- f_c varies linearly from f_c' to f_{cc}';
- equivalent rectangular stress distribution for $f_c < f_c'$ with a_1= 0.781 and β_1=0.855;
- compression and tension steel has yielded;
- intermediate steel is in the elastic domain;
- FRP in compression is ignored;

For confined concrete, $C_{cc} = \phi_c \frac{f_c' + f_{cc}'}{2} A_{cc}$

Where, A_{cc} = Area under confined concrete

$$A_{cc} = R^2\left(\cos^{-1}\left(\frac{R - (c - c')}{R}\right)\right) - \left(R - (c - c')\right)\sqrt{2R(c - c') - (c - c')^2}$$

= 24472.2 mm^2

$$C_{cc} = 1 \times \frac{35 + 39.5}{2} \times 24472.2 = 243.3 \text{ kN}$$

For unconfined concrete, $C_c = \phi_c \alpha_1 f_c' A_{\beta_1 c'}$

Where, $A_{\beta_1 c'}$ = Area under unconfined concrete

$A_{\beta_1 c'} = A_c - A_{c-\beta_1 c'}$ = 24472.2 – 8315.6 = 16156.6 mm^2

C_c = 1×0.781×35×16156.6 = 451.0 kN

For bars in compression, $C_s = \phi_s f_y A_s'$ = 1×460×600 = 276 kN

For intermediate bars, $F_{sj} = \phi_s \varepsilon_{sj} E_s A_{sj}$

$\varepsilon_{sj3} = \frac{\varepsilon'_{cc} \times (d_3 - c)}{c} = \frac{0.00575 \times (207.5 - 112.5)}{112.5} = 0.0049$

$F_{sj3} = \phi_s \varepsilon_{sj3} E_s A_{sj3}$ = 1×0.0049×200000×400 = 402.8 kN >$\phi_s f_y A_{sj} = 1 \times 460 \times 400$ = 184kN

So, $F_{sj3} = 184$ kN

$F_{sj} = 184$ kN

For bars in tension, $T_s = \phi_s f_y A_s$ = 1×460×200 = 92 kN

For sprayed-GFRP in tension, $T_{FRP} = \phi_{frp} f_{frp} A_{frp,t}$

Where, $A_{frp,t}$ = area of sprayed system under tension

= t × (2πR-R $\boldsymbol{\theta}$) = 3×(2×3.1416×152.5-152.5×2.6) = 1688.9 mm^2

T_{FRP} = 1×115×1688.9 = 193.2 kN

Now, $P_r = C_{cc} + C_c + C_s - F_{sj} - T_s - T_{FRP}$= 243.3+451.0+276-184-92-193.2=501.1 kN

$M_{cc} = C_{cc}\left(R - (c - c')\frac{2f'_c + f'_{cc}}{3f'_c + 3f'_{cc}}\right) = 243.3\left(152.5 - (112.5 - 68.33)\frac{2*35+39.5}{3*35+3*39.5}\right)$ = 31.8 kN.m

$M_c = C_c\left(R - c + c'\left(1 - \frac{\beta_1}{2}\right)\right) = 451.0\left(152.5 - 112.5 + 68.33\left(1 - \frac{0.85}{2}\right)\right)$ = 35.3 kN.m

$M_{cs} = C_{s1}(R - d_1) + C_{s2}(R - d_2)$ = 1×460×200(152.5-42.5) + 1×460×400(152.5-97.5) = 20.2 kN.m

$M_{sj} = F_{sj3}(d_3 - R)$ = 184(207.5-152.5) = 10.1 kN.m

$M_{Ts} = T_s(d_3 - R)$ = 92(262.5-152.5) = 10.12 kN.m

$M_{FRP} = T_{FRP}$ R = 193.2 × 152.5 = 29.47 kN.m

$M_r = M_{cc} + M_c + M_{cs} + M_{sj} + M_{Ts} + M_{FRP}$ = 137.045 kN.m

Lateral load = 137.045/1.525= 89.9 kN